INFORMATION TO USERS

This manuscript has been reproduced from the microfilm master. UMI films the text directly from the original or copy submitted. Thus, some thesis and dissertation copies are in typewriter face, while others may be from any type of computer printer.

The quality of this reproduction is dependent upon the quality of the copy submitted. Broken or indistinct print, colored or poor quality illustrations and photographs, print bleedthrough, substandard margins, and improper alignment can adversely affect reproduction.

In the unlikely event that the author did not send UMI a complete manuscript and there are missing pages, these will be noted. Also, if unauthorized copyright material had to be removed, a note will indicate the deletion.

Oversize materials (e.g., maps, drawings, charts) are reproduced by sectioning the original, beginning at the upper left-hand corner and continuing from left to right in equal sections with small overlaps. Each original is also photographed in one exposure and is included in reduced form at the back of the book.

Photographs included in the original manuscript have been reproduced xerographically in this copy. Higher quality 6" x 9" black and white photographic prints are available for any photographs or illustrations appearing in this copy for an additional charge. Contact UMI directly to order.

UMI

A Bell & Howell Information Company
300 North Zeeb Road, Ann Arbor MI 48106-1346 USA
313/761-4700   800/521-0600

UMI Number: 9712644

Copyright 1996 by
Xu, James Jin

UMI Microform 9712644
Copyright 1997, by UMI Company. All rights reserved.

UMI

300 North Zeeb Road
Ann Arbor, MI 48103

ABSTRACT

LOCAL STRESSES ON LATERAL PIPE-NOZZLE
WITH 45° DEGREE ANGLE INTERSECTION

by
James Jin Xu

This dissertation presents a comprehensive study of local stresses, due to internal pressure around a pipe-nozzle with 45 degree angle intersection. The resulting circumferential and longitudinal stresses on the pipe around the pipe-nozzle region are normalized as local stress factors and plotted as function of beta, β, (the radius of the nozzle/the radius of the pipe) and gamma, γ, (the radius of the pipe/the thickness of the pipe) through the finite element method. The range of beta, β, is from 0.1, to 1.0, and gamma, γ, from 10 to 300. Comprehensive studies were made for the boundary parameters, such as α_p (pipe length / pipe mean radius) and α_n (nozzle length / nozzle mean radius), the optimized numbers of nodes around the pipe-nozzle juncture and total elements of the model. To justify a wide range of application of the 45° degree pipe-nozzle angles, extensive studies and a set of plots are provided to show that local stress factors vary with the pipe-nozzle intersection angle, from 90° to 30°.

An approximate theoretical analysis, which is based on thin-shell theory together with stress multipliers for the peak stresses at the both inside and outside crotch points, has derived to compare the data from 3D finite element models.

This study concludes that the maximum local stress is in the circumferential direction and occurs at the inside crotch point. The 45° intersecting angle yields relatively less local

stresses when the pipe-nozzle intersecting angle other than 90° must be used for operational purposes. The local pressure stresses in the pipe-nozzle juncture are mostly in tension except on the inside surface of pipe in longitudinal direction. For certain combinations of β and γ, however, the longitudinal stress at point C (see Figure 2) on the outside surface of pipe may be compressive also.

Twelve (12) plots of local pressure stress factors are provided in this thesis allows design engineers of pressure vessel to compute local stress on both the outside and the inside shell of pipe when the pipe-nozzle intersecting angle is 45°. A numerical example is given.

LOCAL STRESSES ON LATERAL PIPE-NOZZLE
WITH 45° DEGREE ANGLE INTERSECTION

by
James Jin Xu

A Dissertation
Submitted to the Faculty of
New Jersey Institute of Technology
in Partial Fulfillment of the Requirements for the Degree of
Doctor of Philosophy

Department of Mechanical Engineering

October 1996

Copyright @ 1996 by James Jin Xu

ALL RIGHTS RESERVED

APPROVAL PAGE

LOCAL STRESSES ON LATERAL PIPE-NOZZLE
WITH 45° DEGREE ANGLE INTERSECTION

James Jin Xu

Dr. Benedict C. Sun, Dissertation Advisor   Date
Associated Professor of Engineering Technology, NJIT

Dr. Berhard Koplik, Committee Chair   Date
Professor and Chairperson
of the Department of Mechanical Engineering, NJIT

Dr. Rong-Yaw Chen, Committee Member   Date
Professor, Associate Chairperson and Graduate Advisor
of the Department of Mechanical Engineering, NJIT

Dr. Ansel C. Ugural, Committee Member   Date
Professor of the Department of Mechanical Engineering, NJIT

Dr. C. T. Thomas Hsu, Committee Member   Date
Professor of Civil and Environmental Engineering, NJIT

BIOGRAPHICAL SKETCH

Author: James Jin Xu

Degree: Doctor of Philosophy

Date: October 1996

Undergraduate and Graduate Education:

- Doctor of Philosophy in Mechanical Engineering,
  New Jersey Institute of Technology,
  Newark, New Jersey, 1996

- Master of Science in Mechanical Engineering,
  New Jersey Institute of Technology,
  Newark, New Jersey, 1992

- Bachelor of Science in Chemical Machinery Engineering,
  ZhengZhou Institute of Technology,
  ZhengZhou, China, 1982

Major: Mechanical Engineering

Position Held:

Mechanical Design Engineer
Werner & Pfleiderer Corporation
663 East Crescent Ave.
Ramsey, NJ 07446

Membership:

Member of American Society of Mechanical Engineers
Member of American Society of Heating, Refrigerating and Air-Conditioning
Engineers

This Dissertation
is dedicated to my parents, my wife and
all my family members.

v

ACKNOWLEDGMENT

The author wishes to express his sincere appreciation to his Dissertation advisor, Dr. Benedict Sun, for his guidance, friendship, and moral support throughout this research.

Special thanks to Dr. Bernard Koplik, Dr. Rong-Yaw Chen, Dr. Ansel C. Ugural , Dr. C. T. Thomas Hsu for serving as members of the committee and their kind suggestions and supports.

The author is grateful to the Department of Mechanical Engineering, NJIT for the Research Assistantship through the Fall of 1991 to the Spring of 1992.

Also, the author would like express his gratitude to his wife for her love, understanding and support to the achievement of this dissertation.

TABLE OF CONTENTS

TABLE OF CONTENTS
(Continued)

LIST OF TABLES

LIST OF FIGURES

x

LIST OF FIGURES
(Continued)

LIST OF FIGURES
(Continued)

LIST OF FIGURES
(Continued)

NOMENCLATURES

α_p = pipe length/pipe mean radius

α_n = nozzle length/nozzle mean radius

β = nozzle radius/pipe mean radius

β_g = see equation (6),

β_p = see equation (25)

β_n = see equation (29)

γ = pipe mean radius/pipe thickness

$\varepsilon_{\phi p}$, $\varepsilon_{\phi n}$ = circumferential strain

v = Poisson's ratio

σ_{ap}, σ_{an} = meridional membbrane stress

σ_{bp}, σ_{bn} = meridional bending stress

σ_{cp}, σ_{cn} = circumferential membrane stress

θ = angle between pipe and nozzle on the symmetric plan alone the pipe axis

a = shell radius

E = Young's modules

D = see equation (5)

D_p = see equation (24)

D_n = see equation (28)

h = shell thickness

K_r = radial nozzle stress factor

K_{nr} = non - radial nozzle stress factor

xv

NOMENCLATURES
(Continued)

L_p = length of pipe

L_n = length of nozzle

M_0 = bending moments at the edge of shell, lb-in./in.

M_{xp}, M_{xn} = shell bending moments, lb-in./in.

M_x = shell moment resultants, lb-in./in.

N_x = meridional direct stress resultants, lb/in..

$N_{\phi p}$, $N_{\phi n}$ = circumferential direct stress resultants, lb/in.

N_ϕ = circumferential direct stress resultants, lb/in.

p = internal pressure

Q_0 = shear force at the edge of pipe, lb/in.

Q_{xp}, Q_{xn} = transverse shear stress resultants, lb/in

R_p = pipe mean radius

R_n = nozzle mean radius

t_p = pipe thickness

t_n = nozzle thickness

u = displacement in x direction

v = displacement in ϕ direction

w = displacement in r direction

$\partial w_p/\partial x_p$, $\partial w_n/\partial x_n$ = rotations

x_p, x_n = coordinates along shell meridians for pipe and nozzle respectively

NOMENCLATURES
(Continued)

x, ϕ, r = coordinates for general cylindrical shell

X, Y, Z = globe coordinates for 3D modelling

Z = intensity of load

Subscripts

p = pipe, main shell

n = nozzle, branch

CHAPTER 1

INTRODUCTION

Pipe tees and lateral connections are essential components in process and power generation facilities for functional purposes. The lateral tee or nozzle makes an elliptical opening in the pipe or vessel which cause the higher stress concentration than the standard 90° nozzle. The high local stresses at the juncture of these connections cause major safety concerns especially in nuclear power design.

The commonly used laterals have the intersection angles of 30°, 45°, and 60°, respectively. Although considerable investigations have been available on nozzle junctions and branches under internal pressure and other external loadings by experimental, analytical and numerical methods, they are limited to the 90° intersection. The fundamental difficulty in the analysis of pipe-nozzle is that they are not axisymmetric and the curve of intersection is a nongeodesic curve. This thesis investigates the effect of these lateral connection variations in angle θ on the local stresses due to internal pressure, and it also presents a comprehensive data of local stress factors for the 45° pipe-nozzle connection, shown in Figure 1. In the figure, points A and B are designated as outside and inside crotch points, respectively.

Using ALGOR finite element analysis package, the pipe-nozzle juncture is simulated by using a full pipe-nozzle model. To ensure proper convergence of the numerical results on the local stresses, comprehensive studies are made to optimize the models with 96

1
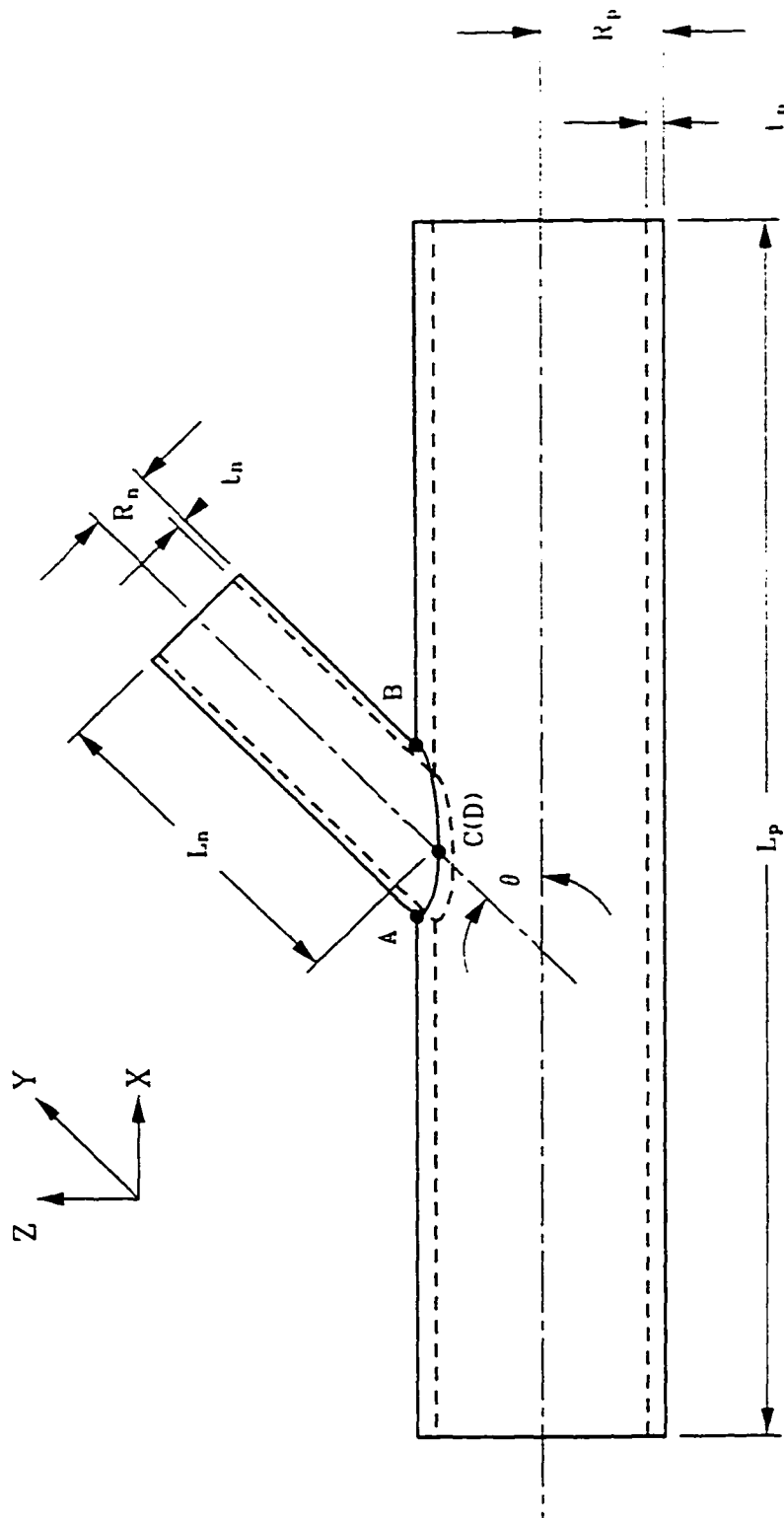
Figure 1: Pipe-nozzle configuration
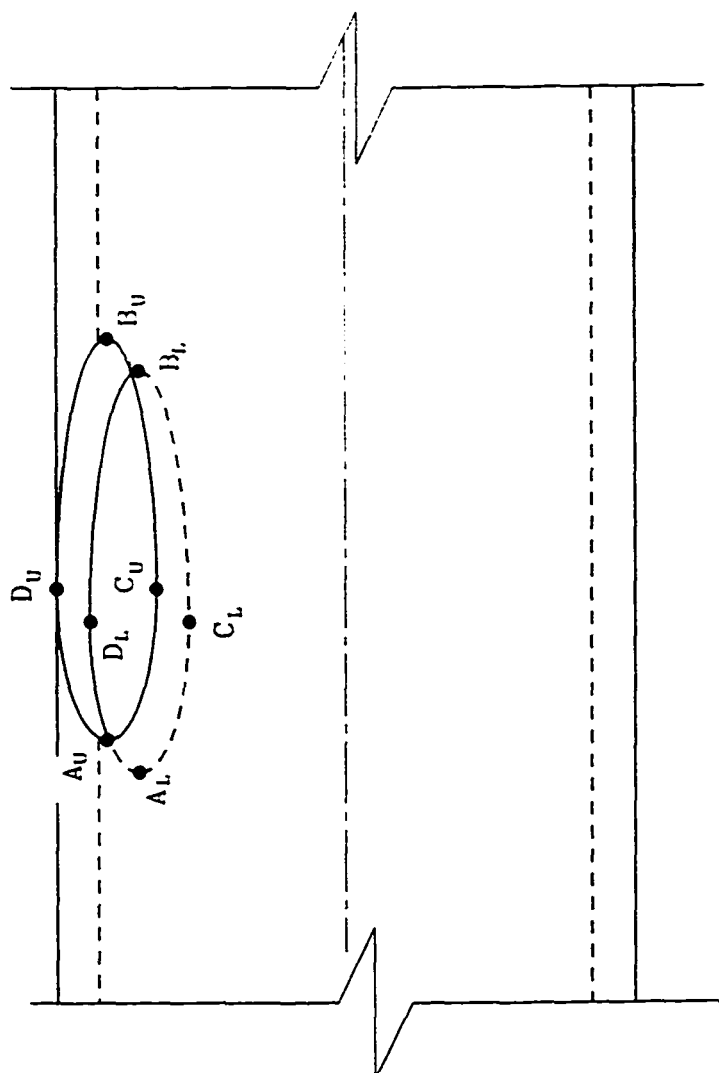
Figure 2: Data points configuration

nodes on the pipe-nozzle junction, and the values for the geometry parameter are 10.0 for α_p (pipe length / pipe mean radius) and 5.0 for α_n (nozzle length / nozzle mean radius). These values ensure that boundary conditions at the end of the pipe and nozzle will not effect the accuracy of the numerical results. Assuming that the membrane pressure stresses in the pipe and the nozzle are identical, the nozzle thickness is proportional to the pipe thickness by a factor beta, β, i.e. $t_n = \beta t_p$.

To provide a comprehensive range of local stress results for design engineers and stress analysts, this thesis presents twelve plots of local stress factors for both the circumferential and longitudinal stresses at points A, B, and C, respectively, as shown in Figure 2, of which six plots are for the stresses on the outside surface of pipe and the remaining six are for the inside surface. In these plots, the geometrical parameter β (nozzle mean radius / pipe mean radius) range from 0.1 to 1.0 with an increment of 0.1 and the γ (pipe mean radius / pipe thickness) range from 10 to 300 in ten random selected intervals. The local stress factors are defined by normalizing the resulting local stresses by the applied internal pressure value.

CHAPTER 2

LITERATURE SURVEY

There exist many theoretical analyses, experimental data and finite element analysis on the local stresses of the pipe-nozzle intersection since the 1950s. However, they are either mainly concerned about the pipe-nozzle intersection with 90 degree angle or have various limitations which can only be applied to certain special cases.

K.R. Wichman, A.G. Hopper and J.L. Mershon [1] published WRC Bulletin No. 107 in 1965. It suggested a method to calculate the local stresses of spherical and cylindrical shells with a nozzle due to external loading. The theory of this bulletin is based on a study by Bijlaard published in 1955 [2]. His work is based on the thin-shell theory and double Fourier series solutions. The latest revision of Bulletin No. 107 was published in March 1979. Due to the mathematical limitation of Bijlaard's work, Bulletin No. 107 can only apply to problems of lug or a solid trunnion at 90° intersection angle with the vessel. It does not recommend any specific method in analyzing an actual nozzle connection to a pressure vessel, either cylindrical or spherical. The induced normal stresses were reported as membrane and bending stress factors in biaxial directions. The shear stresses due to external shear forces and torsional moments are obtained through approximated formulas. Finally, stresses from various nozzle loads are summed in their respective directions before the principal stresses and stress intensity are calculated.

5

Mirza and Gupgupoglu [3] [4] in 1988 introduced a 17-node doubly curved shell finite element model to simulate the case of longitudinal moments applied at discrete points around the circumference of the vessel. The results from the finite element method were in agreement with WRC 107 [1], but were not applicable to pipe-nozzle other than 90° intersection.

J.L. Mershon et al. published the WRC Bulletin No. 297 in August 1984 [5]. It is a supplement to WRC 107 and is specifically applicable to round nozzles on cylindrical vessels. This bulletin was based on Professor Steele's theoretical work [6] for larger γ (radius/thickness) values than what is provided in WRC 107 [1]. Steele's theoretical work considers an opening on the shell together with restraining effect of nozzle wall. The β values are limited to 0.5.

Sadd and Avent [7] in 1982 studied a trunnion pipe anchor by the finite element method. The model is analyzed for the case of internal pressure and various end moment loadings. With Georgia Tech ICES STRUDL finite element package, a quadrilateral element with six degrees of freedom at each of the four corner nodes was utilized. The α_p value is taken as 8.0 for their models. Data are provided for a beta, β, (trunnion mean radius/pipe mean radius) range from 0.5 to 1.0 and gamma, γ, (pipe radius/pipe thickness) range from 5 to 20.

Tabone and Mallett [8] in 1987 established a finite element model of a nozzle in a cylindrical shell subjected to internal pressure, and out-of-plane moment. This model used ANSYS 3-D finite elements and the analysis considered the elastic behavior at small

displacements. Two elements along the thickness direction of the nozzle and vessel were employed in this study. It resulted in an estimation of limited loads based on extrapolation of the load-versus-inverse-displacement curves. An expression is given for the effect of the combined loadings for a case in which the internal pressure reduces the moment capability of the nozzle by approximately 35 percent.

H. Sun, B.C. Sun and H. Herman [9] [10] in 1991 published comprehensive results of studies on local pipe stresses using the finite element method. These papers reported a series bending and membrane stress factors for local circumferential and longitudinal stresses on the pipe region of the pipe-nozzle intersection due to all six external loading components.

J. Ha, B.C. Sun and B. Koplik [11] in 1994 presented a comprehensive study of local stresses around a pipe-nozzle due to internal pressure using the finite element method. In this paper, the local pressure stresses for both the pipe and nozzle around the pipe-nozzle juncture are normalized into pressure stress factors which are then plotted as functions of geometrical parameters, β and γ. The ranges of these stress factors cover β from 0.1 to 1.0, γ from 10 to 300. To ensure proper convergence, the optimized numbers is 8 for α_p, 4 for α_n, respectivelly. Their model contains 96 nodes around the pipe-nozzle juncture, and 3000 ~ 4000 elements for the full model. For accuracy and faster convergence, ten separate finite element models were established, one for each β value.

From above literature survey, it is obvious that in the past decades few studies were available on the local stresses around pipe-nozzle with 45 degree angle. The theoretical

analysis of local stresses around pipe-nozzle intersection involve tremendous mathematical difficulties due to the absence of axial symmetry. Instead of an ordinary differential equation for the pipe-nozzle stress field, partial differential equations with various non-symmetrical terms are needed for the pipe-nozzle geometry which led to extreme difficulties in obtaining the exact equilibrium equations of force and moment at the juncture of the pipe-nozzle. The approximate solution are restricted to a fairly small range of the intersection curvatures since the mid-surfaces of the pipe-nozzle intersection is generally not a geodesic curve. There exists neither analytical nor experimental data for pressure vessel designer to analyze the stresses on pipe-nozzle with 45 degree angle with neither external loading, nor internal pressure. A comprehensive database to calculate these local stresses are needed by industry.

CHAPTER 3

THEORETICAL ANALYSIS

Analytical methods for local stresses around the pipe-nozzle under internal pressure involve tremendous mathematical difficulties caused by the absence of axial symmetry and non-geodesic curve on either the pipe or the nozzle. Several researchers have achieved some approximate solutions for certain locations on the juncture of pipe-nozzle based on certain special geometrical configurations and assumptions [12] [13] [14] [15] [16]. The linear stress distribution through the thickness of the pipe-nozzle intersection and the continuity conditions of axial membrane stress, circumferential strain, rotation of normal, and bending moment at the intersection of pipe-nozzle connection, are commonly assumed in most of the approximated theoretical solutions. However, their studies are limited by the location and special geometry configuration and most of them only discussed the 90° pipe-nozzle intersection.

3.1 General Thin-shell Theory

In terms of the components of displacement and their partial derivatives, the basic thin shell theory equation was established by Timoshenko [17][18] for a radial loading per unit surface. Let the components of displacement be u, v, and w respectively in the direction of x, ϕ, and r (see Figure 3a). The equilibrium equations are as following:

9

$$\frac{\partial^2 u}{\partial x^2} + \frac{1-v}{2a^2} \cdot \frac{\partial^2 u}{\partial \phi^2} + \frac{1+v}{2a} \cdot \frac{\partial^2 v}{\partial x \partial \phi} - \frac{v}{a} \cdot \frac{\partial w}{\partial x} = 0 \tag{1}$$

$$\frac{1+v}{2} \cdot \frac{\partial^2 u}{\partial x \partial \phi} + \frac{1}{a} \cdot \frac{\partial^2 v}{\partial \phi^2} + a\frac{1-v}{2} \cdot \frac{\partial^2 v}{\partial x^2} - \frac{1}{a}\frac{\partial \varpi}{\partial \phi} = 0 \tag{2}$$

$$v\frac{\partial u}{\partial x} + \frac{1}{a}\frac{\partial v}{\partial \phi} - \frac{w}{a} - \frac{h}{12}\left[a\frac{\partial^4 w}{\partial x^4} + \frac{2}{a}\frac{\partial^4 w}{\partial x^2 \partial \phi^2} + \frac{\partial^4 w}{a^3 \partial \phi^4} \right]$$

$$= -\frac{ap(1-v^2)}{Eh} \tag{3}$$

3.2 Cylindrical Shell with Axial Symmetric Loadings

When a cylindrical shell is loaded symmetrically with respect to its axis and the thickness of shell is constant, a fourth order differential equation is obtained [17][18]:

$$\frac{\partial^4 w}{\partial x^4} + 4\beta_g^4 w = \frac{Z}{D} \tag{4}$$

where

$$D = \frac{Eh^3}{12(1-v^2)} \tag{5}$$

$$\beta_g^{\,4} = \frac{Eh}{4a^2 D} = \frac{3(1-v^2)}{a^2 h^2} \tag{6}$$

For a long circular pipe submitted to the action of bending moment M_0 and shearing forces Q_0, both uniformly distributed along the edge $x = 0$ shown in Figure 3b, the expression for w is given by solving equation (4) in the case there is no pressure Z distributed over the surface of the shell:

$$w = \frac{e^{-\beta x}}{2\beta_g^{\,3} D}\left[\beta_g M_0\left(\sin\beta_g x - \cos\beta_g x\right) - Q_0 \cos\beta_g x\right] \tag{7}$$

At the load end, $x = 0$

$$(w)_{x=0} = -\frac{1}{2\beta_g^{\,3} D}\left(\beta_g M_0 + Q_0\right) \tag{8}$$

$$\left(\frac{dw}{dx}\right)_{x=0} = -\frac{1}{2\beta_g^{\,2} D}\left(2\beta_g M_0 + Q_0\right) \tag{9}$$

$$\left(\varepsilon_\phi\right)_{x=0} = -\left(\frac{w}{a}\right)_{x=0} = \frac{1}{2\beta_g^{\,3} Da}\left(\beta_g M_0 + Q_0\right) \tag{10}$$

3.3 Approximated Solution for 45° Lateral Tee or Nozzle

An approximate method for the elastic stresses at the crotch of a branch pipe connection under internal pressure is developed based on thin-shell theory together with stress

(a) Coordinate for general
cylindrical shell.
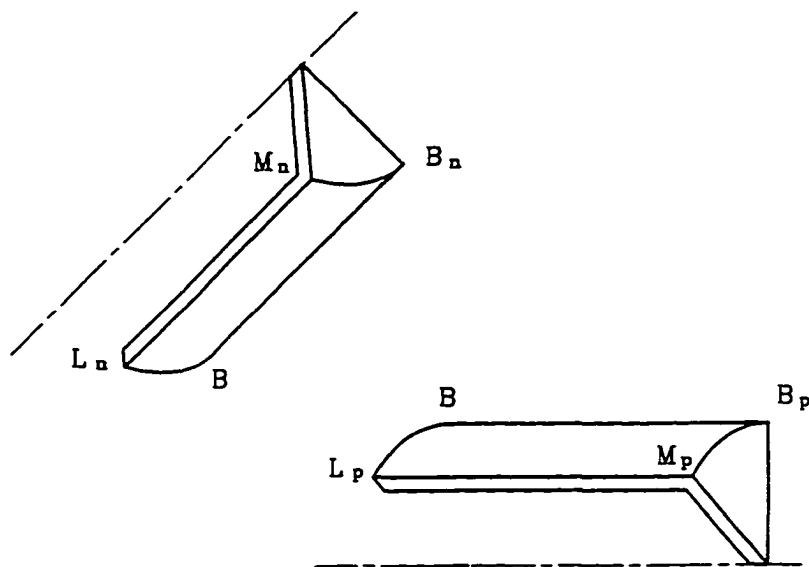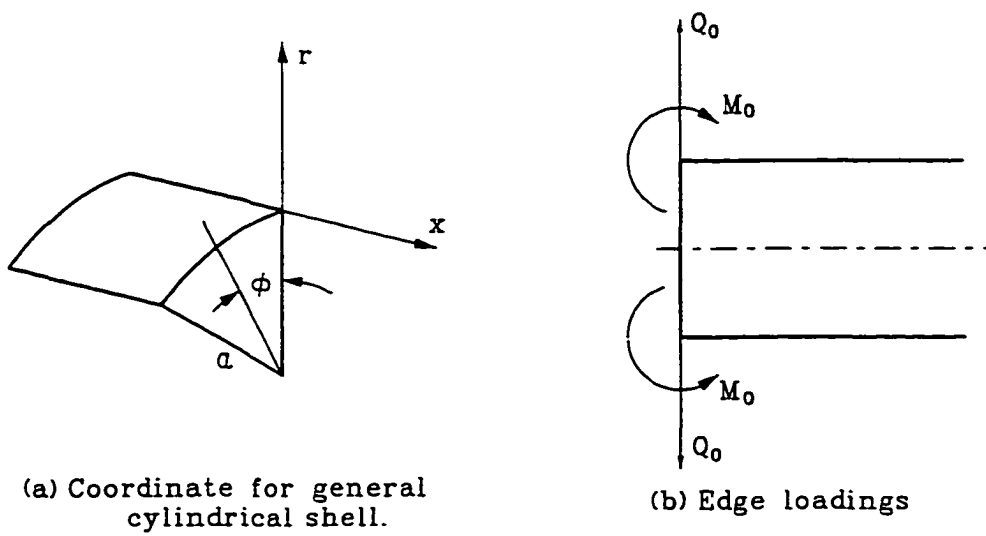
(b) Edge loadings

(c) Presentative cylinder panels

Figure 3: General cylindrical shell configuration

13
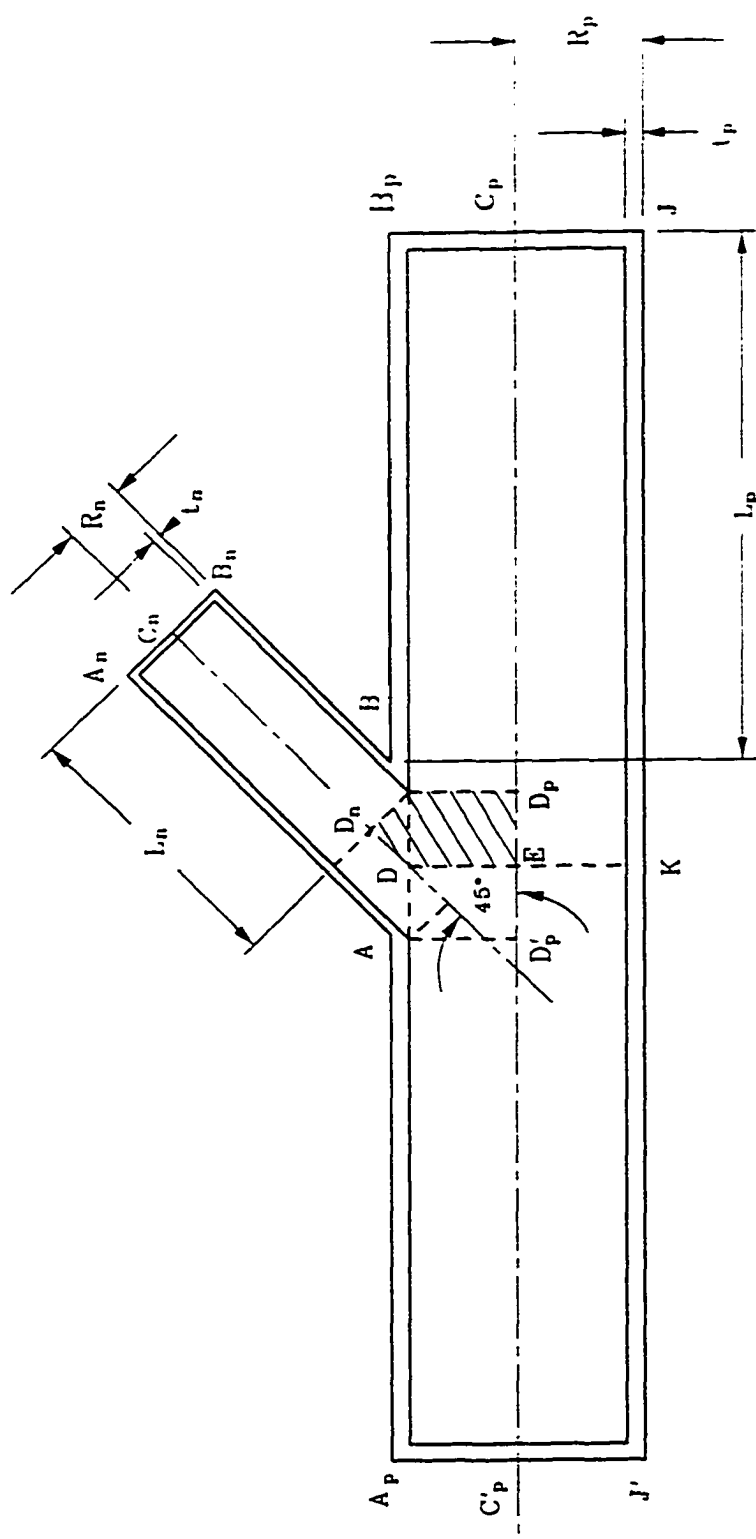
Figure 4: Section used for calculating forces in overall equilibrium equation
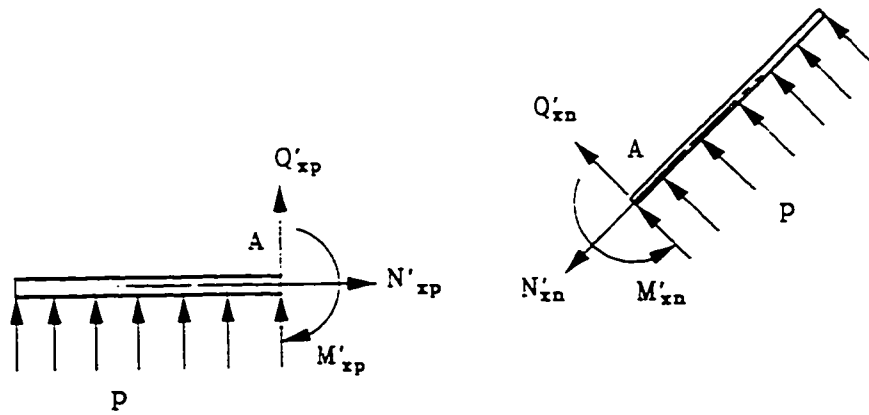
(a). Forces at point A
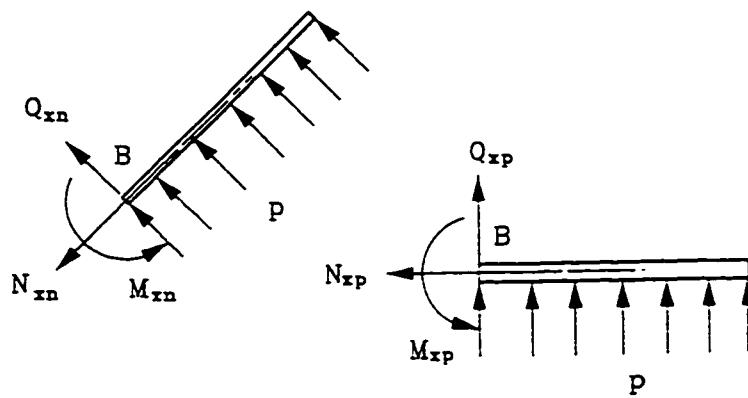
(b). Forces at point B

Figure 5: Edge loading on cylinder strip
due to internal pressure

multipliers for the peak stress at the crotch point. Lind [19] developed an overall equilibrium equation for a tee branch connection with 90° degree angle. Lind's equation represents a balance of forces across the mid-plane of the structure. In the case of pipe-nozzle with 45° degree intersection, referring to Figure 4, the area to balance the tensile forces along the shell is modified in this study.

The tensile forces on the cross section $C_\alpha B_\alpha BB_p C_p JK$ of the structure are set equal to the resultant force of the pressure acting on area $C_\alpha B_\alpha BB_p C_p JKD$. If it is assumed that both the main shell and the branch are long and that stress along KJ is the nominal hoop stress, then the pressure times area, $EC_p JK$, is balanced by the tensile force along $C_p JK$. Then, this requires that the tensile force on $C_\alpha B_\alpha BB_p C_p$ balance the pressure times area $C_\alpha B_\alpha BB_p C_p ED$, which includes sub-areas $C_\alpha B_\alpha BD$ ($R_n \cdot L_n$), $BB_p C_p D_p (R_p \cdot L_p)$, $DBD_p E$ ($R_p \cdot R_n \cdot \cos 45°$) and $D_\alpha BD$ ($R_n \cdot R_n/2$). The force balance equation then becomes

$$\int_{C_\alpha B_\alpha BB_p C_p} N_\phi \, dx = p \left(R_p L_p + R_n L_n + \frac{R_n^2}{2} + R_p R_n \sqrt{2} \right)$$

(11)

Expressions for the edge shearing forces Q_{xp} and Q_{xn} acting on the cylindrical panels $BB_p M_p L_p$ and $BB_\alpha M_\alpha L_n$ at the junction point B (Figure 3c) are derived by Updike [20] to be

$$\int_{BB_p C_p} N_\phi \, dx = Q_{xp} R_p + p R_p L_p$$

(12)

$$\int_{C_\alpha B_\alpha B} N_\phi \, dx = Q_{xn} R_n + p R_n L_n$$

(13)

Summing equations (12) and (13) and invoking (11) results in

$$Q_{xp}R_p + Q_{xn}R_n = p(\frac{R_n^2}{2} + R_p R_n \sqrt{2})$$
(14)

The rotation of the shell normal and the circumferential strain of each of the strips meeting at point B of Figure 5 are matched by satisfying the equations due to the continuity conditions

$$\frac{dw_p}{dx_p} + \frac{dw_n}{dx_n} = 0$$
(15)

$$\varepsilon_{\phi p} = \varepsilon_{\phi n}$$
(16)

Equilibrium of a shell element at the junction point B of the strips is satisfied by means of the equations:

$$M_{xn} = M_{xp}$$
(17)

$$\sqrt{2}(N_{xn} - Q_{xn})/2 = Q_{xp}$$
(18)

$$\sqrt{2}(N_{xn} + Q_{xn})/2 = N_{xp}$$
(19)

where the edge loads M_{xp}, M_{xn}, N_{xp}, N_{xn}, Q_{xp} and Q_{xn} are shown in Figure 5. Equations (18) and (19), are solved for N_{xp} and N_{xn}, yield the expressions

$$N_{xp} = Q_{xp} + \sqrt{2}Q_{xn} \tag{20}$$

$$N_{xn} = Q_{xn} + \sqrt{2}Q_{xp} \tag{21}$$

If the derivatives in the circumferential direction of stress and the deformation variable are neglected and stresses due to ovaling deformation are ignored, the equation governing the stresses in the cylindrical strip BB_p reduce to those of a complete circular cylindrical shell of radius, R_p, subjected to axisymmetric loading. In terms of the internal pressure, p, and the edge loads, M_{xp}, Q_{xp}, and N_{xp}, of Figure 5, the flexibility relations for semi-infinite cylindrical shell are determined by equations (9) and (10) as

$$dw_p / dx_p = M_{xp} / \beta_p D_p - Q_{xp} / 2\beta_p^2 D_p \tag{22}$$

$$\varepsilon_{\phi p} = Q_{xp} / 2\beta_p^3 D_p R_p - M_{xp} / 2\beta_p^2 D_p R_p + pR_p / Et_p - vN_{xp} / Et_p \tag{23}$$

where

$$D_p = Et_p^3 / 12(1 - v^2) \tag{24}$$

$$\beta_p^4 = 3(1 - v^2) / R_p^2 t_p^2 \tag{25}$$

Likewise, the governing equations for nozzle $B_n B$ reduce to equations for finite cylindrical shell of radius R_n subjected to axisymmetric loading. With section $BB_n C_n D_n$ as a plane of symmetry the flexibility relations in terms of the internal pressure, p, and the edge

loads, M_{xn}, Q_{xn} and N_{xn} of Figure 5, the flexibility relations for semi-infinite cylindrical shell are determined by equations (9) and (10) as

$$dw_n \, / \, dx_n = M_{xn} \, / \, \beta_n D_n - Q_{xn} \, / \, \beta_n^{2} D_n \tag{26}$$

$$\varepsilon_{\phi n} = Q_{xn} \, / \, 2\beta_n^{3} D_n R_n - M_{xn} \, / \, 2\beta_n^{2} D_n R_n + pR_n \, / \, Et_n - vN_{xn} \, / \, Et_n \tag{27}$$

where

$$D_n = Et_n^{3} \, / \, 12(1 - \mathbf{v}^{2}) \tag{28}$$

$$\beta_n^{4} = 3(1 - \mathbf{v}^{2}) \, / \, R_n^{2} t_n^{2} \tag{29}$$

Equations (20) and (21) is used to eliminate N_{xp} and N_{xn} from equations (23) and (27). Equations (20) and (24) are then used to eliminate dw_p/dx_p and dw_n/dx_n from equation (20). Therefore, Q_{xp}, Q_{xn}, M_{xp}, and M_{xn} may be obtained from the reduced equations (14), (15), (16), and (17).

Equations for meridional and circumferential direction stresses are

$$\sigma_a = N_x \, / \, t \tag{30}$$

and

$$\sigma_c = N_\phi / t = E\varepsilon_\phi + v\sigma_\phi \tag{31}$$

The meridional bending stresses is obtained from

$$\sigma_b = 6M_x / t^2 \tag{32}$$

while the circumferential bending stresses due to local bending are obtained by multiplying the meridional stresses by Poisson's ratio.

The stresses at point A may be obtained by the same method as for point B except that the equation (14) is substituted by

$$Q_{xp}R_p + Q_{xn}R_n = p\left[R_p R_n \sqrt{2} - \frac{R_n^2}{2} \right] \tag{33}$$

From equations (14) and (33), one can observe the local stresses at the inside crotch point B, are larger than those at outside crotch point A. Based on this approximate mathematic method, the local stresses at crotch points A and B on the pipe-nozzle junction have been computed for several case. The approximate solutions in a range of β from 0.6 to 0.8 and γ larger than 100 are close to the results from the 3-D finite element models in this thesis with 5% to 30% difference (see numerical example in Chapter 7).

CHAPTER 4

THREE DIMENSIONAL FINITE ELEMENT MODEL

4.1 General

The finite element method for stress analysis fully utilizes the advantages of computer capacity in performing speedy and reliable calculations for a wide range of engineering design problem. This is particularly true when the problem is difficult to solve by a traditional mathematic model or when the geometrical model is too complex. In the study of the problem of the pipe-nozzle connection, a gamma, γ, value (the ratio of radius to the thickness of pipe) of 10 is often considered as a lower bound for the applicability of thin shell theory. Since pipe is considered as a thin shell for most cases, the numerical analysis in this study is based on the quadrilateral thin shell element models.

3D finite element models are generated by a well developed finite element analysis package, ALGOR [21] [22], with each specific β value. The pipe-nozzle system here is modeled by using plate/shell elements based on 3-node and 4-nodes. Material properties, such as Young's Modulus, Poisson's ratio, thermal expansion and density, are assigned to the elements. The models are constructed of elements by locating points (nodes) using coordinates in the global coordinate system. The elements are defined by a way in which the nodes are connected. Each node has six potential degrees of freedom. This means that a given node may displace in three translational degrees of freedom, and also in three rotational degrees of freedom. The translation refers to the movement of a node along the

20

X, Y, or Z axes (or any combination of the three), while rotation refers to the movement of a node about the X, Y, or Z axes (or any combination). Boundary conditions are set by restricting various degrees of freedom.

The Algor system will solve the following equations.

Static Stress Analysis

$$\{F\} = [K]\,\{D\}$$

where : $\{F\} =$ force vector

$[K] =$ stiffness matrix

$\{D\} =$ the displacement vector (stresses are back-calculated from this vector)

Model Analysis

$$[K] \times \{D\} = [M] \times [D] \times [W]^2$$

where: $[D] =$ displacement matrix (mode shapes)

$[W]^2 =$ diagonal matrix containing eigenvalues

$[M] =$ mass matrix

For the analysis, the following assumptions are made:

1). The material is assumed to be homogeneous and isotropic.

2). The resulting stresses are within the proportional limit of the material and obeys Hook's law.

3). The influences of self-weight are neglected.

4). There are no transitions, fillets, or reinforcing pad at the junction.

5). In the pipe-nozzle model, the boundary conditions in each case does not significantly effect the results of the computation since the parameters α_p(pipe length / pipe mean radius) is assigned as large as 10.0 and α_n(nozzle length / nozzle mean radius) is assigned as large as 5.0.

For the convergence requirement of the finite element method, several models with different number of element, node number around the intersection , geometric parameters, and boundary condition have been studied.

To simulate the true pipe-nozzle geometry, full finite element models (see Appendix F for figures) are employed with a symmetric plan (X-Z plan) . The number of element is approximately 4000 to 5000 for the whole finite element models (see Table 4.1), which is required to develop large number of elements and generate sufficient meshes to provide sufficient convergence to the stress results.

Table 4.1: The number of nodes and elements in 3D models

β	number of nodes	number of elements
0.1	10796	5520
0.2	9298	4750
0.3	8592	4386
0.4	9484	4884
0.5	8472	4286
0.6	10540	5384
0.7	9752	5028
0.8	8886	4554
0.9	8784	4484
1.0	10044	5122

4.2 Convergence Studies

The convergence of the finite element models have been carefully studied which included the following factors:

1). The numbers of the elements for the 3-D finite element models.

2). The numbers of the node points at the juncture of pipe-nozzle.

3). The optimum values of α_p (pipe length/pipe mean radius).

4). The optimum values of α_n (nozzle length/nozzle mean radius).

5). Boundary conditions.

To ensure the accuracy of the finite element model, several samples have been tested, such as the cases of closed end cylinder and small hole on the plate, which completely match the available results from theoretical analysis [17] [18] [23].

24

4.2.1 The Number of Elements for the Finite Element Models

The more the number of nodes and elements has, the more accuracy of the results for the finite element model is, but the more running time will be required. Table 4.2 indicates that, for model No.3, the stress results for a 4286 elements model has 0.134% in difference of the results from a 6122 elements model (model #5) but the running time is reduced almost 37.5%. Therefore, the optimum number of elements for the models in this work is between 4000 ~ 5500.

Table 4.2: Comparison of models with different element numbers

Model	No. of Element	Max. Stress, psi	Improv. , %	Run Time, min
No. 1	2422	78313	——	90
No. 2	3634	83076	4.53	160
No. 3	4286	83687	0.73	200
No. 4	5384	83792	0.125	260
No. 5	6122	83799	0.01	320

The data in Table 4.2 are based on a model with $\beta = 0.5$ and $\gamma = 50$ under internal pressure of 100 psi.

4.2.2 The Number of the Node Points at the Juncture of Pipe-nozzle

Previous researchers [11] [24] have shown as the number of node points on the pipe-nozzle junction increase to 96 the stresses converged asymptotically when the pipe-nozzle intersected with 90 degree angle. For the 45 degree pipe-nozzle junction, the studies show that the same value is obtained, which is shown in Figures A1 through A12 in Appendix A when a typical model is employed with $\beta = 0.5$, $\gamma = 50$ and the number of node range from 72 to 112.

4.2.3 The Optimum Values of α_p and α_n

The boundary parameters, α_p and α_n, should be large enough to obtain a converged solution of various stresses. Previous researchers [11] [24] have shown the values of α_p and α_n are 8 and 4, respectively. These were done for stresses due to internal pressure when the pipe-nozzle intersected with 90 degree angle. For the 45 degree pipe-nozzle juncture, the previous values of α_p and α_n may not be sufficient since there exists only one symmetric plan. Figures B1 to B12 in Appendix B show the percentage of improvement with next larger α_p to the previous α_p, and Figures C1 to C12 in Appendix C show the percentage of improvement with larger α_n to the previous α_n. It is evident that $\alpha_p = 10$ and $\alpha_n = 5$ are the optimum values that the boundary conditions would not have any significant effect on the solution of the stresses at the pipe-nozzle junction due to internal pressure.

4.2.4 Boundary Conditions

In the real pipe-nozzle system, both pipe and nozzle are considered as closed end system which means the local pressure stresses at the pipe-nozzle juncture are superimposed with the membrane pressure stresses. Meanwhile, in order to prevent the thermal expansion stresses from occuring, the vessel and nozzle are usually modelled with simply supported.

Table 4.3 shows the comparison of data from this study with Ha's data [11], which does not have longitudinal membrane stress contribution since his model is assumed with clamped boundary conditions on the ends of pipe and nozzle, and his pipe-nozzle model is not closed. one can see that the stress factors for both models vary about 9 to 15% at the critical point A or B where the local stresses are mainly caused by the local circumferential stress. The affect to point C or D is from -1.5 to 52%. However, it is believed that the models used in this studies with simply supported boundary condition and closed ends should more closely simulated the real application in engineering.

From the 3D finite element models used in this study, the stresses away from the intersection area approach to PR/T in circumferential direction and approach to $PR/2T$ in logitudinal direction when the closed ends are simply supported. This indicate the real situation that the local stresses are no longer affect the stress field at the location away from the nozzle area.

Table 4.3: Comparison of local stress factors from different boundary conditions

Pressure stress factors	Data from this work	Ha's stress* factors	Pecentage different %
Longitudinal stress factor at A_U	328	386	15.8
Longitudinal stress factor at A_L	-256	-284	9.8
Circumferential stress factor at A_U	438	517	15.2
Circumferential stress factor at A_L	218	255	14.5
Longitudinal stress factor at C_U	-42.8	-90.4	52.6
Longitudinal stress factor at C_L	-34.3	-40.2	14.6
Circumferential stress factor at C_U	59.1	75.5	21.7
Circumferential stress factor at C_L	-70	-68.9	-1.5

*open ends with clamped boundary conditions.

In the Table 4.3, the models in both work have the same geomatric parameters with

$\beta = 0.5$, $\gamma = 50$, and the intersecting angle is $90°$ degree.

4.3 Normalization Studies

Normalization studies have verified the validity of using β(R_n/R_p) and γ (R_p/t_p) as the geometric parameters under internal pressure. Several cases of normalization studies have been made as discussed in the following:

1). Two models with the same geometric parameters, i.e. β, γ, but under different internal pressure has been studied. Parameters for these two models are listed in Table 4.4. The local stresses and stress factors from those models are listed in Table 4.5, which has shown that the normalized of pressure stress factor by a randomly selected applied internal pressure is valid.

Table 4.4: Geometric parameters and dimensions of models for normalization study one

Parameters	Model #1	Model #2
p	100 psi	125 psi
α_p	10	10
α_n	5	5
β	0.4	0.4
γ	50	50
L_p	100 in	100 in
R_p	10 in	10 in
t_p	0.2	0.2
L_n	20 in	20 in
R_n	4 in	4 in
t_n	0.08	0.08 in

29

Table 4.5: Local stress comparison of models for normalization study one

Model No.	Model #1		Mdel #2	
	Stress, psi	Stress* factors	stress, psi	Stress* factors
Longitudinal stress at A_U	45,508	455.08	56,885	455.08
Longitudinal stress at A_L	-29,256	-292.56	-36,570	-292.56
Circumferential stress at A_U	50,157	501.57	62,696	501.57
Circumferential stress at A_L	28,307	283.07	35,384	283.07
Longitudinal stress at B_U	53,248	532.48	66,560	532.48
Longitudinal stress at B_L	-41,009	-410.09	-51,261	-410.09
Circumferential stress at B_U	79,241	792.41	99,051	792.41
Circumferential stress at B_L	42,800	428.00	53,500	428.00
Longitudinal stress at C_U	-3,393	-33.93	-4,242	-33.93
Longitudinal stress at C_L	-12,746	-127.46	-15,933	-127.46
Circumferential stress at C_U	6,279	62.79	7,848	62.79
Circumferential stress at C_L	-9,452	-94.52	-11,815	-94.52

* Stress factor is local stress normalized by the applied internal pressure for each case.

2). Table 4.7 shows that the local stresses from two models of different size but with the same geometric parameters, such as β, γ, α_p and α_n and under the same internal pressure. This verifies the validity of using β, γ, α_p and α_n as geometric parameters for this study. The parameters and dimensions for two test models are listed in Table 4.6

Table 4.6: Geometric parameters and dimensions of models for normalization study two

Parameters	Model #1	Model #2
p	100 psi	100 psi
α_p	10	10
α_n	5	5
β	0.4	0.4
γ	50	50
L_p	100 in	200 in
R_p	10 in	20 in
t_p	0.2	0.4
L_n	20 in	40 in
R_n	4 in	8 in
t_n	0.08	0.16 in

Table 4.7: Local stress comparison of models for normalization study two

Model No.	Model #1, psi	Mdel #2, psi
Longitudinal stress at A_U	45,508	45,508
Longitudinal stress at A_L	-29,256	-29,256
Circumferential stress at A_U	50,157	50,157
Circumferential stress at A_L	28,307	28,307
Longitudinal stress at B_U	53,248	53,248
Longitudinal stress at B_L	-41,009	-41,009
Circumferential stress at B_U	79,241	79,241
Circumferential stress at B_L	42,800	42,800
Longitudinal stress at C_U	-3,393	-3,393
Longitudinal stress at C_L	-12,746	-12,746
Circumferential stress at C_U	6,279	6,279
Circumferential stress at C_L	-9,452	-9,452

CHAPTER 5

STUDY ON THE EFFECT OF PIPE - NOZZLE
INTERSECTING ANGLES

This thesis has studied the local stresses around the pipe-nozzle junction, due to an internal

pressure when the angle of intersection varies from 90° to 30° by using a typical model with

β value of 0.5 and γ value of 50 under internal pressure, p, of 100 psi. When the angle of

intersection is at 90°, it is a typical pipe-nozzle, which many literature exist both in theoretical

and numerical approaches [1], [10], [11], [20], [25], [26], etc. However, few results exist in

literature for a pipe with lateral connection. Among all the lateral nozzle (tee), the 45° of

intersection is the most popular one in industrial applications. Local stress studies for these

lateral nozzle are very rare or non-existent due to the difficulties in mathematical modelling

of the actual geometries.

This study selects the angle of intersection varying from 90°, 75°, 60°, 45°, 38°, 34°

to 30°. Local stresses under this study are both the circumferential and longitudinal stress on

both the outside and inside surfaces of the pipe-noozle juncture. Figure 2 shows these stress

points, A_U, A_L, B_U, B_L, etc around the pipe-nozzle juncture. The local stress factors are

defined by normalizing these resulting local stresses with the internal pressure. These local

stress factors are then plotted as function of the intersection angles as shown in Figure D1 to

through D12 in Appendix D.

From these figures, one notes that the 90° intersection exhibits the most favorable

local stresses. These stresses increase as the angle of intersection decreases from 90° and

33

become more severe when the angle of intersection is less than 45°. The inside crotch point has the worst stresses and the local stresses in circumferential direction are generally higher than that in the longitudinal direction. For an intersection angle other than 90°, the inside crotch point, point B, would have higher stress than the opposite side, point A. Points A and B would have the same local stresses if the intersection is orthogonal. The points C and D always yield symmetric local pressure stresses due to symmetry with the pipe axis. From the above, conclusions are drawn to justify why the 45° lateral is the most popular one as far as the local stresses are concerned.

Some analytical and experimental investigations of the stress distribution around non-radial holes in flat plates [27] [28], which may be considered as a pipe with very large radius, have shown that the maximum stresses occur in the vessel on the major axis of the elliptical opening close to the nozzle [29] [30], and are greater with nozzles of increased non-radiality, which is the same conclusion from the plots in Appendix D. According to the ASME Boiler and Pressure Vessel Code [31], the stress concentration factors for non-radial nozzle in spherical and cylindrical vessels can be approximately related to that for the same radial nozzle by following relation:

$$K_{nr} = K_r [1 + (\tan \theta)^{3/4}] \qquad (34)$$

where

K_{nr} = non-radial nozzle stress concentration factor

K_r = radial nozzle stress concentration factor

θ = angle the axis of the nozzle makes with the normal to the vessel wall

From equation (34), the stress concentration factor goes up sharply with the angle of non-radiality. As indicated, this equation is especially applicable at the acute internal lip and external crotch where it has been found that the maximum stress occurs and fatigue failure originates, which agrees with the results from the 3-D finite element models in this study. One can get the same conclusion from Figure 6 to Figure 9. The stress concentration factors increase with the intersection angle changing from 90° to smaller angles, and goes up sharply when the angle is less than 45°. The plots of pressure stress factors at point B close to the plots of the equation. The pressure stress factors at point A have less value than point B, and those at the point C have much less values than those at point A and B on both the outside and the inside surfaces of the pipe in both longitudinal and circumferential directions. Therefore, the crotch point B is the critical design point due to internal pressure.

In Figure 6 ~ 9, the left Y axis shows the local stress factors due to internal pressure, which is the ratio of local pressure stress to applied internal pressure; the right Y axis shows the stress concentration factors, which is the ratio of local pressure stress to membrane stress away from nozzle area in the same direction.
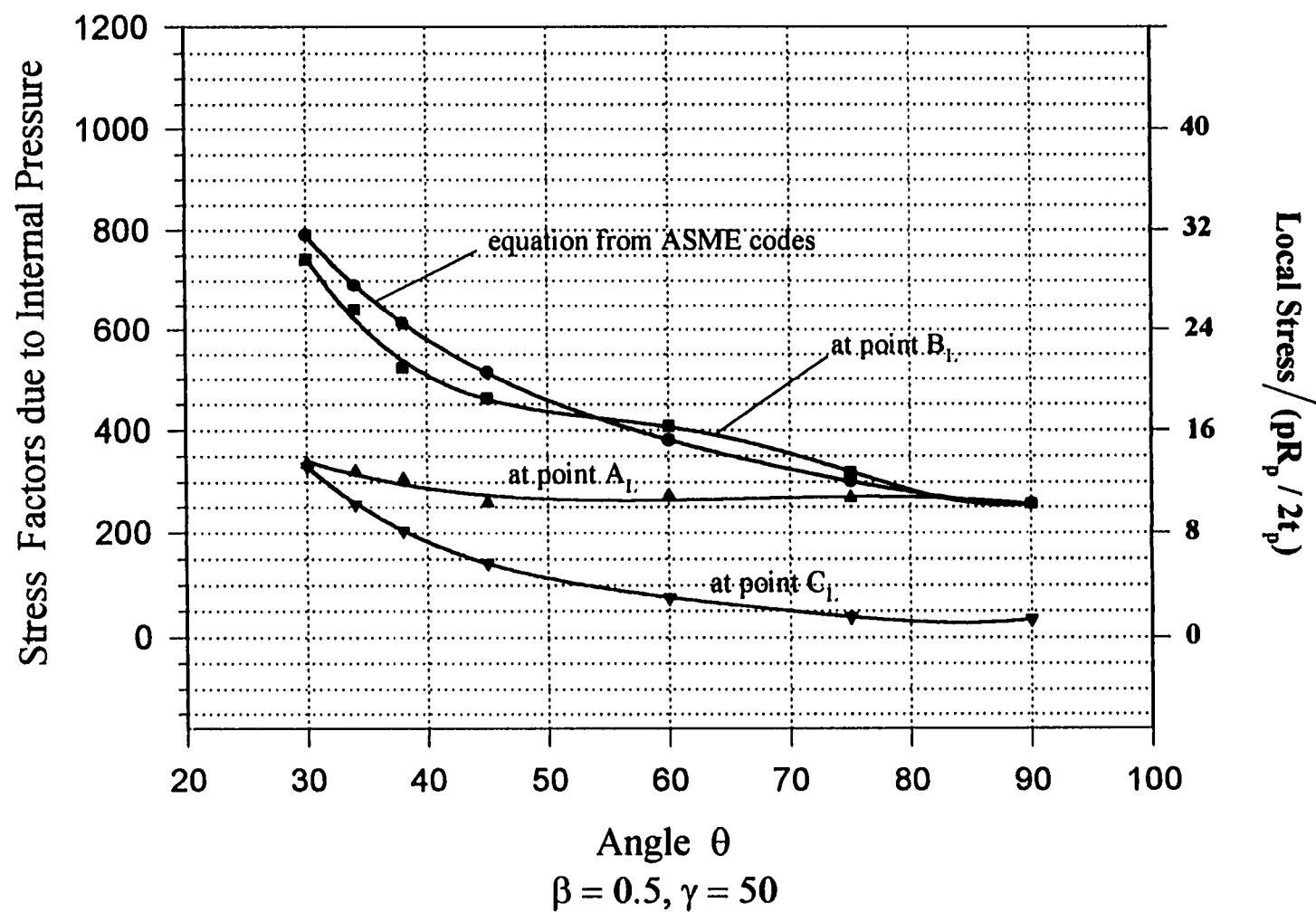
For longitudinal direction:

$$\text{Stress concentration factors} = \text{local stress} / (pR_p / 2t_p).$$
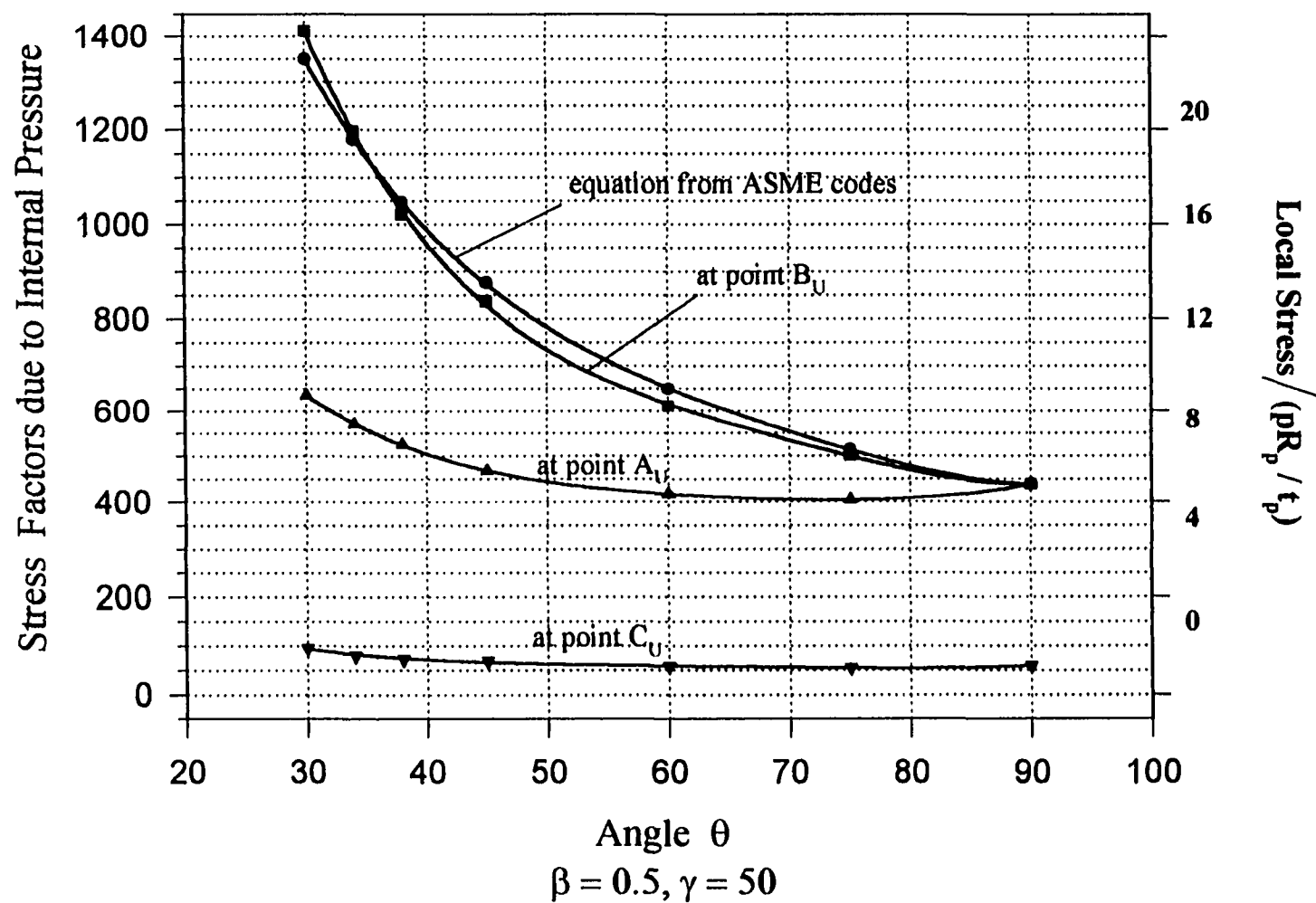
For circumferential direction:

$$\text{Stress concentration factors} = \text{local stress} / (pR_p / t_p).$$
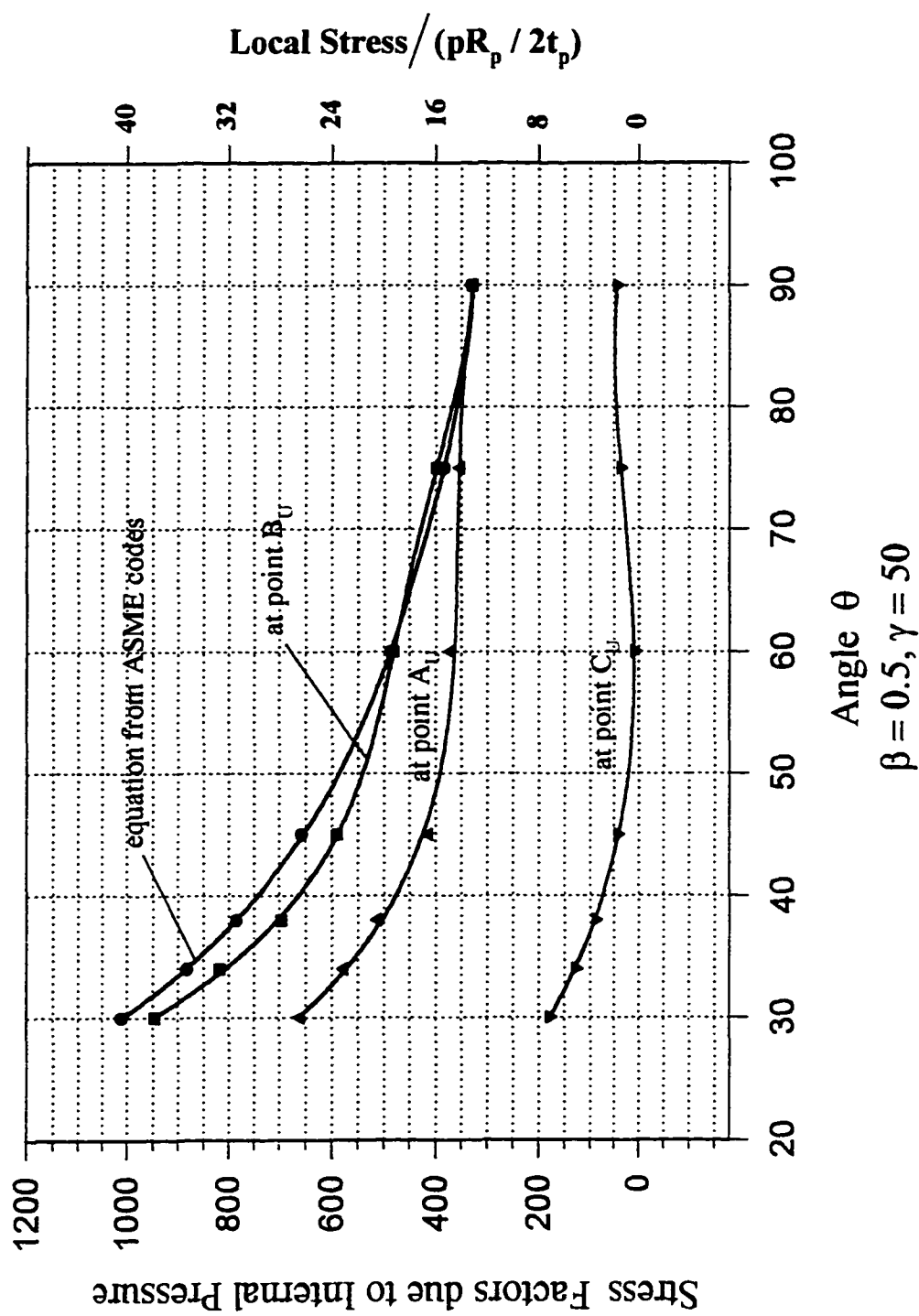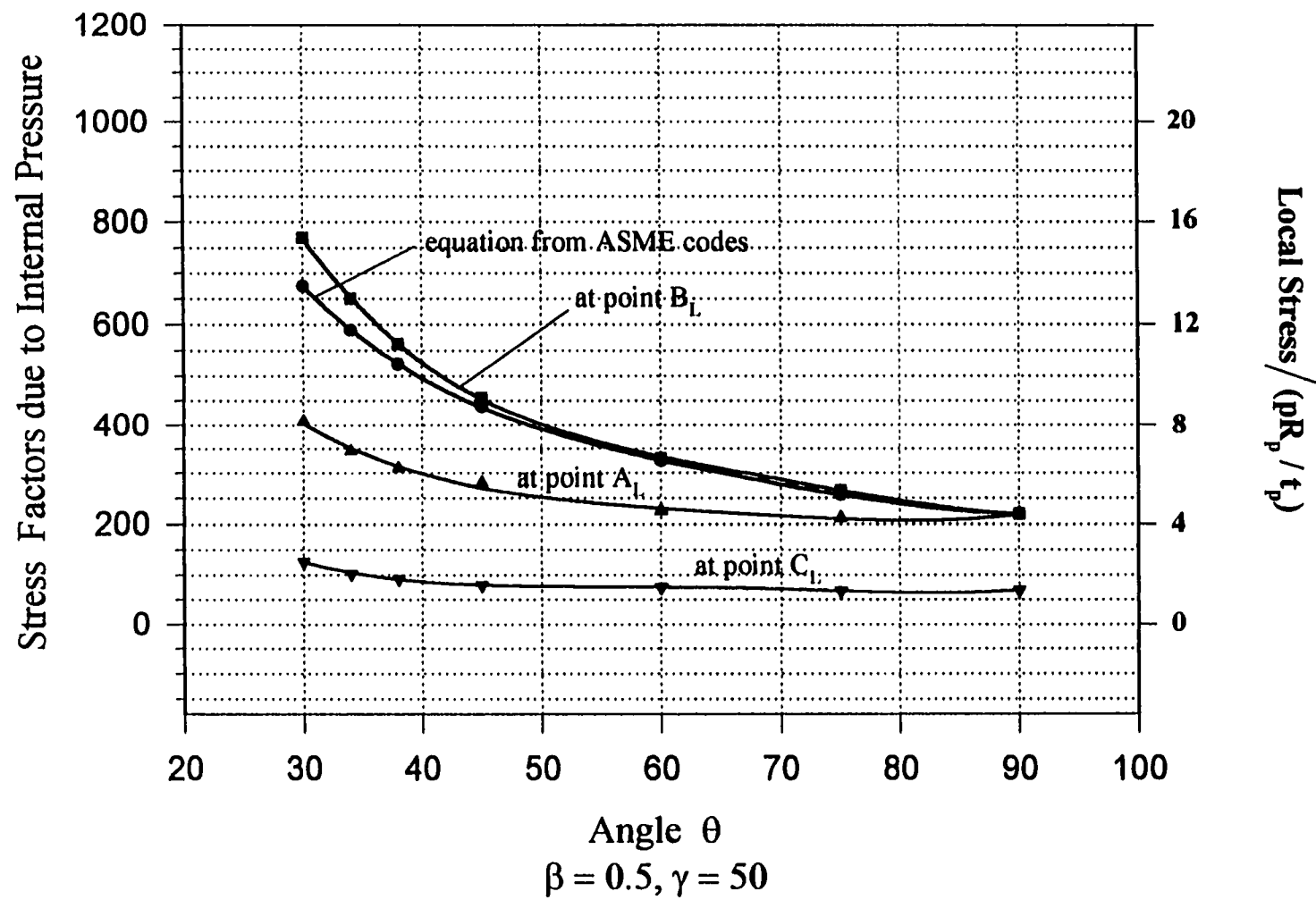
Figure 6: Comparison of longitudinal stress factors at outside surface of pipe with ASME code

$\beta = 0.5, \gamma = 50$

Figure 7: Comparison of longitudinal stress factors at inside surface of pipe with ASME code

Figure 8: Comparison of circumferential stress factors at outside surface of pipe with ASME code

$\beta = 0.5, \gamma = 50$

Figure 9: Comparison of circumferential stress factors at inside surface of pipe with ASME code

CHAPTER 6

THE LOCAL STRESSES
ON THE PIPE NEAR THE PIPE - NOZZLE JUNCTURE

To study the local stresses in the area near the nozzle, a typical model is employed with α_p = 10, α_n = 5, L_p = 200 in., nozzle radius, R_n = 10 in. , the pipe radius R_p = 20 in. and the pipe thickness is 0.4 in. which yield β = 0.5, γ = 50. The local stress factors are plotted as function of x which is the distance from the center of nozzle. Since the nozzle and pipe intersect with 45°, the distance from point A or B is $1.414R_n$ which is not equal to the radius of the nozzle. From the plots from Figure G1 to Figure G8 in Appendix G, the stress factors from point A or B decrease fast within a range of the half of the distance between the point A or B to the center of the nozzle. The local stresses approach to the membrane stress value when x approximetly reach to the twice of the distance from point A or B to the center of nozzle, which agrees wuth the theory of reinfored opennings for the design of reinforcement in the nozzle area as suggested by Harvey [23].

CHAPTER 7

NUMERICAL EXAMPLES

For the local pressure stresses around pipe-nozzle with $45°$ degree intersection, one can

obtain the data from twelve plots of stress factors in Appendix E.

Example: An 50.25 in. outside diameter, with 0.25 in. thickness, pipe is intersected

by a 35.125 in. nozzle with 0.175 in. thickness. The internal pressure is 100 psi. In this

example, the mean radius of the pipe, $R_p = 25$ in., the mean radius of nozzle is $R_n = 17.5$ in..

Assume any other nozzles, trunnion, or pipe bend is at least 250 in. away from this nozzle

Table 7.1: Geometric parameters and dimensions of the sample model

α_p = Pipe length / Pipe mean radius	10
α_n = nozzle length / nozzle mean radius	5
β = Nozzle radius / Pipe mean radius	0.7
γ = Pipe radius / Pipe thickness	100
L_p = Pipe length	> 250 in
R_p = Pipe mean radius	25 in.
L_n = Nozzle length	>176 in.
R_n = nozzle mean radius	17.5 in.
t_p = Pipe thickness	0.25 in.
t_n = nozzle thickness	0.175 in.

41

and the nozzle has a minimum length of 176 in. The detail information is listed in Table 7.1.

The results are listed in Table 7.2.

Table 7.2: Local stresses from Appendix E for numerical example

Data point	Stress factor	Stress, psi	From figure
Longitudinal stress at A_U	867.72	86772	E1
Longitudinal stress at A_L	-640.25	-64025	E2
Circumferential stress at A_U	946.20	94620	E3
Circumferential stress at A_L	499.43	49943	E4
Longitudinal stress at B_U	1706.36	170636	E5
Longitudinal stress at B_L	-1363.34	-136334	E6
Circumferential stress at B_U	2473.91	247391*	E7
Circumferential stress at B_L	1418.72	141872	E8
Longitudinal stress at C_U	-138.20	-13820	E9
Longitudinal stress at C_L	-413.04	-41304	E10
Circumferential stress at C_U	179.62	17962	E11
Circumferential stress at C_L	-209.55	-20955	E12

* maximum local pressure stress

In this example, the circumferential membrane stress under internal pressure away from the pipe-nozzle area is

$$\sigma_c = \frac{pR}{T} = \frac{100 \times 50}{0.25} = 20000(psi)$$

which is 13.35 times less than the maximum local stress located at the inside crotch point B.

When the elastic modulus is different from 30×10^6 psi, new local pressure stress may be obtained by multiplying the ratio of new modulus to 30×10^6 psi to the factor.

Table 7.3 listed the comparison of data from 3D finite element model with approximate mathematic solution. Since the approximate mathematic solution have more than 20% off, the results from this method are for reference only.

Table 7.3: Comparison of data from 3D finite element model with approximate solution for numerical example with $\beta = 0.7$, $\gamma = 100$

Data point	Approximate math. solution	3D FEA Model	Difference
Longitudinal stress at B_U	184000	170636	8.3%
Longitudinal stress at B_L	-145800	-136334	7%
Circumferential stress at B_U	187200	247391	24.5%
Circumferential stress at B_L	98010	140872	29%

CHAPTER 8

CONCLUSIONS

8.1 Conclusions on Lateral Connections
with Various Intersecting Angles

From the studies of the effect of the intersection angle, the dimensionless stress factors (local stress/applied internal pressure) have been plotted as a function of angle θ for the stresses at all critical points. Results from Figure D1 to D12 of Appendix D show that:

1). When $\theta = 90°$, the local pressure stresses at points A and B are identical and the same for points C and D due to symmetry. The stress factors for this case exhibit the most favorable value when compared with other angle of intersection.

2). The local pressure stresses increase when the angle of intersection decrease from $90°$, and the increasing of stresses become more severe when the angle of intersection is smaller than $45°$ degree.

3). When the angle of intersection is less than $90°$, the maximum stress occurs at inside crotch point, B, the circumferential stresses on the outside surface are most critical.

8.2 Conclusions on 45° Lateral Connection

From the plots of stress factors for pipe-nozzle connection with 45° degree (Figure E1 to E12 of Appendix E), one conclude that:

1). The increase of the parameter, γ, (R_p/t_p) makes the local pressure stress higher. It is known from WRC Bulletin No. 107 [1] that when γ increases, the local bending stress

44

decreases while the membrane stress increases. One may conclude that the membrane component gives major contribution of the local pressure stresses when the shell is very thin.

2). The highest local pressure stress occurs at the inside crotch point, B, on the outside surface of the pipe in circumferential direction. The stresses increase when β increases. Therefore, the point B will be the critical stress point due to internal pressure.

3). At point A, the highest local stress appears to be around 0.4 of β, i. e., occuring when the nozzle diameter is about 40% of the pipe diameter

4) The local pressure stresses can be many times higher than the circumferential membrane stress. It is 4.5 to 39.6 times higher on outside surface at point B (see Figure G1 to G8 in Appendix G). Therefore, these results provide significant data base for pressure vessel design.

5). The stress at point C, on the transverse plane of the pipe-nozzle intersection, have less value than the points A and B, no matter it is in longitudinal or circumferential direction.

6). The circumferential stresses at points A and B are always in tension. In the longitudinal direction, these stresses are in tension on the outside surface and in compression on the inside surface.

7). At point C, the local stresses on the inside surface are under compression in both longitudinal and circumferential directions, while on the outside surface of the pipe, the stresses in the circumferential direction are always in tension, but the longitudinal stresses may change from tension to compression when γ and β increase, which is shown in Figure E9b in Appendix E.

8). The approximate mathematic solution is close to the data from finite element method in a range of β from 0.6 ~ 0.8 and γ larger than 100 with difference of 5% to 30%, which verified the validity of the data from 3D finite element models.

Since the finite element method is capable of simulating the real geometry of the pipe-nozzle configuration, and meanwhile the convergence of the results are closely monitored through node points, geometric parameters and boundary conditions, the results from the finite element method should be very useful and reliable.

APPENDIX A

FIGURES FOR NODE POINT STUDY

.

47
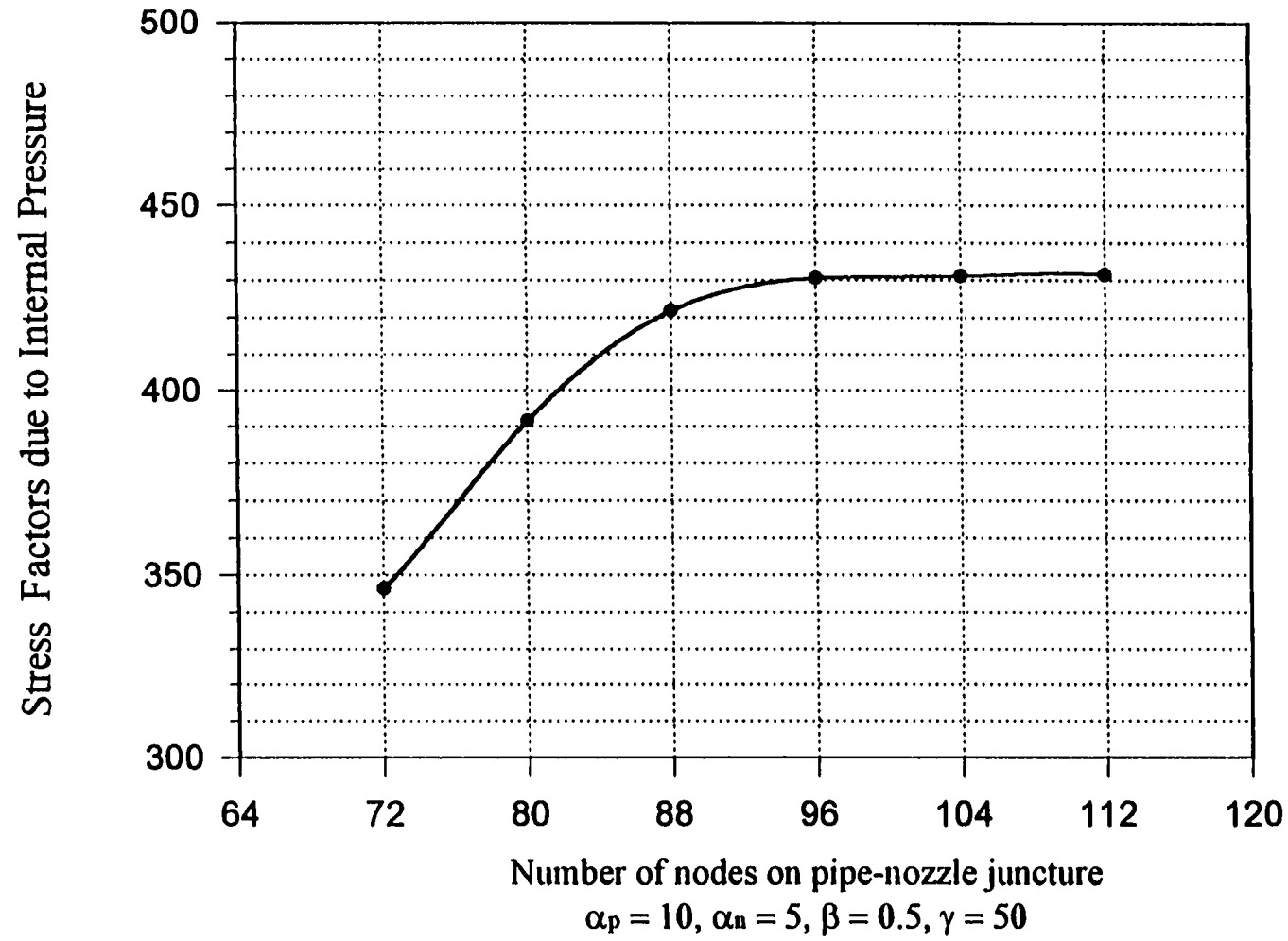
Figure A1: Study on node points at point A_U of pipe in longitudinal direction

$\alpha_p = 10$, $\alpha_n = 5$, $\beta = 0.5$, $\gamma = 50$
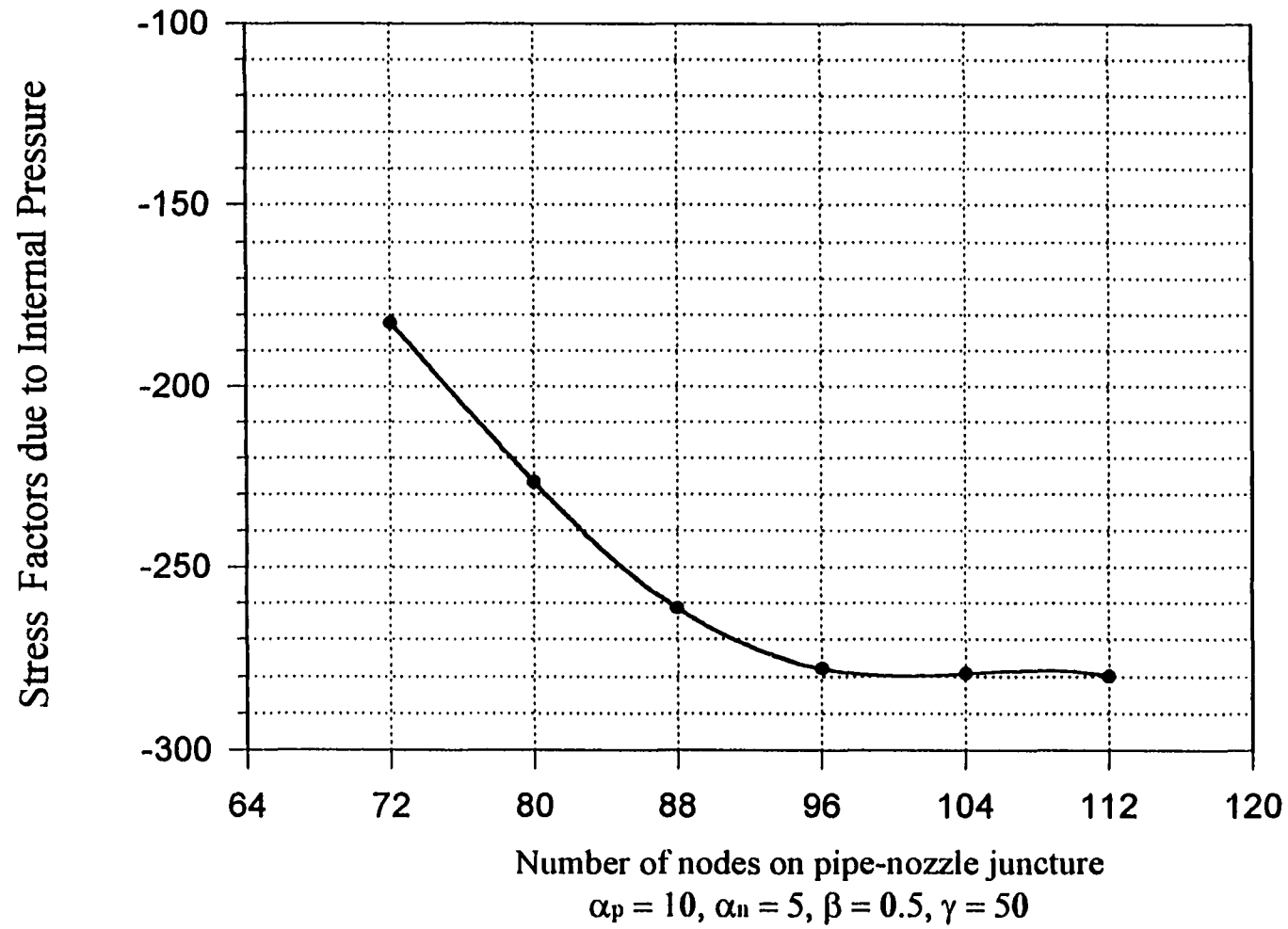
Figure A2: Study on node points at point A_L of pipe
in longitudinal direction

Number of nodes on pipe-nozzle juncture

$\alpha_p = 10, \ \alpha_n = 5, \ \beta = 0.5, \ \gamma = 50$
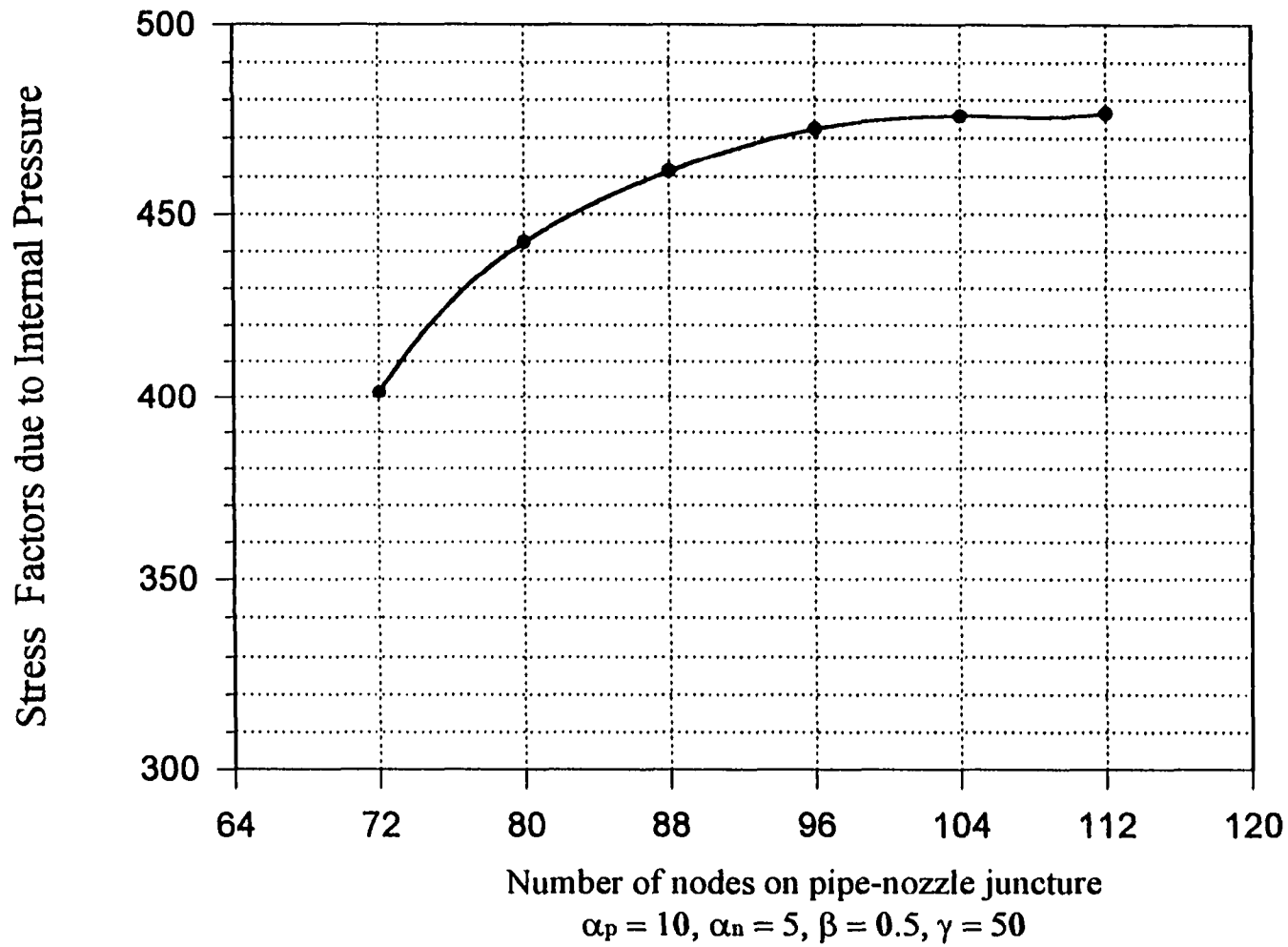
Figure A3: Study on node points at point A_U of pipe
in circumferential direction

$\alpha_p = 10$, $\alpha_n = 5$, $\beta = 0.5$, $\gamma = 50$
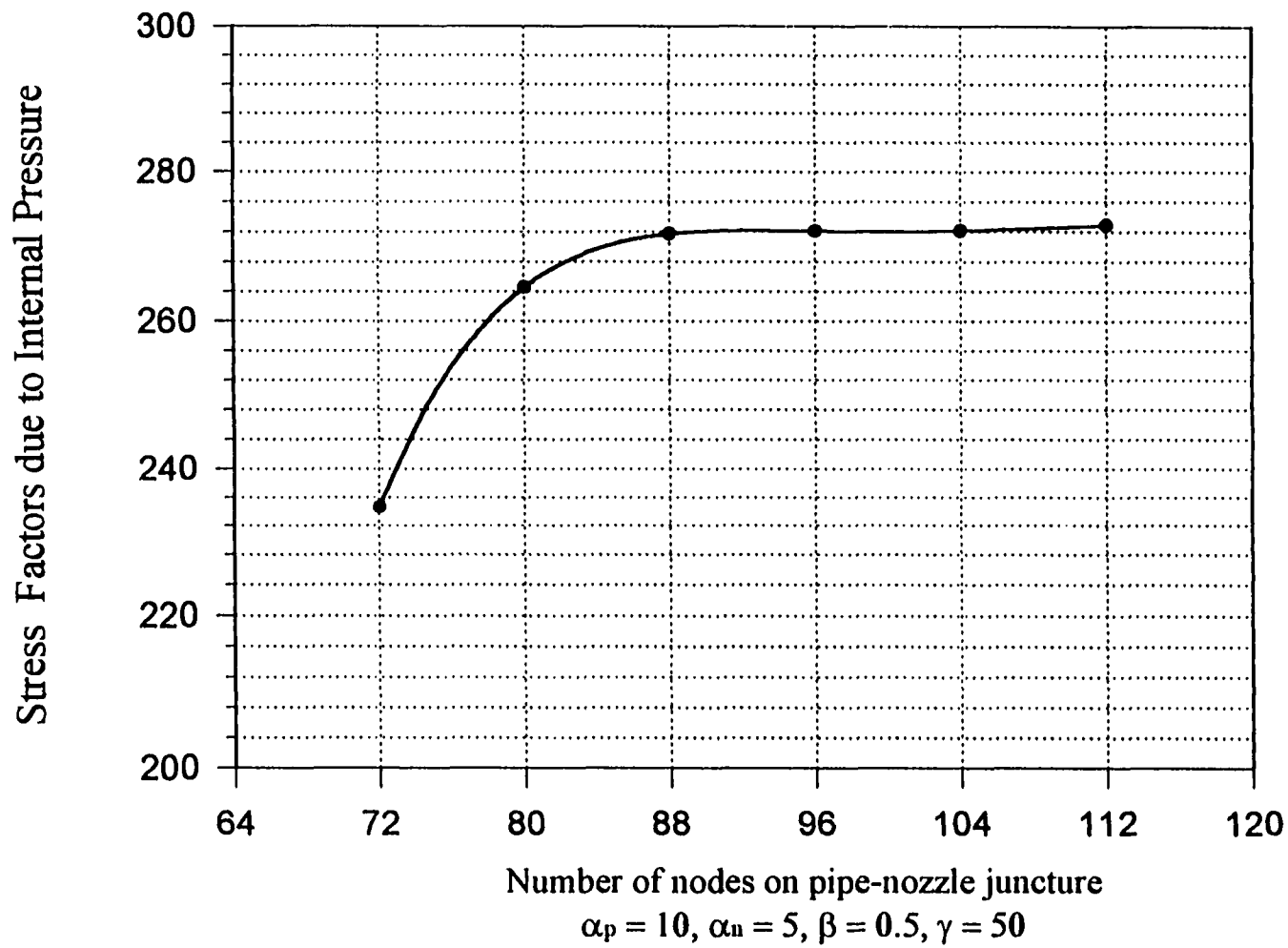
Figure A4: Study on node points at point A_L of pipe in circumferential direction

$\alpha_p = 10$, $\alpha_n = 5$, $\beta = 0.5$, $\gamma = 50$

Number of nodes on pipe-nozzle juncture
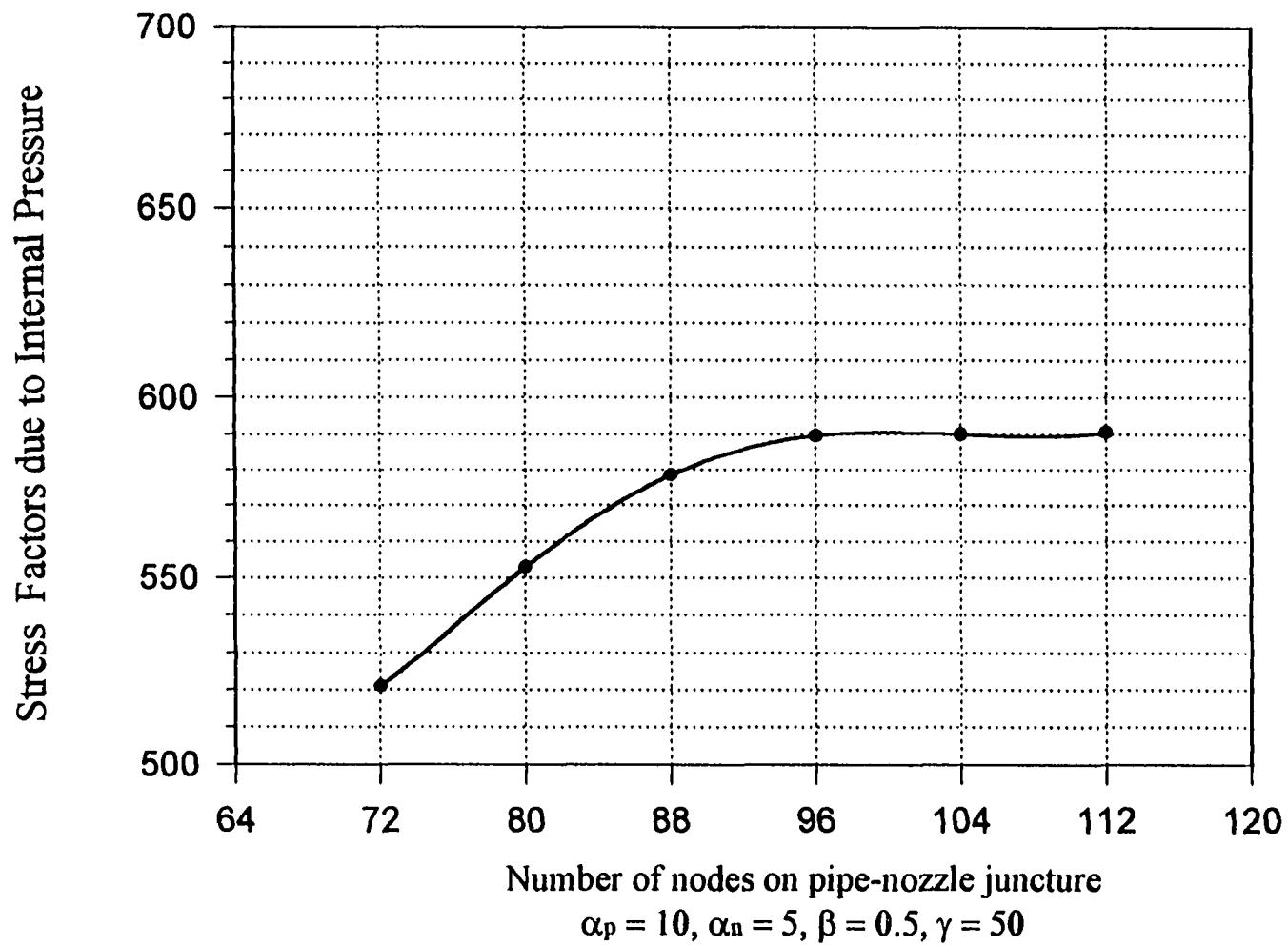
Figure A5: Study on node points at point B_U of pipe
in longitudinal direction

Number of nodes on pipe-nozzle juncture

$\alpha_p = 10$, $\alpha_n = 5$, $\beta = 0.5$, $\gamma = 50$
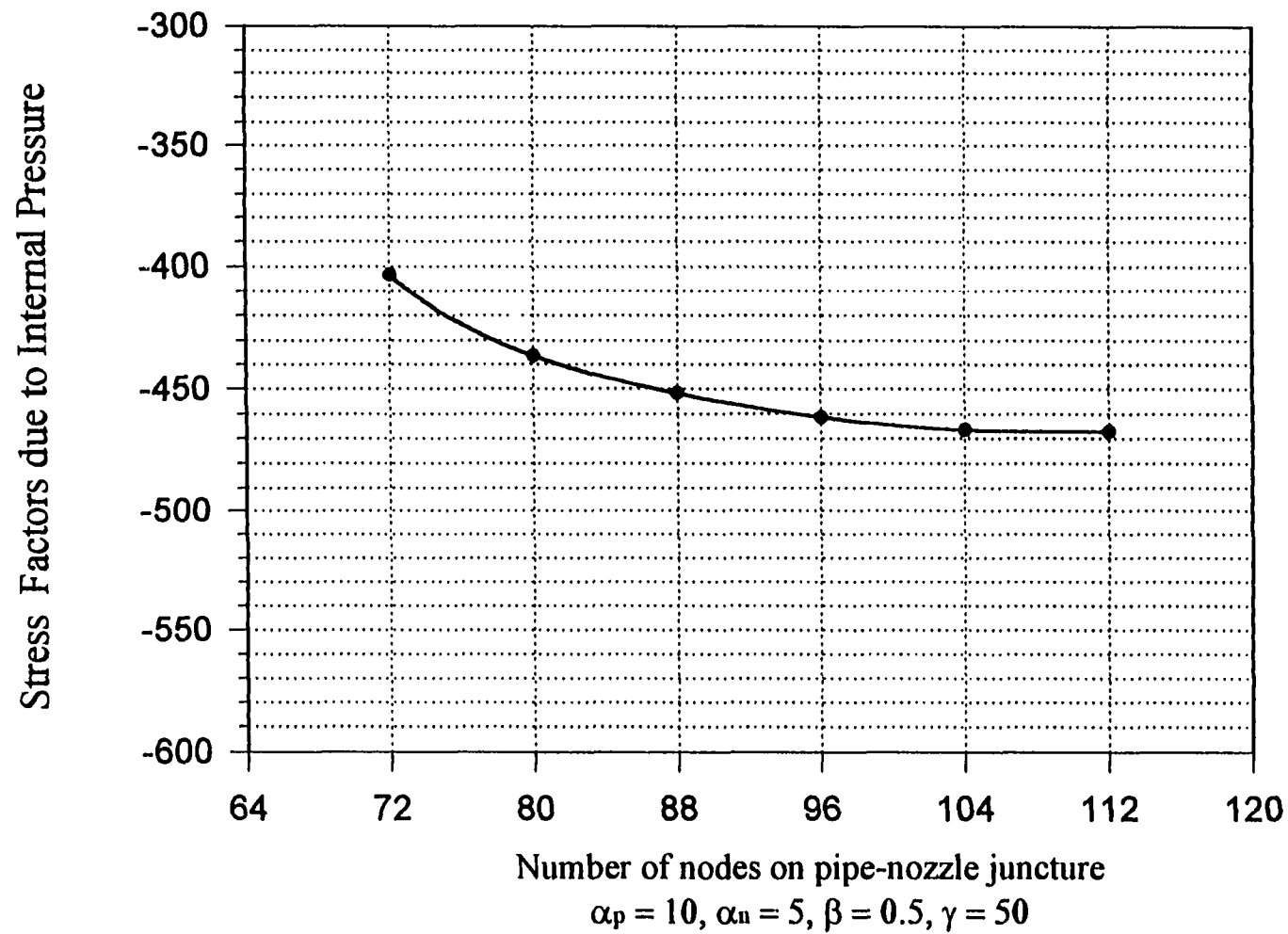
Figure A6: Study on node points at point B_L of pipe
in longitudinal direction

The axes are labelled "Stress Factors due to Internal Pressure" (vertical) and "Number of nodes on pipe-nozzle juncture" (horizontal), with parameters $\alpha_p = 10$, $\alpha_n = 5$, $\beta = 0.5$, $\gamma = 50$.
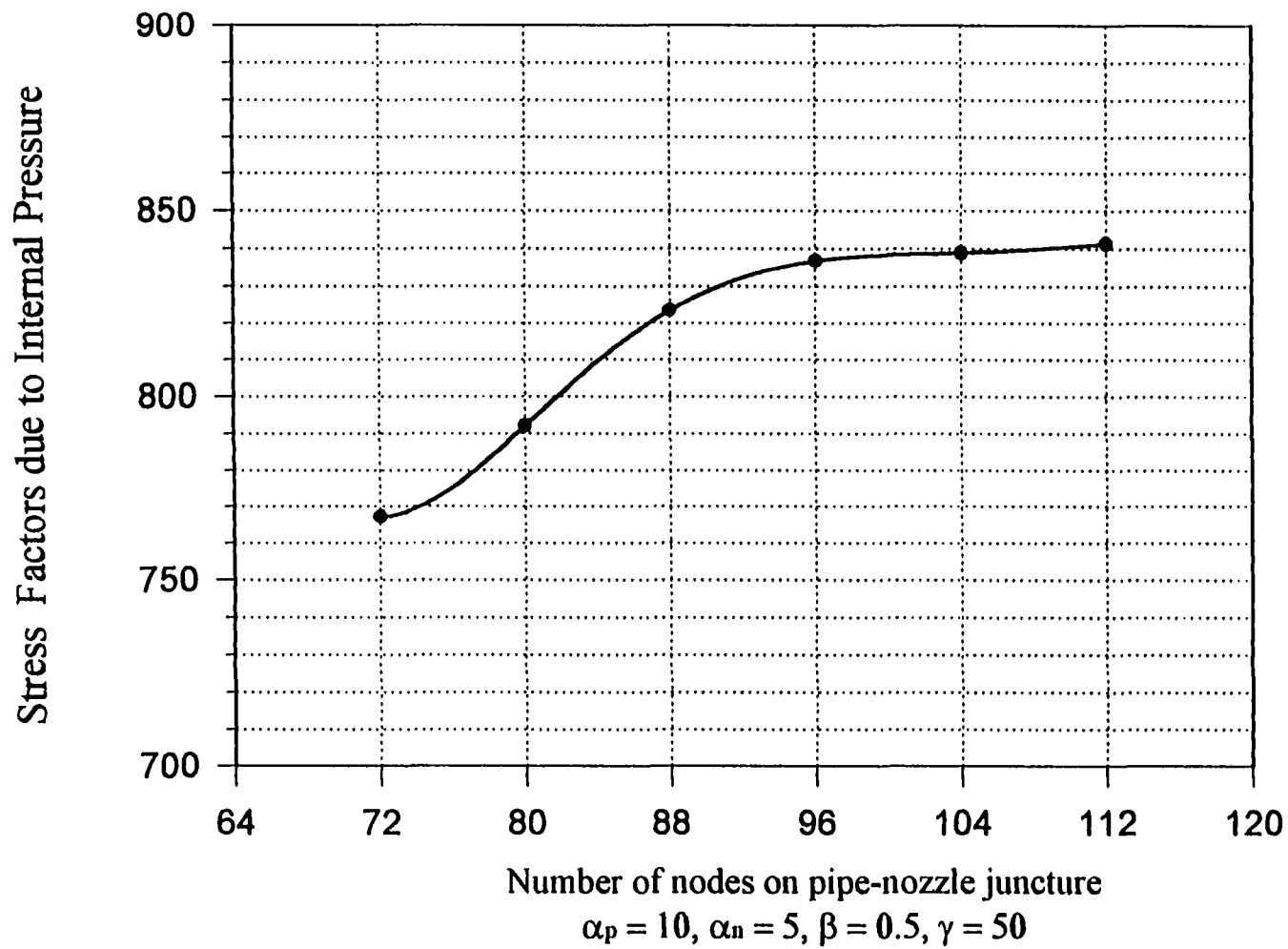
Figure A7: Study on node points at point B_U of pipe
in circumferential direction

Stress Factors due to Internal Pressure

Number of nodes on pipe-nozzle juncture
$\alpha_p = 10$, $\alpha_n = 5$, $\beta = 0.5$, $\gamma = 50$

Number of nodes on pipe-nozzle juncture

$\alpha_p = 10$, $\alpha_n = 5$, $\beta = 0.5$, $\gamma = 50$
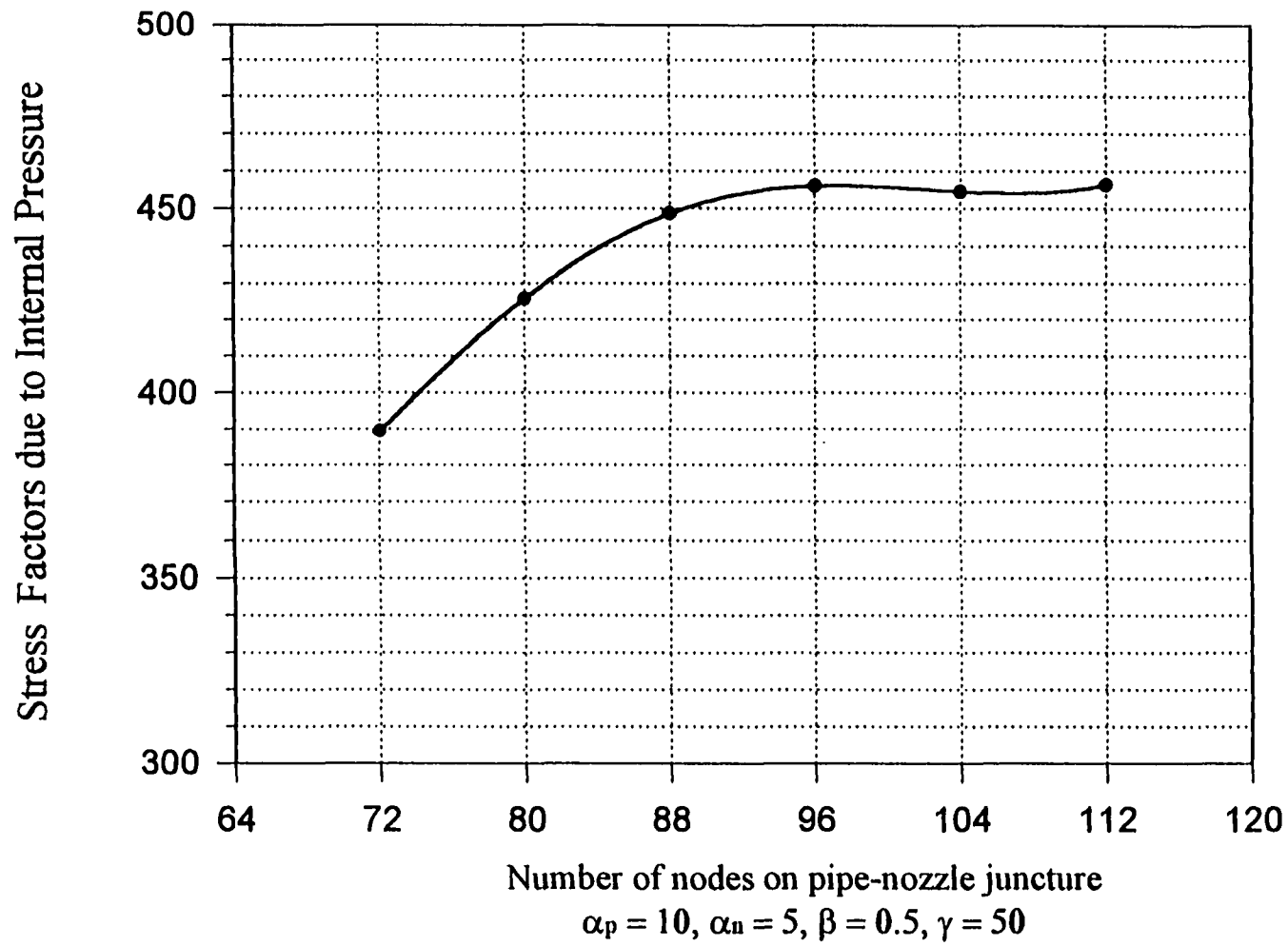
Figure A8: Study on node points at point B_1 of pipe
in circumferential direction

$\alpha_p = 10, \alpha_n = 5, \beta = 0.5, \gamma = 50$

Figure A9: Study on node points at point C_U of pipe
in longitudinal direction
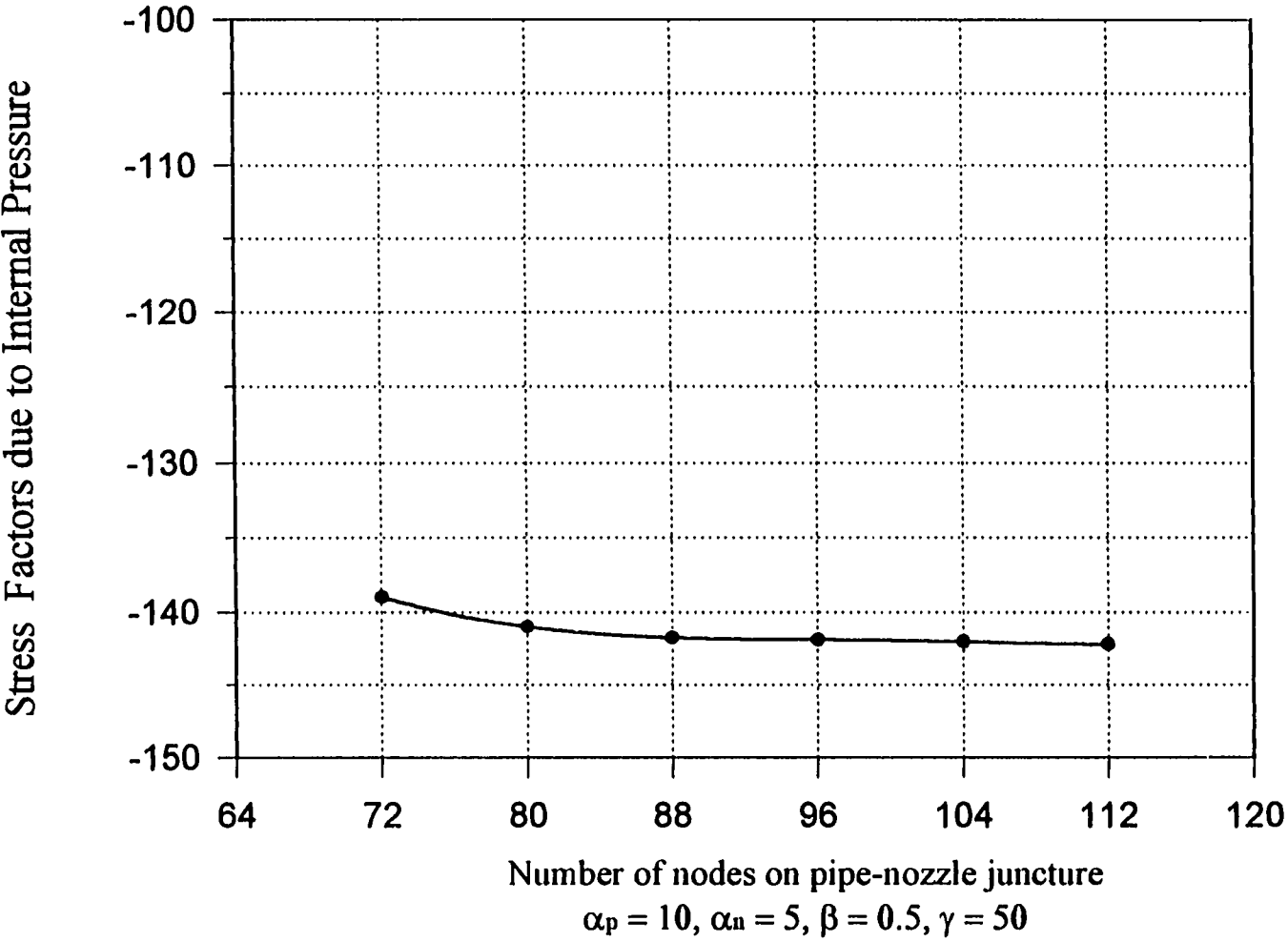
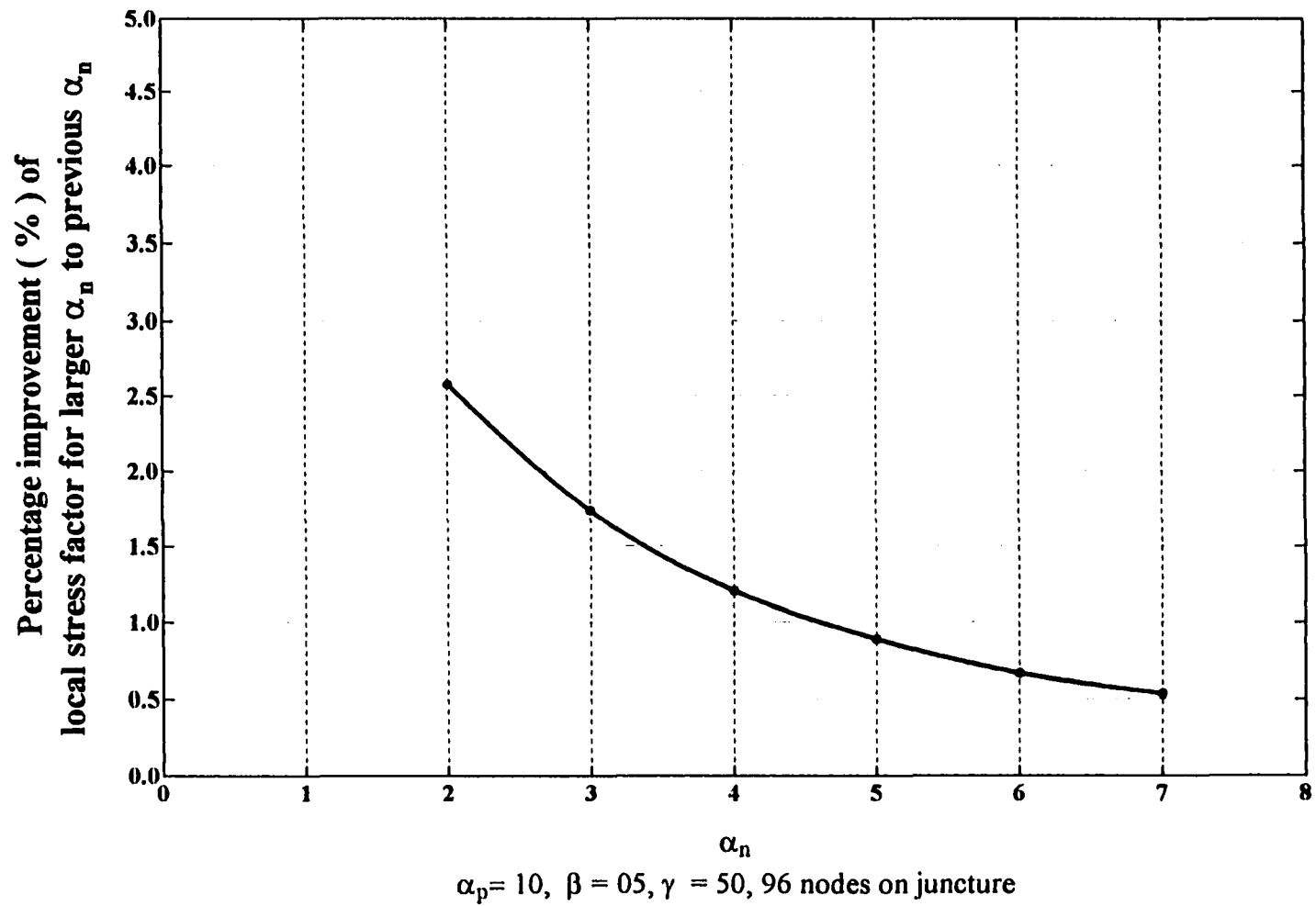**Figure A10:** Study on node points at point C_L of pipe in longitudinal direction

Number of nodes on pipe-nozzle juncture

$\alpha_p = 10$, $\alpha_n = 5$, $\beta = 0.5$, $\gamma = 50$
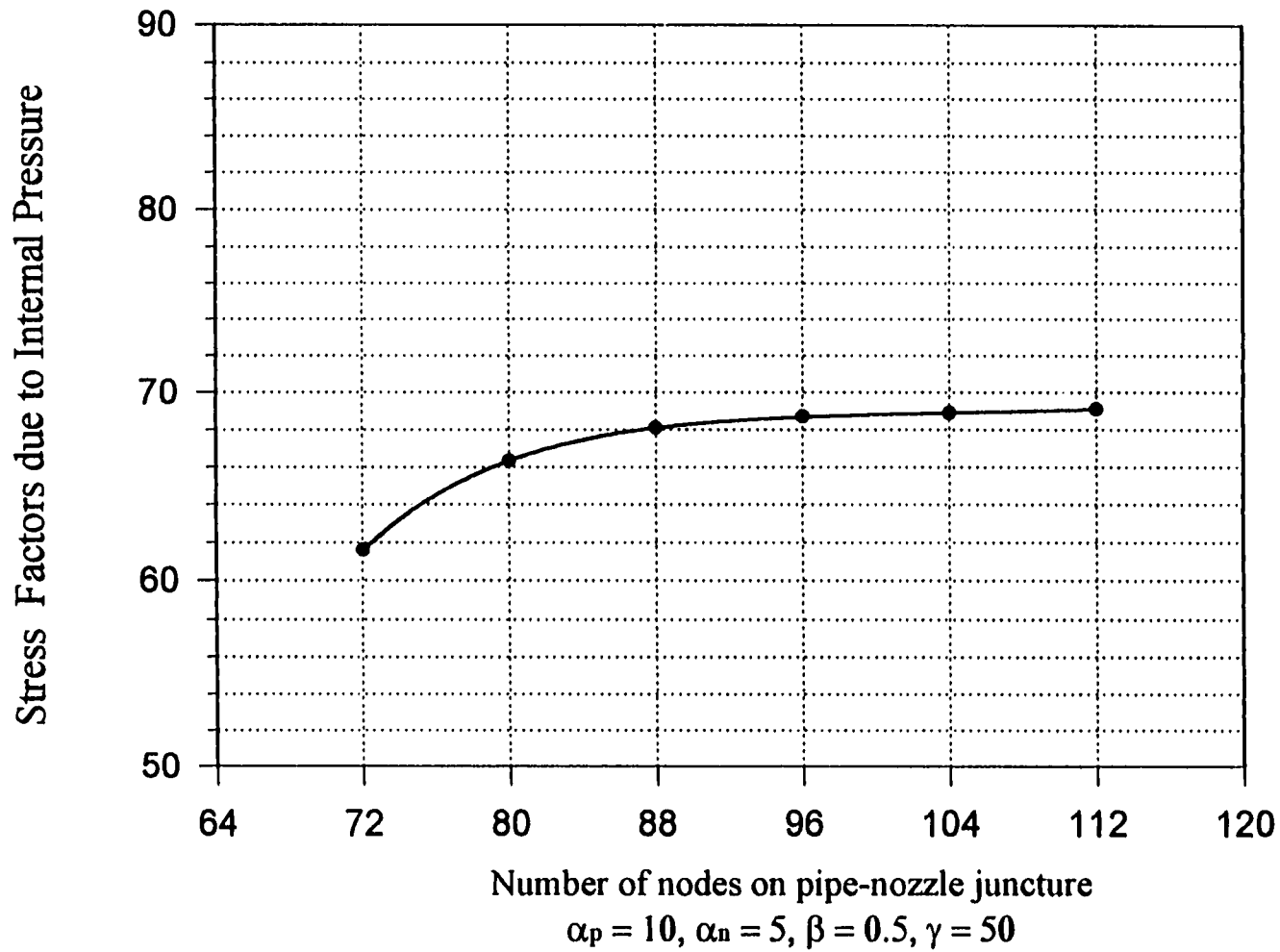
Figure A11: Study on node points at point C_U of pipe in circumferential direction

Number of nodes on pipe-nozzle juncture

$\alpha_p = 10$, $\alpha_n = 5$, $\beta = 0.5$, $\gamma = 50$
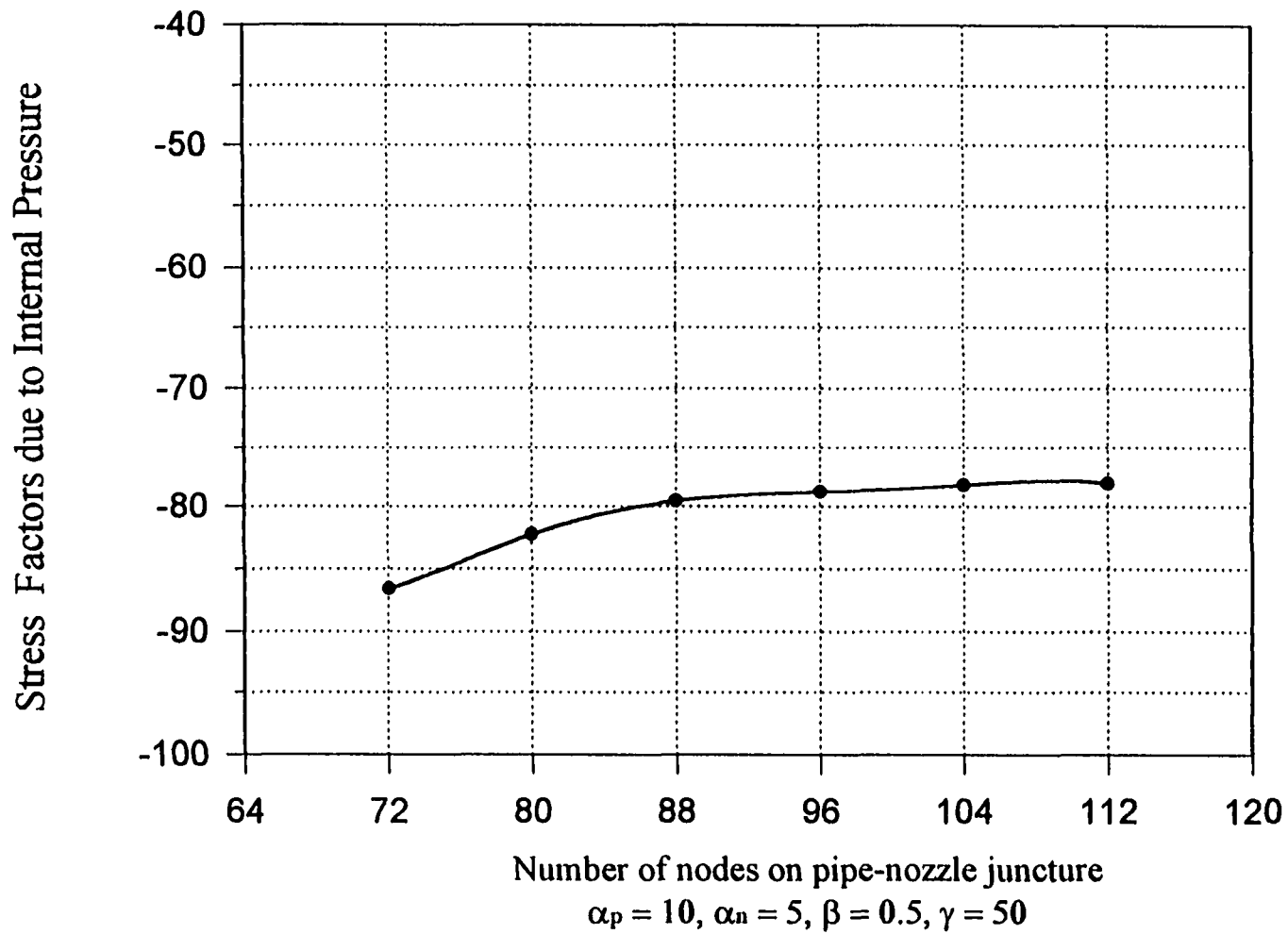
Figure A12: Study on node points at point C_L of pipe
in circumferential direction

$\alpha_p = 10$, $\alpha_n = 5$, $\beta = 0.5$, $\gamma = 50$

APPENDIX B

FIGURES FOR THE CONVERGENCE STUDY OF α_p

60

$\alpha_n = 5, \quad \beta = 05, \gamma = 50, 96$ nodes on juncture
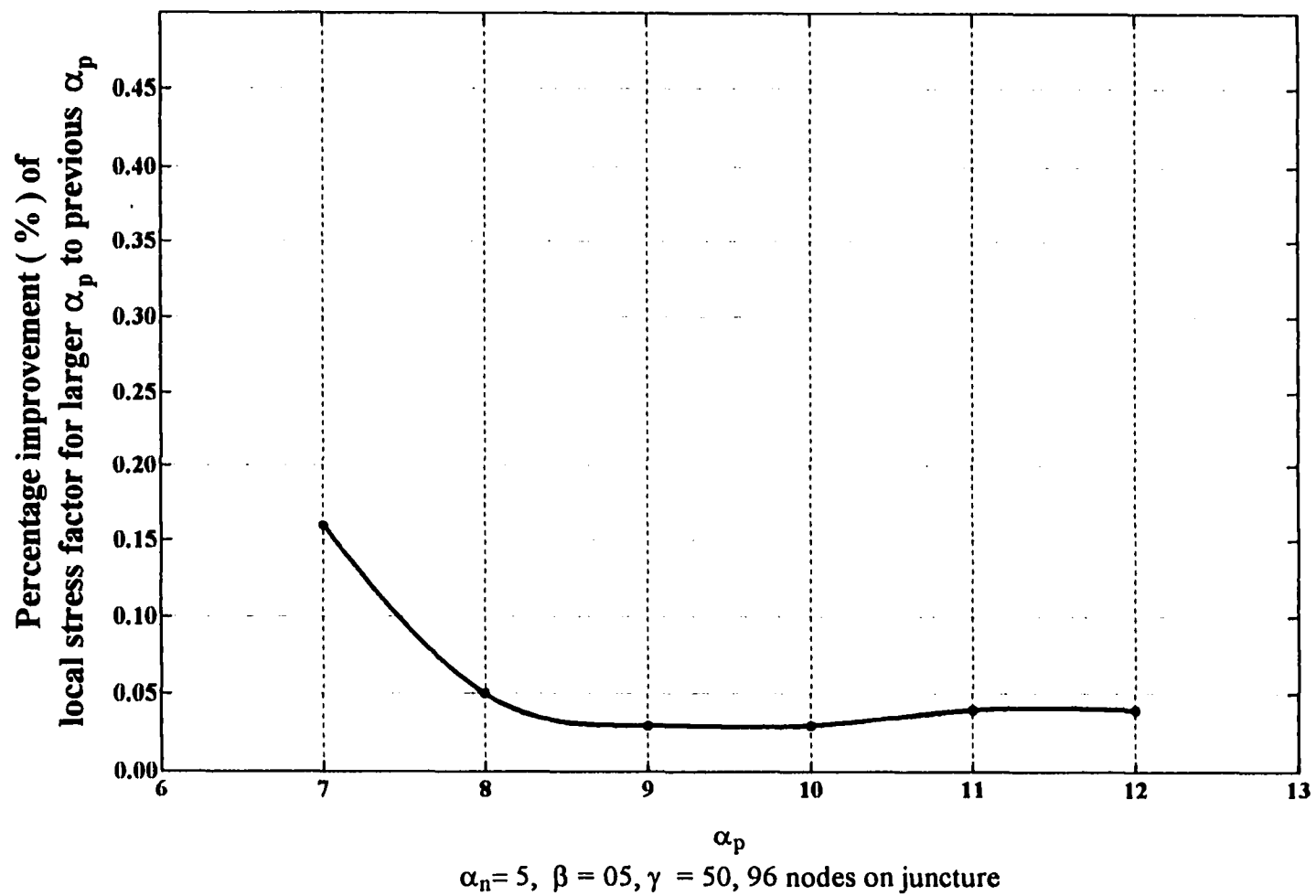
Figure B1: Asymptotic study on α_p at point A_U of pipe in longitudinal direction

$\alpha_n = 5$, $\beta = 05$, $\gamma = 50$, 96 nodes on juncture
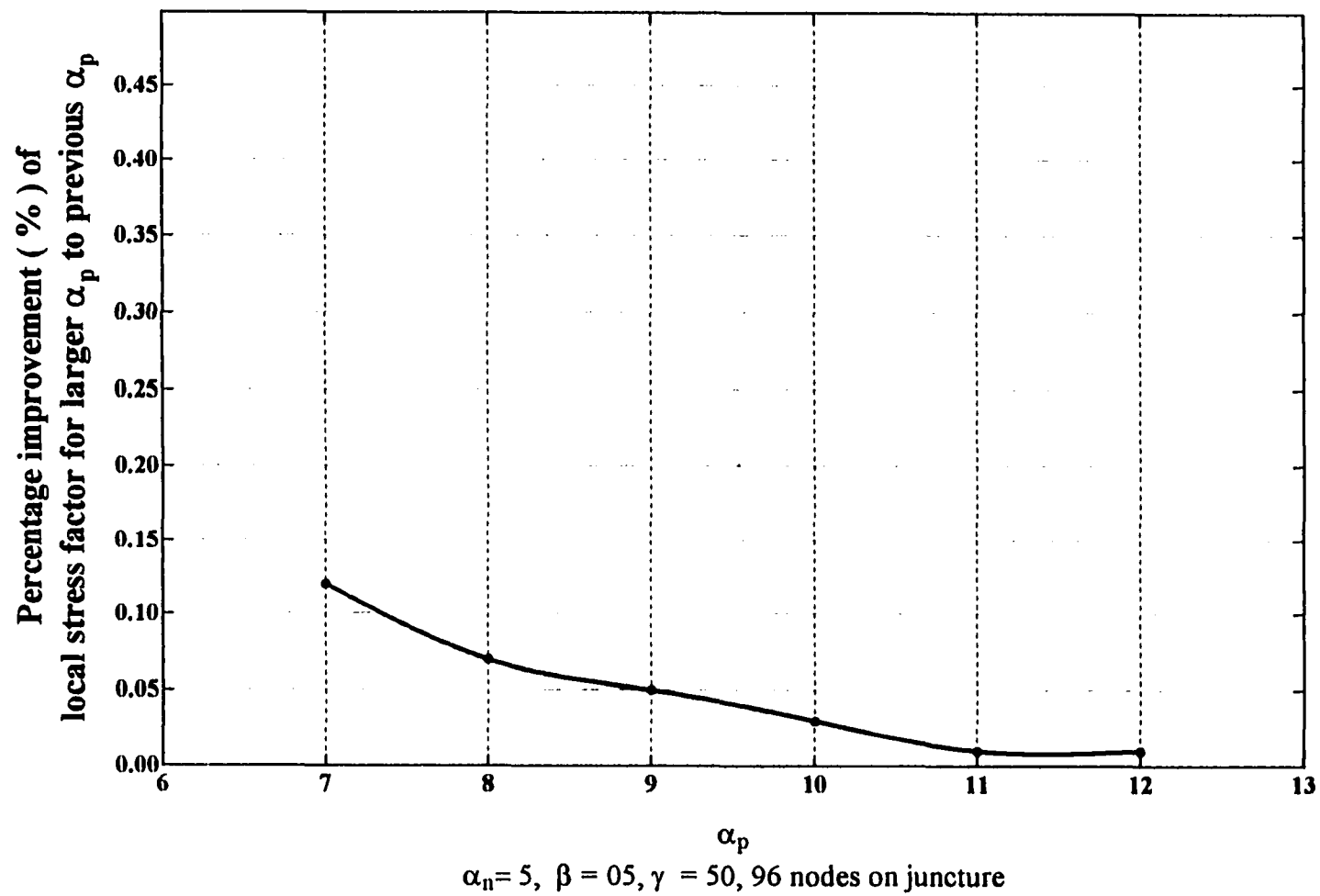
Figure B2: Asymptotic study on α_p at point A_L of pipe
in longitudinal direction

$$\alpha_n = 5, \quad \beta = 05, \gamma = 50, \text{ 96 nodes on juncture}$$
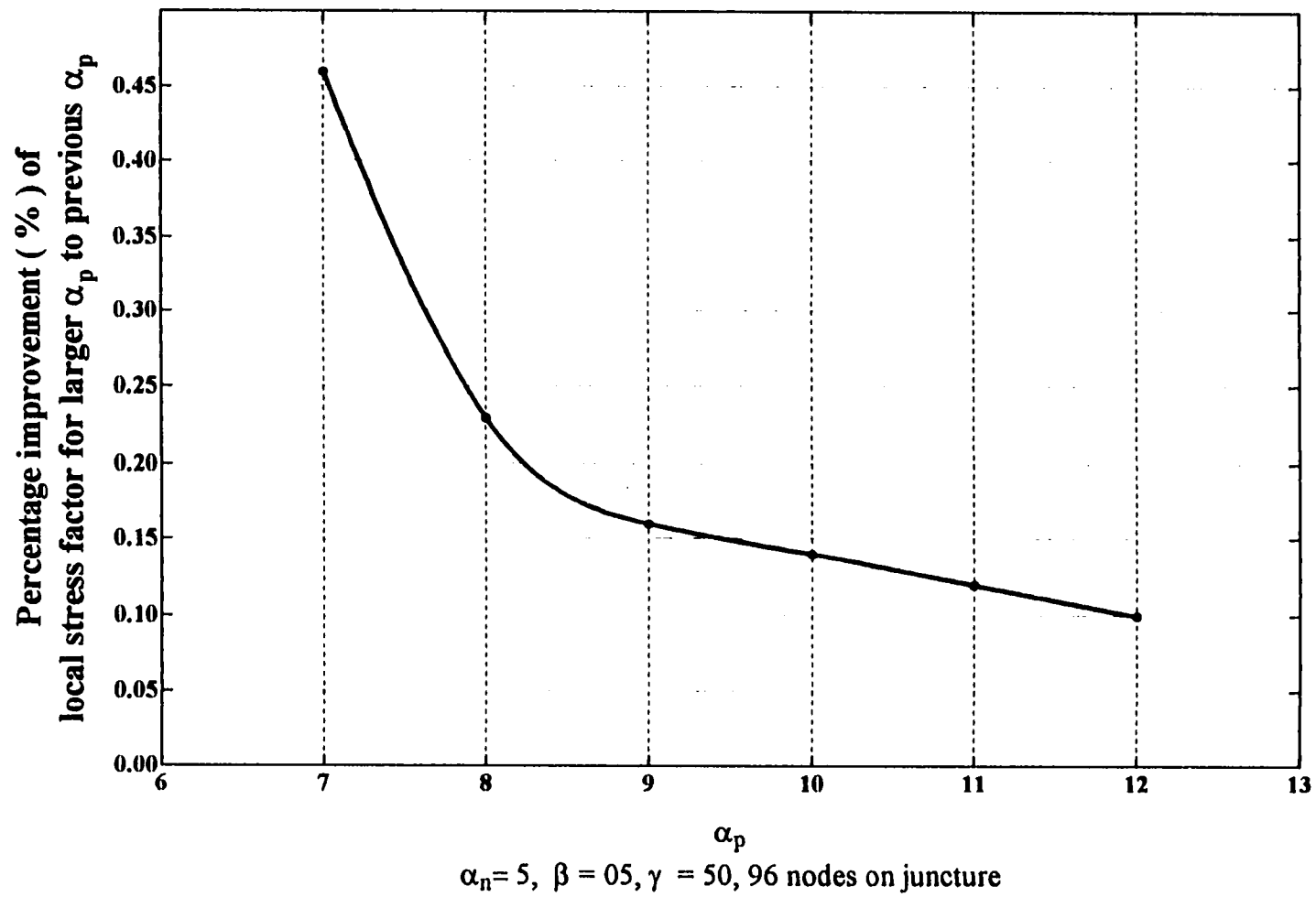
Figure B3: Asymptotic study on α_p at point A_U of pipe
in circumferential direction

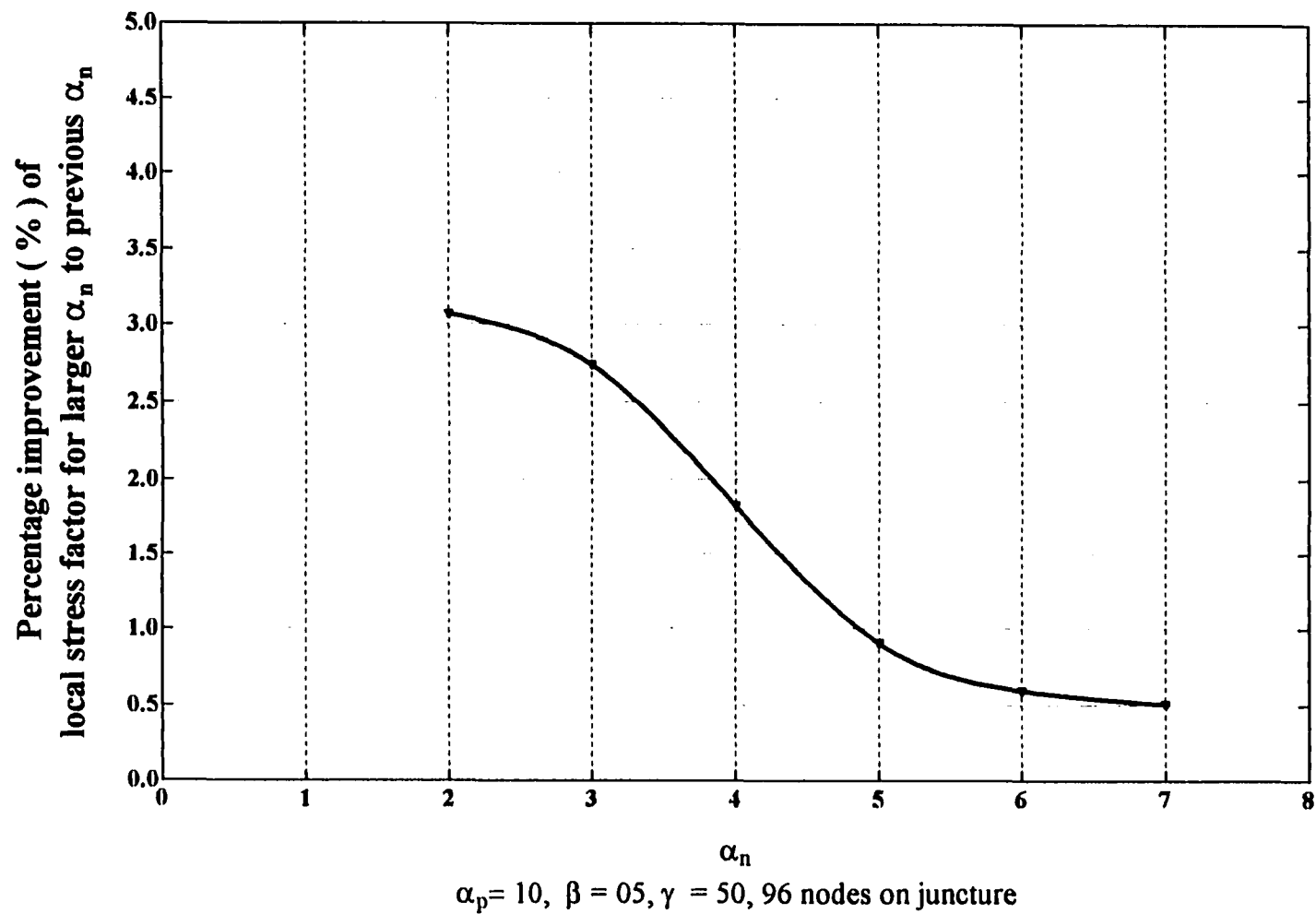$\alpha_n = 5, \quad \beta = 05, \gamma = 50, 96$ nodes on juncture
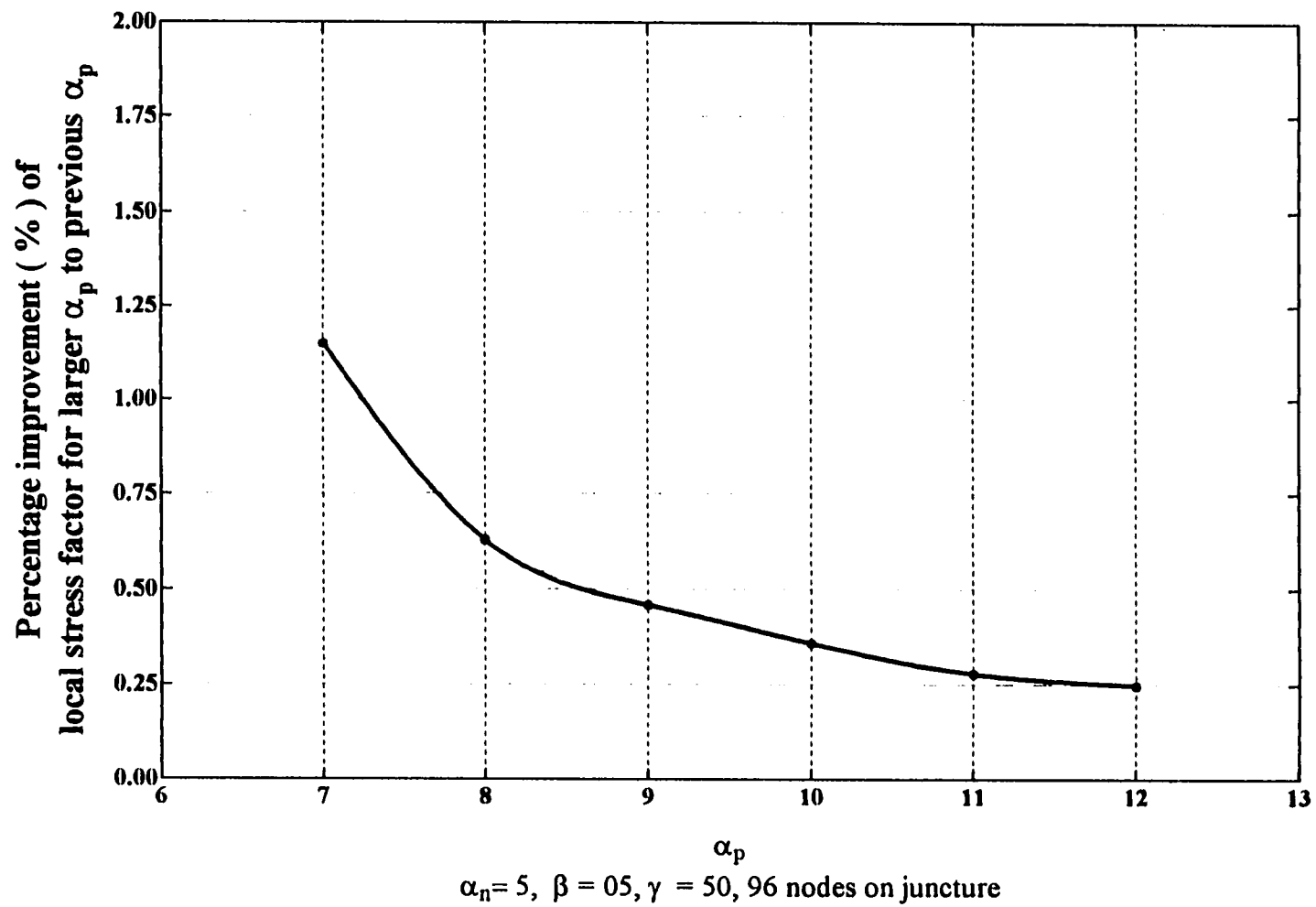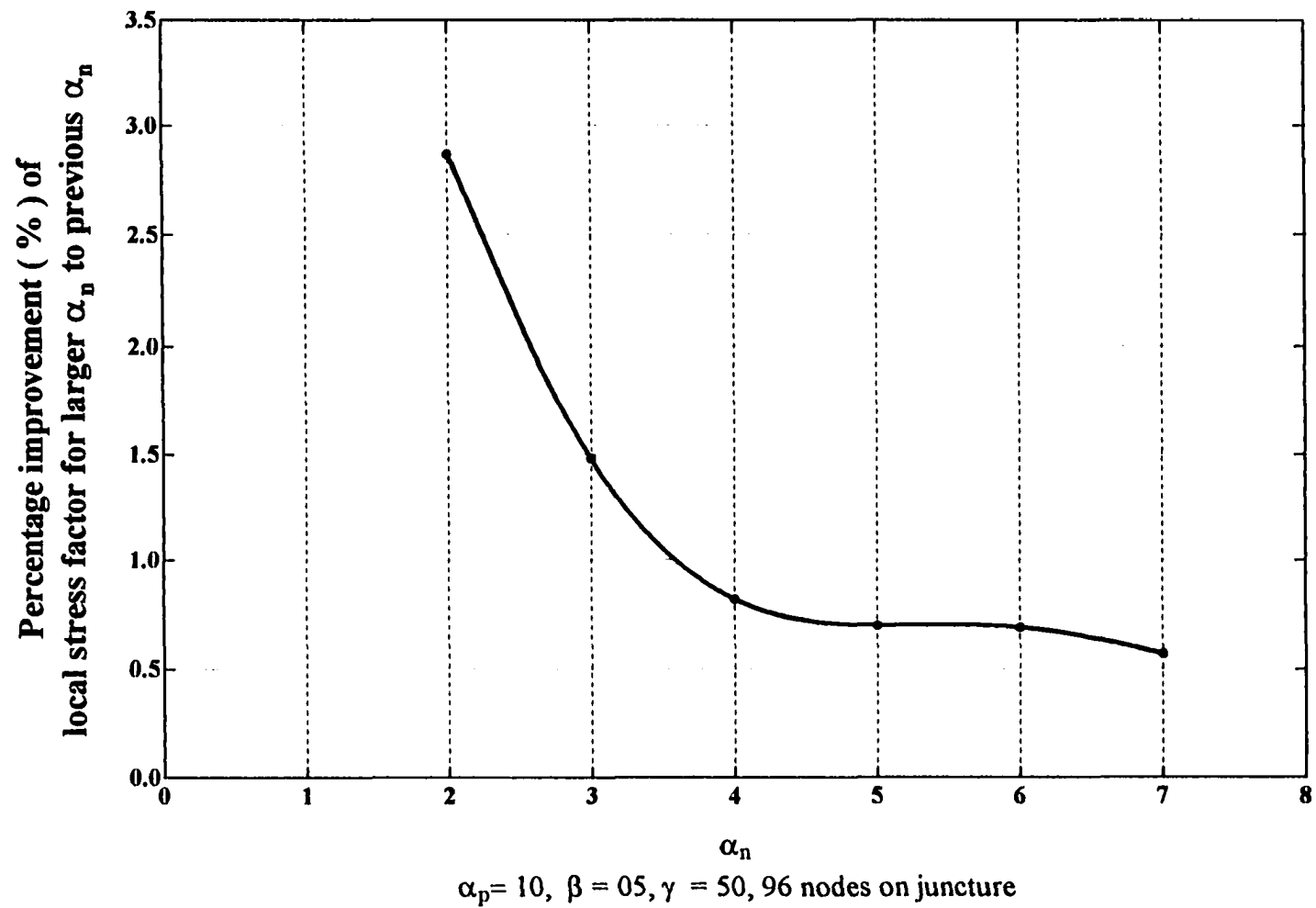
Figure B4: Asymptotic study on α_p at point A_L of pipe
in circumferential direction
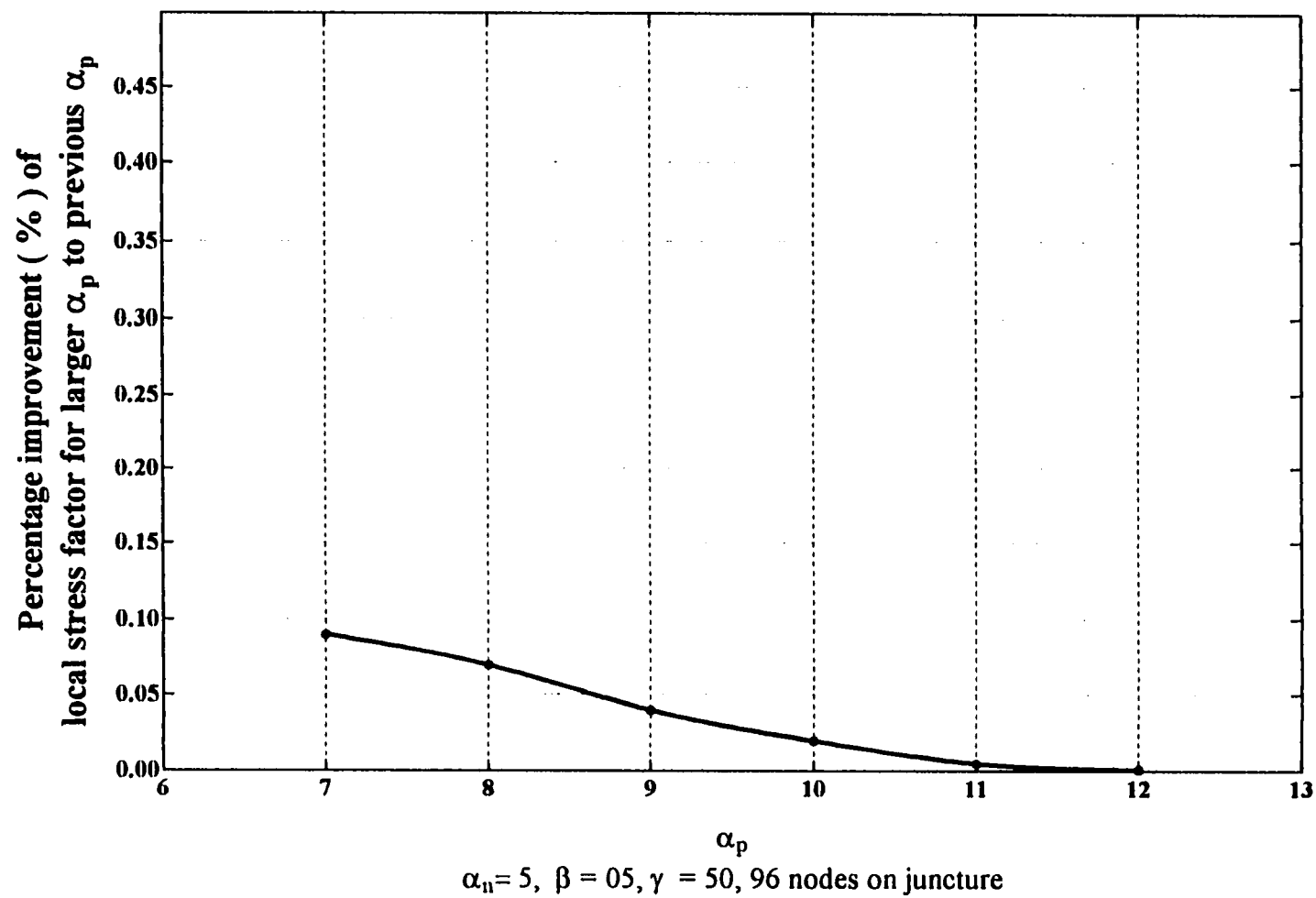
Figure B5: Asymptotic study on α_p at point B_U of pipe
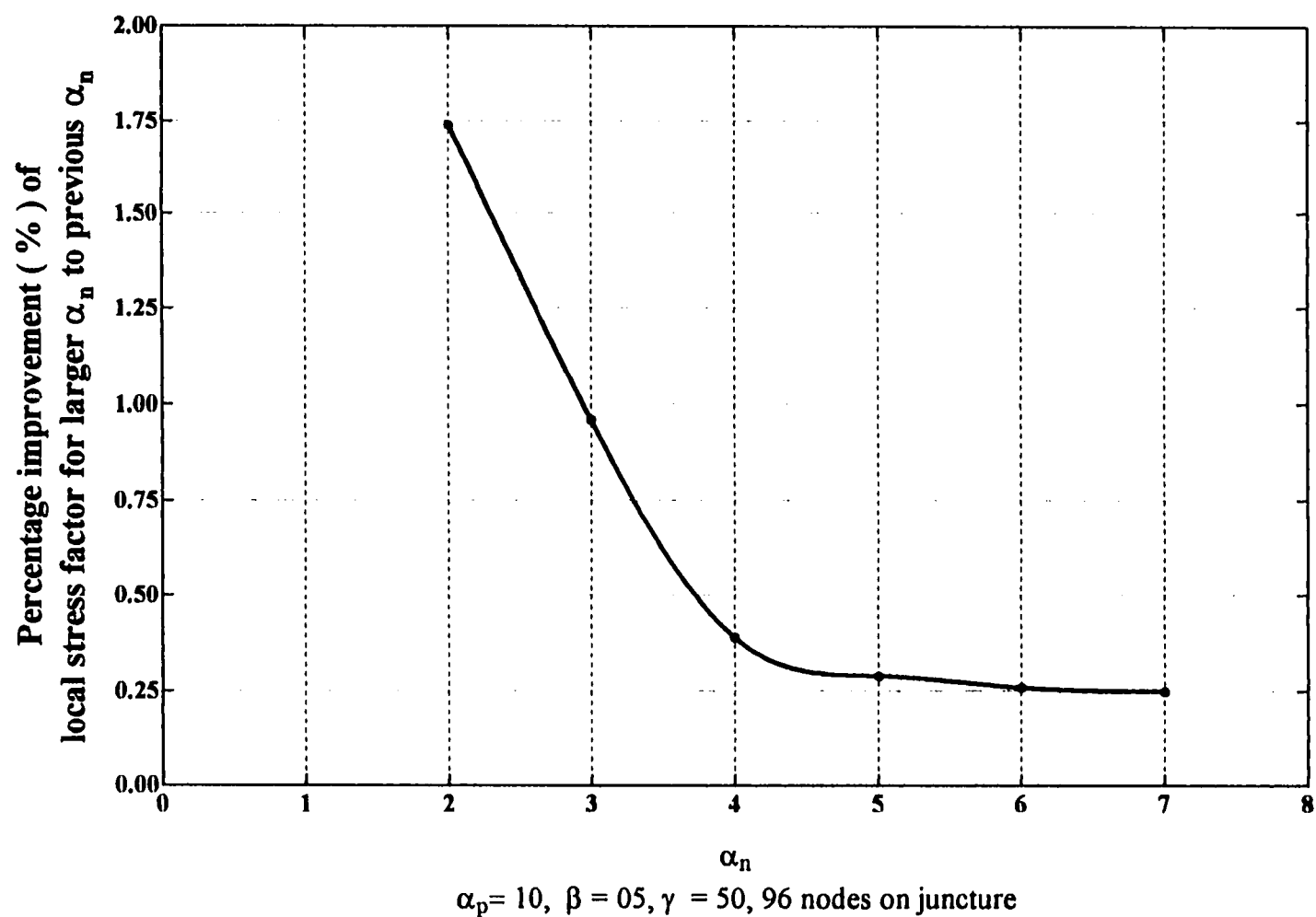in longitudinal direction

$\alpha_n = 5, \ \beta = 05, \gamma = 50, 96$ nodes on juncture

$\alpha_n = 5$, $\beta = 05$, $\gamma = 50$, 96 nodes on juncture
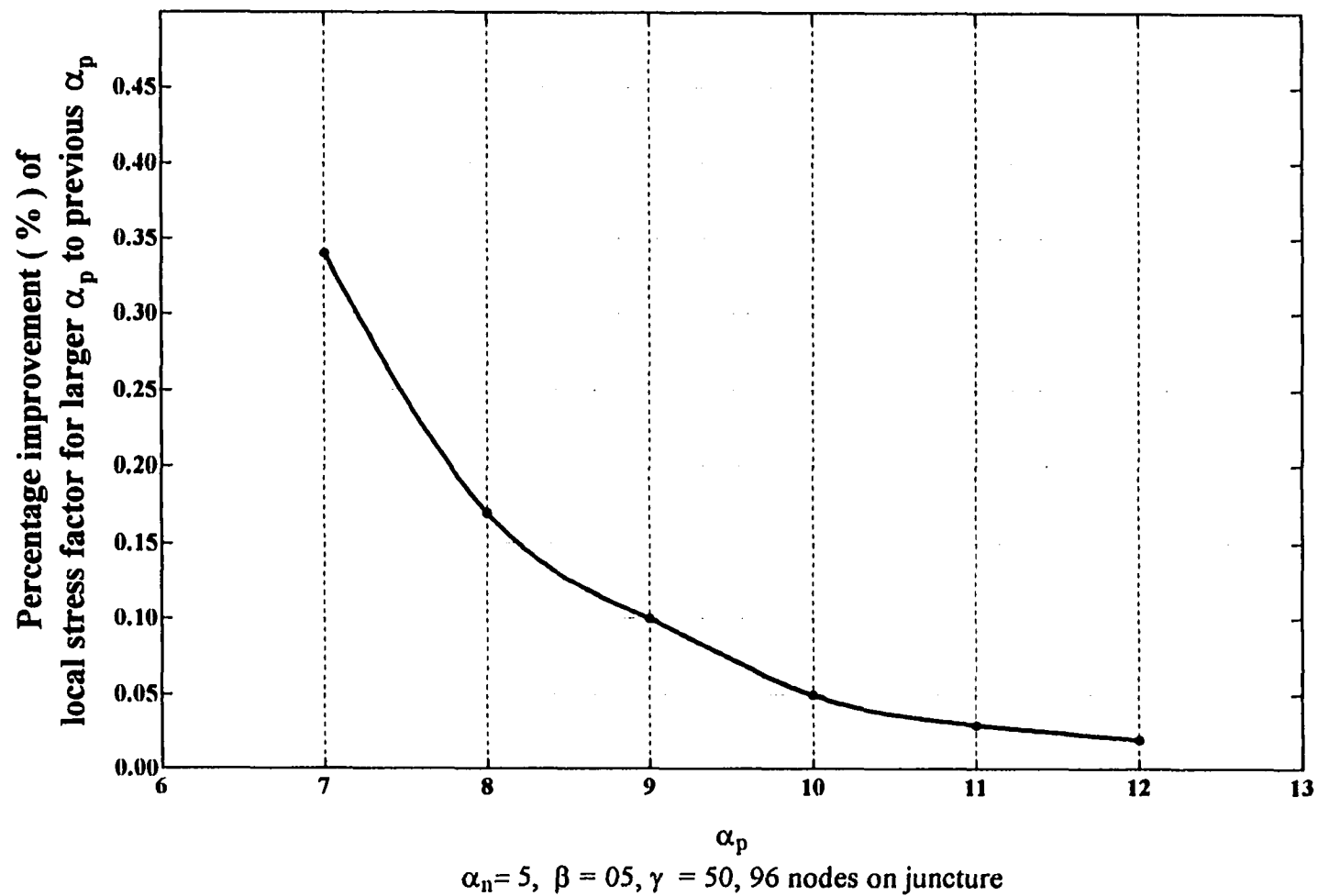
Figure B6: Asymptotic study on α_p at point B_L of pipe in longitudinal direction

$\alpha_n = 5, \quad \beta = 05, \gamma = 50, 96$ nodes on juncture
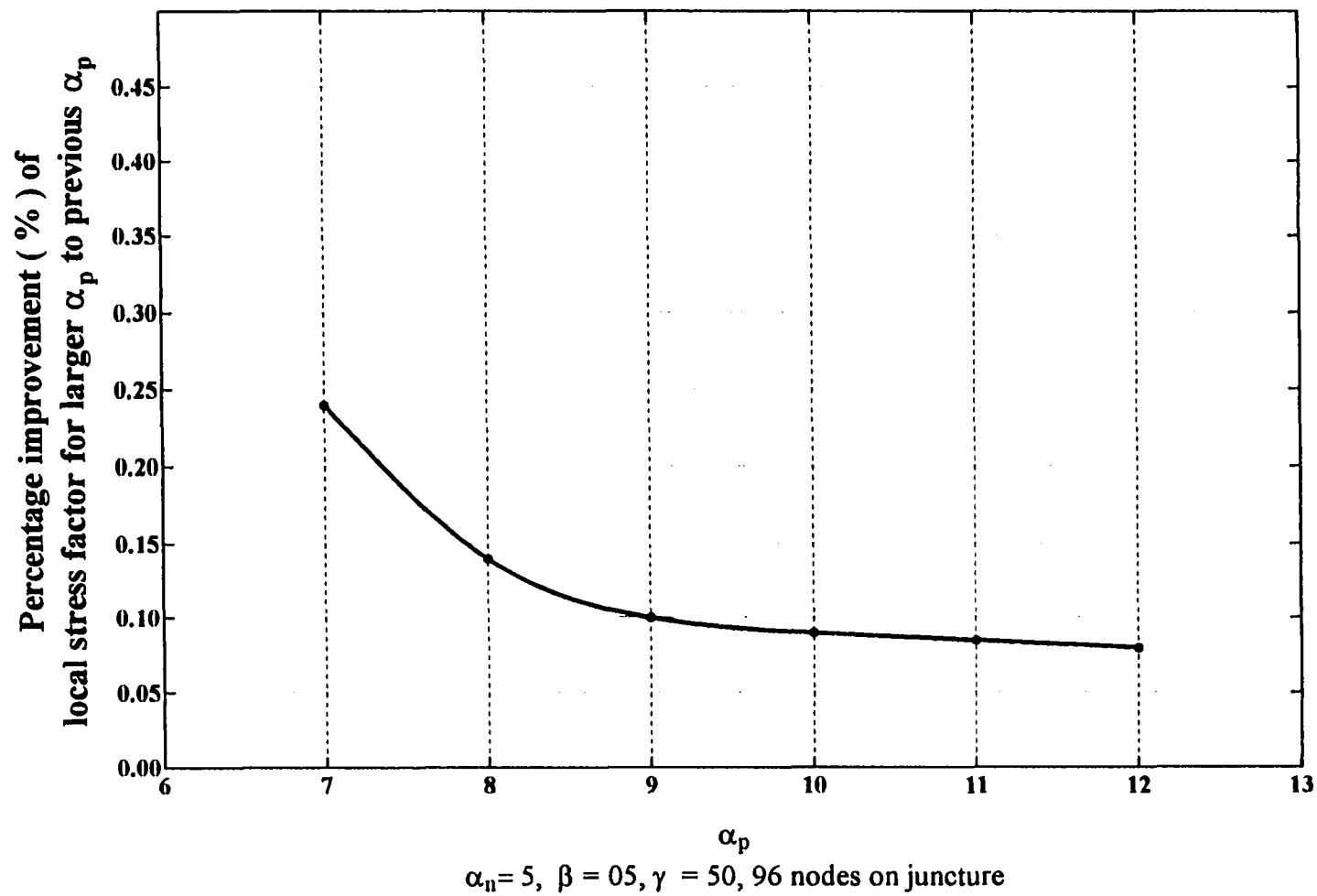
Figure B7: Asymptotic study on α_p at point B_U of pipe in circumferential direction

$$\alpha_n = 5, \quad \beta = 05, \gamma = 50, 96 \text{ nodes on juncture}$$
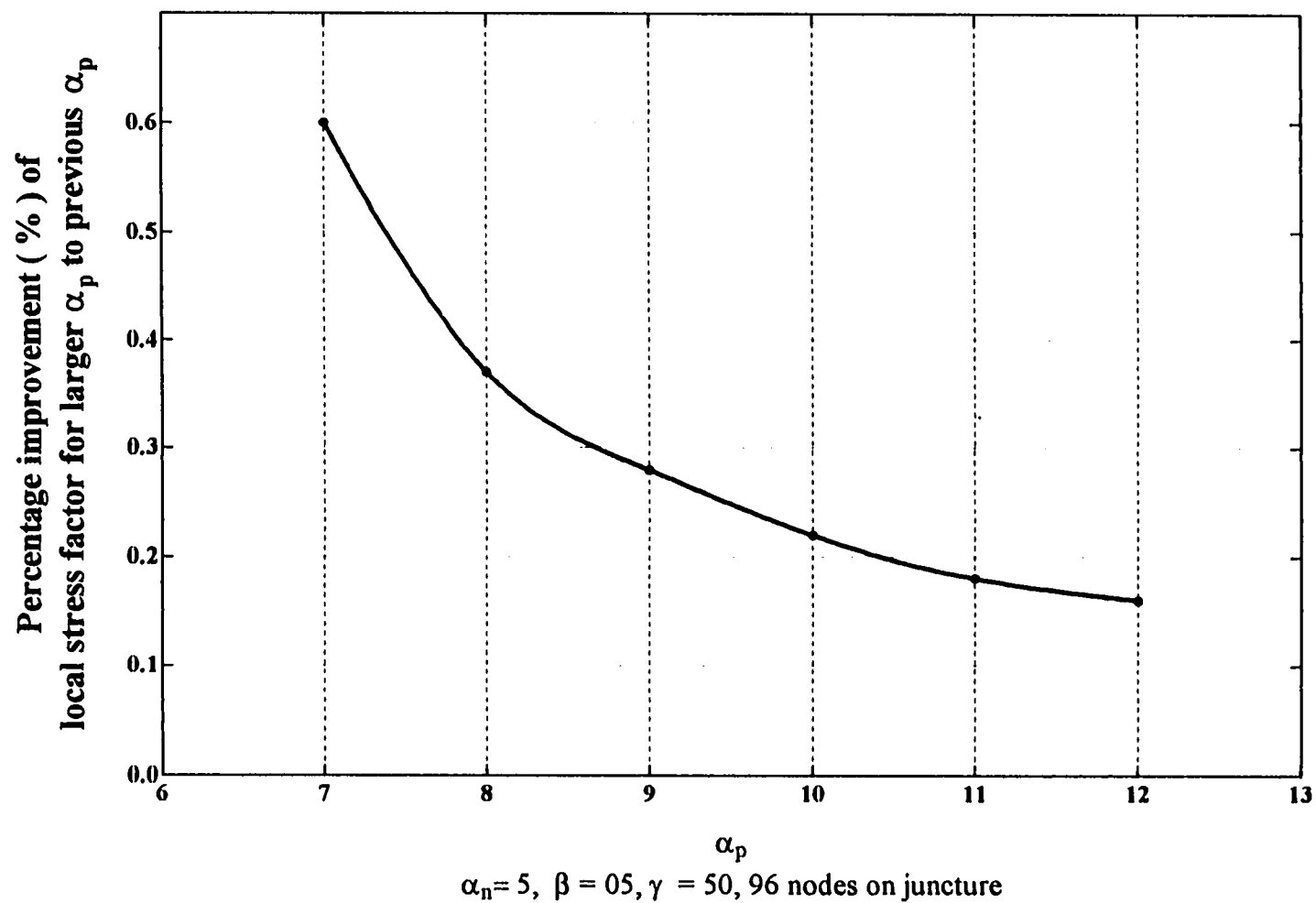
Figure B8: Asymptotic study on α_p at point B_L of pipe
in circumferential direction
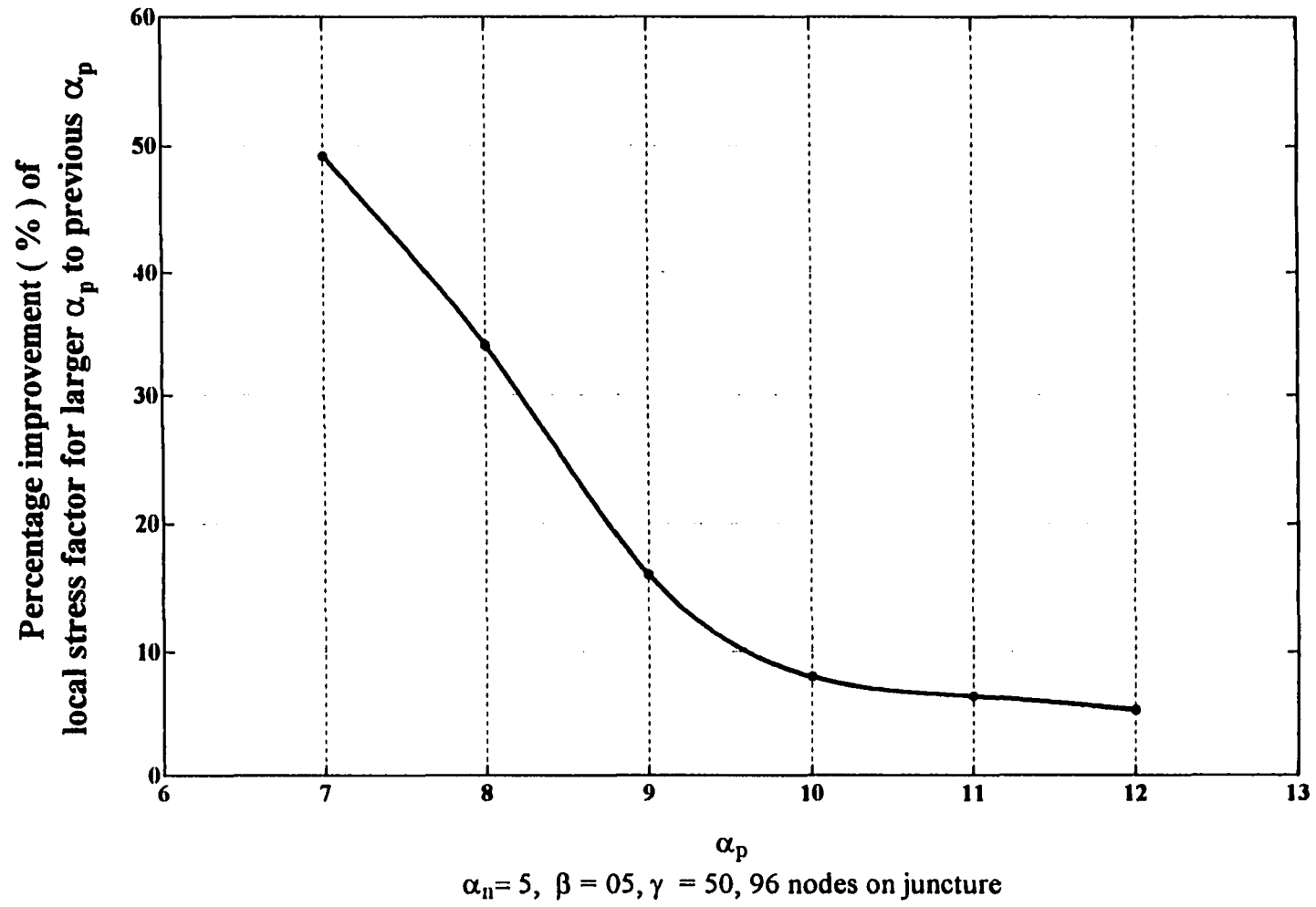
Figure B9: Asymptotic study on α_p at point C_U of pipe
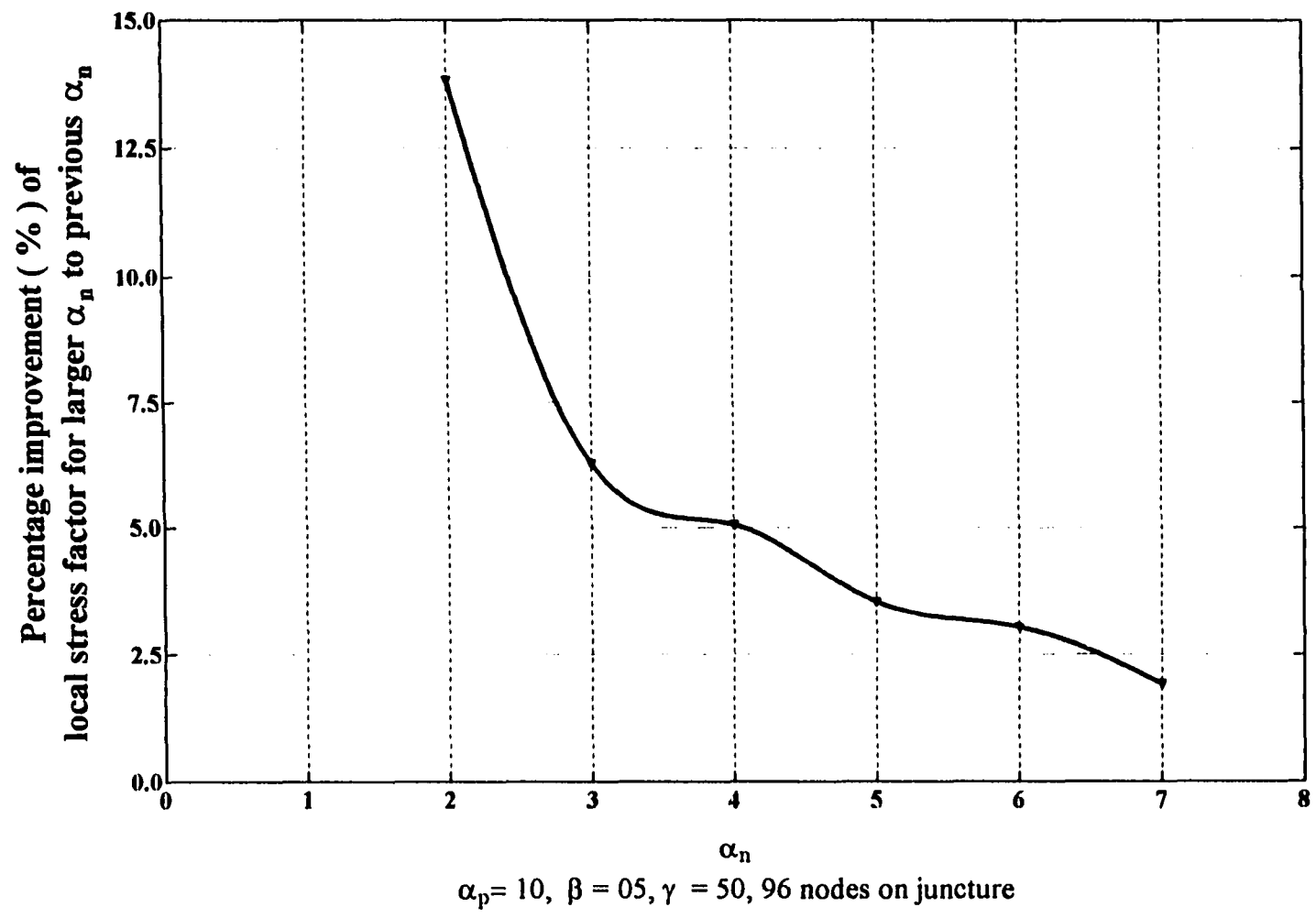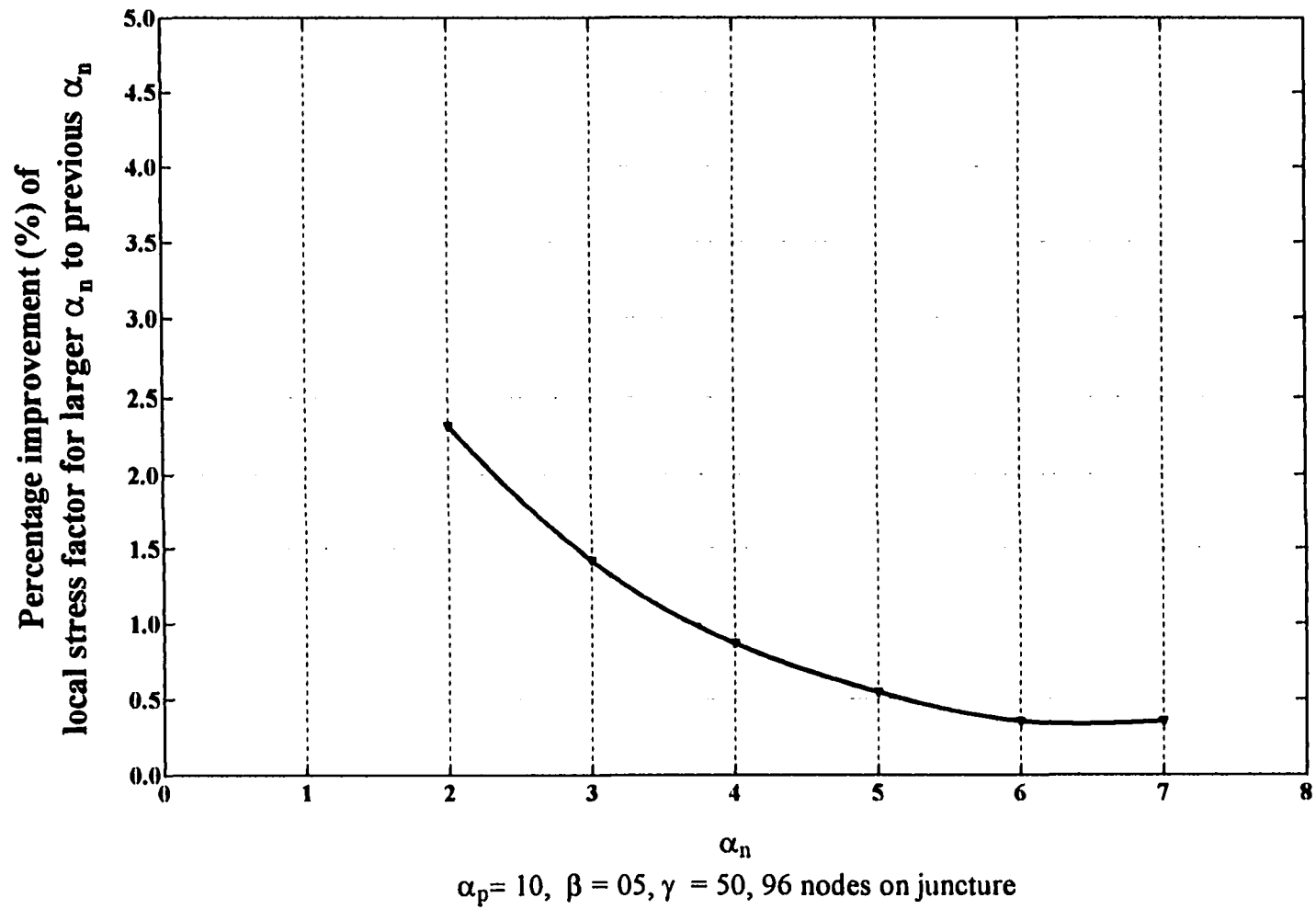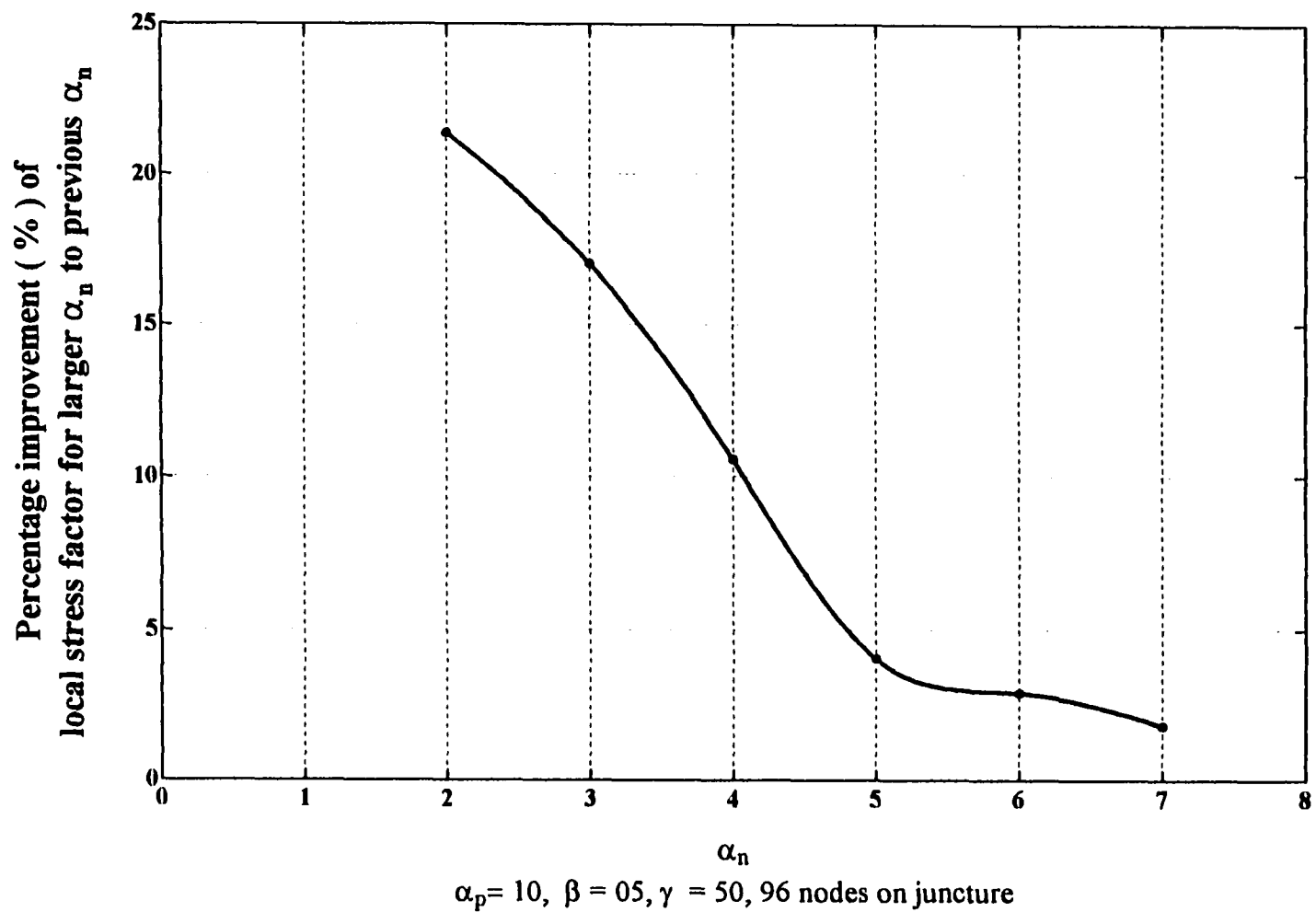in longitudinal direction

$\alpha_n = 5, \ \beta = 05, \gamma = 50, 96$ nodes on juncture

$\alpha_n = 5, \quad \beta = 05, \gamma = 50, 96$ nodes on juncture
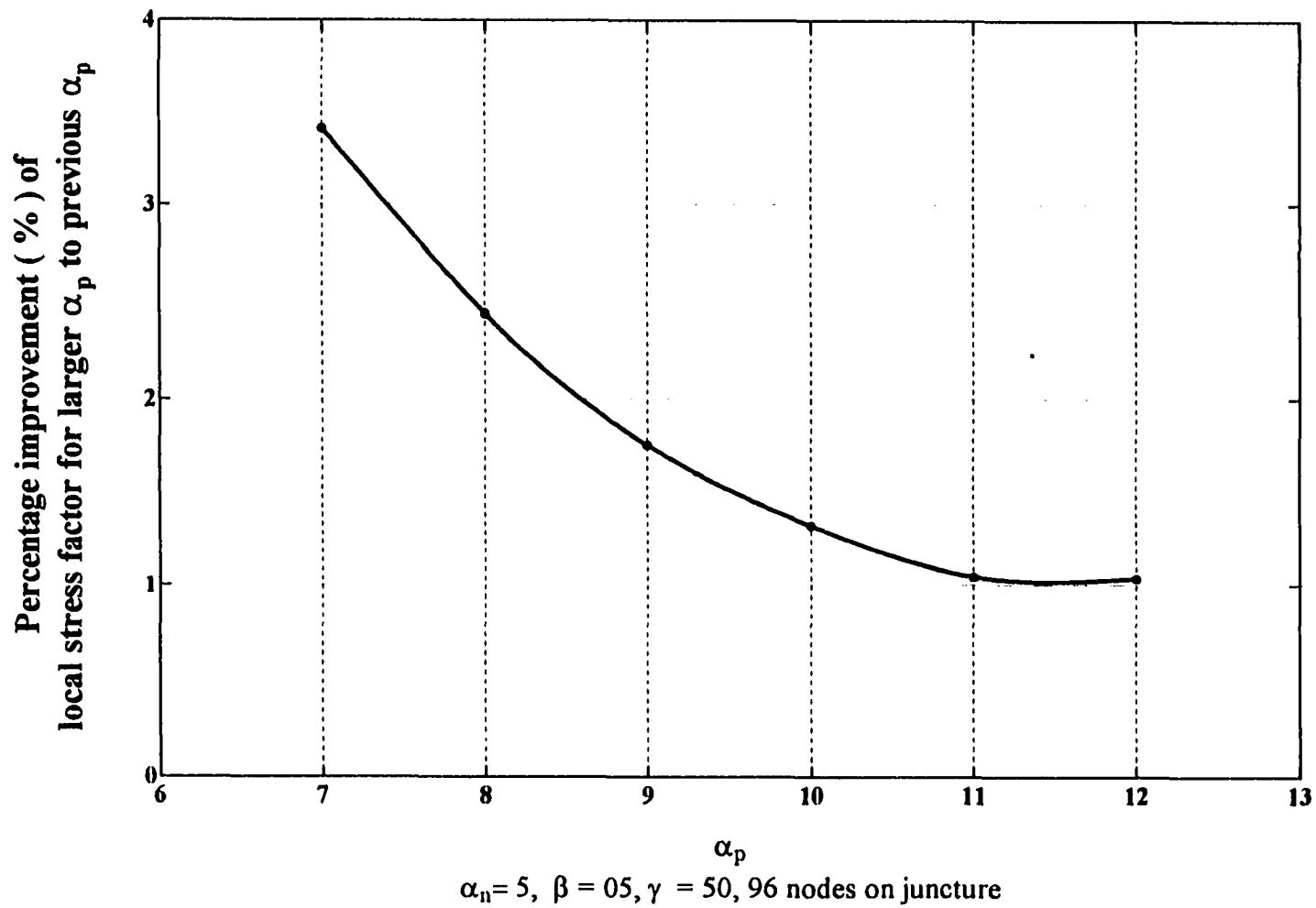
Figure B10: Asymptotic study on α_p at point C_L of pipe in longitudinal direction

$\alpha_n = 5$, $\beta = 05$, $\gamma = 50$, 96 nodes on juncture
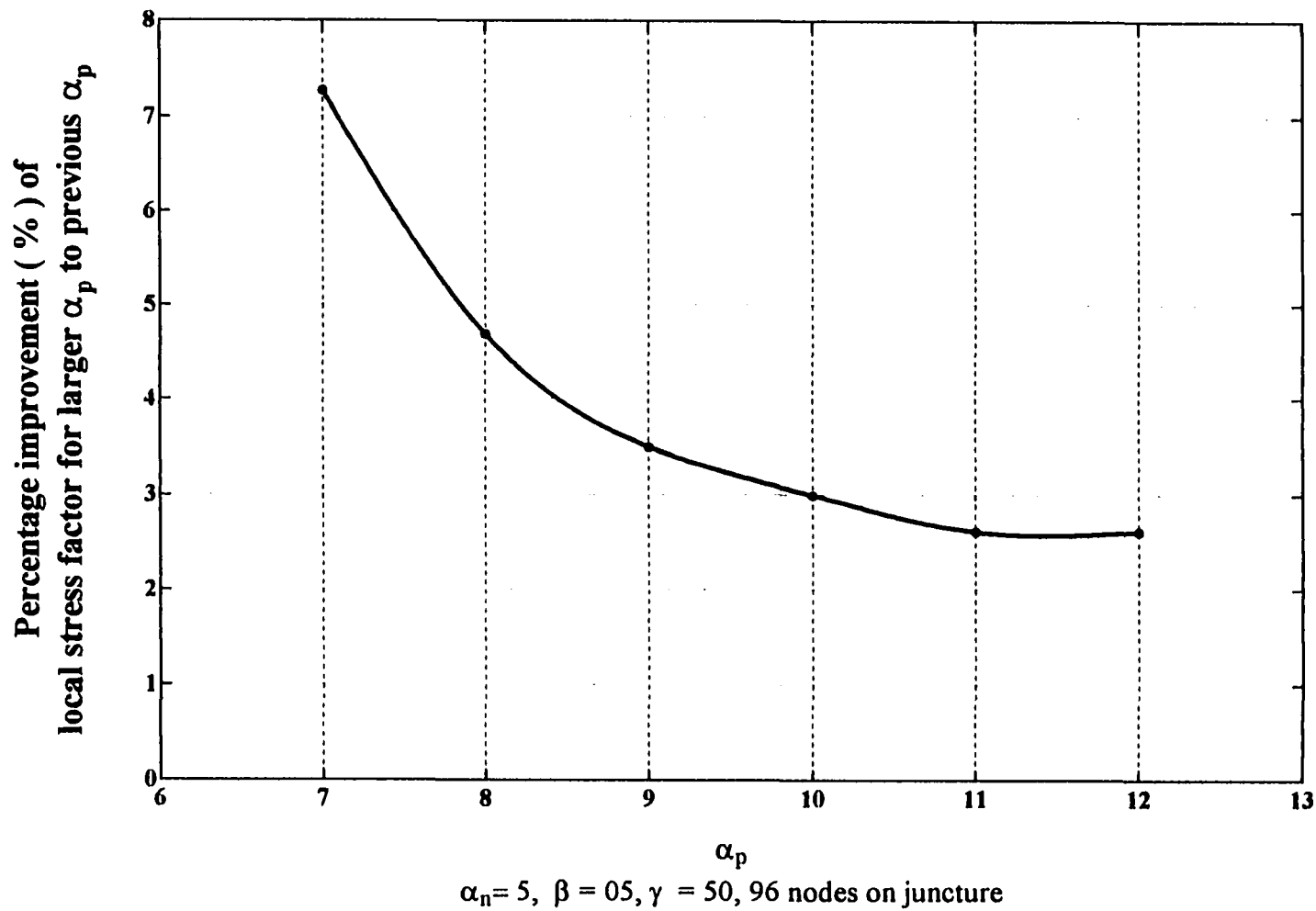
Figure B11: Asymptotic study on α_p at point C_U of pipe
in circumferential direction
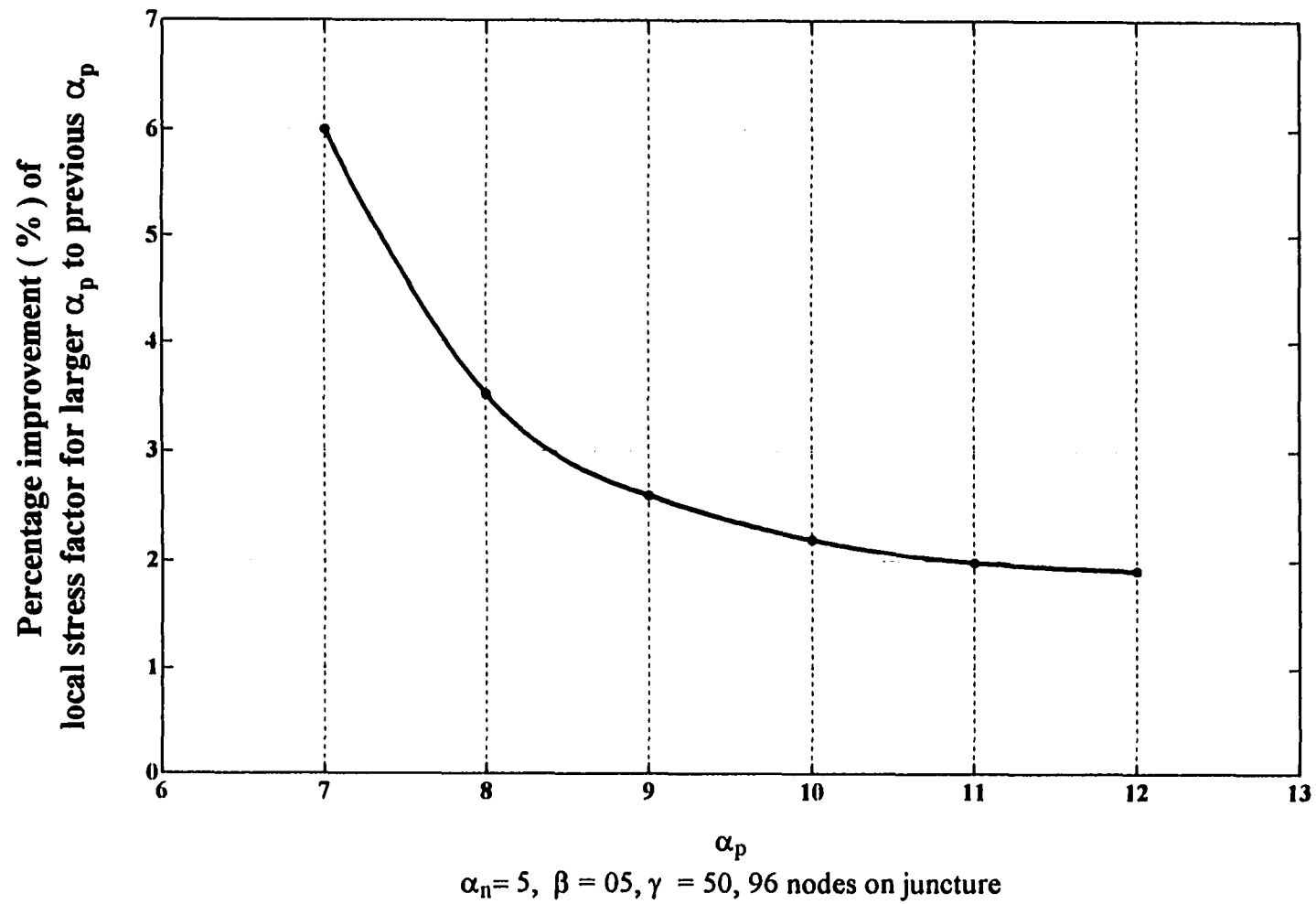
Figure B12: Asymptotic study on α_p at point C_L of pipe
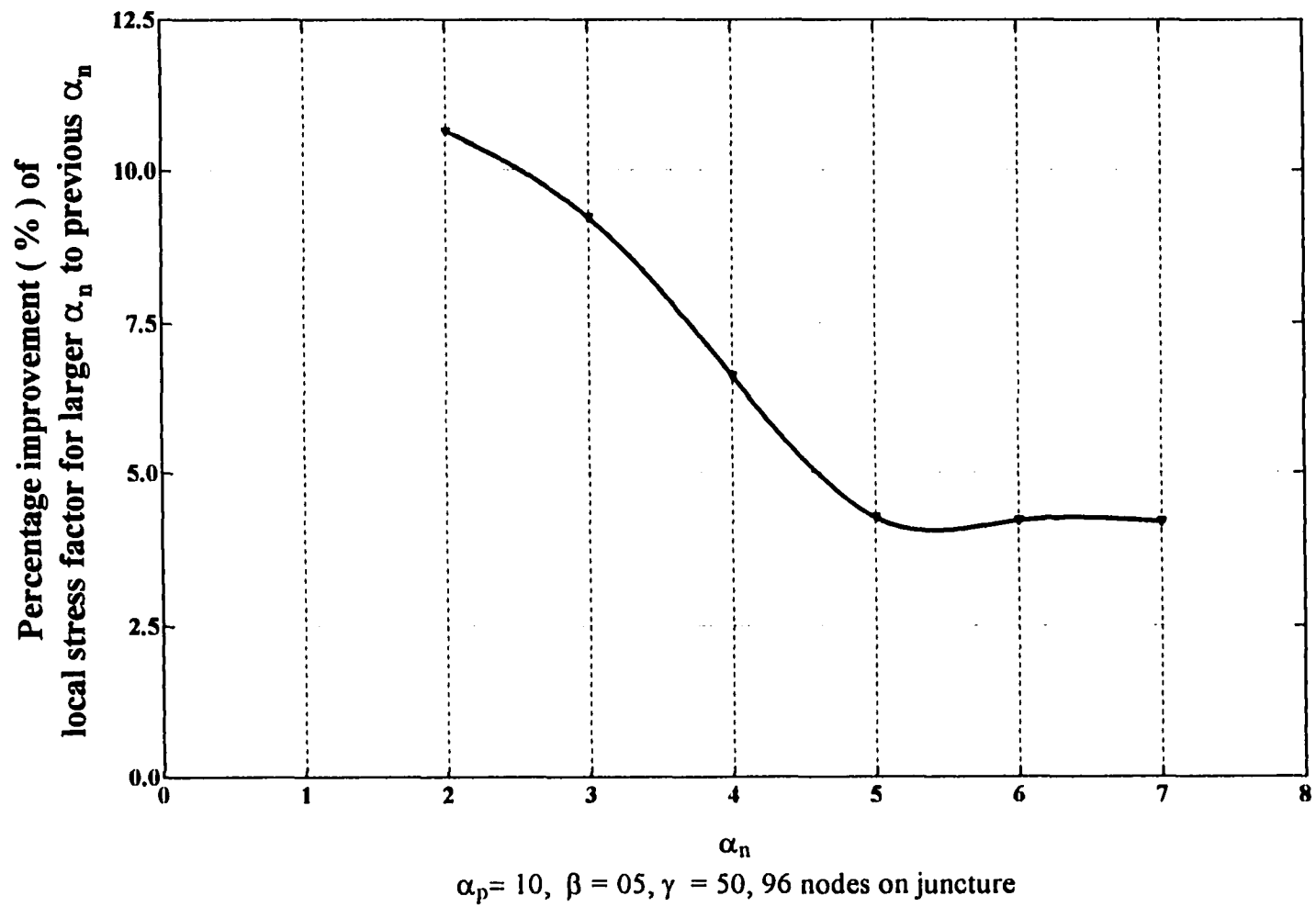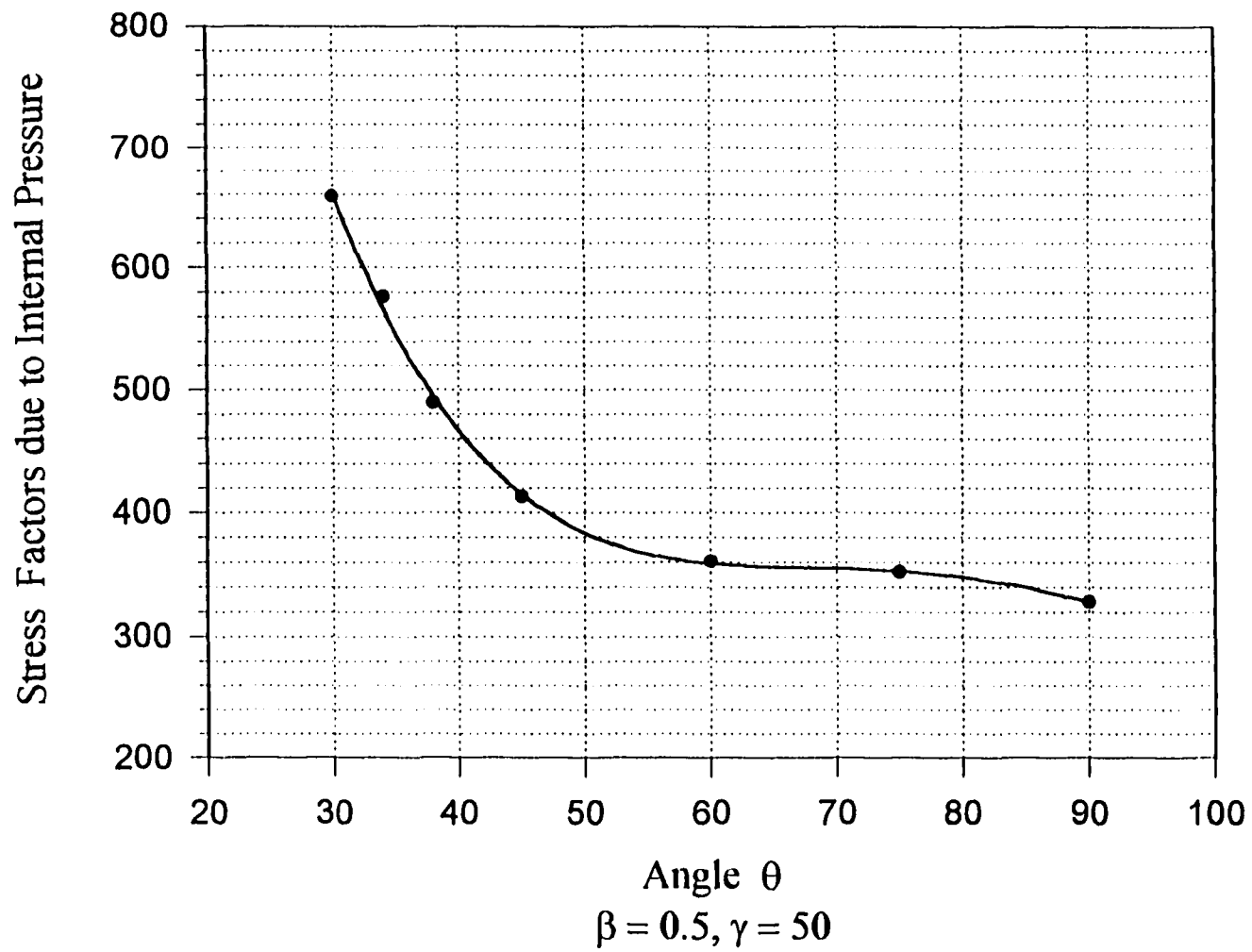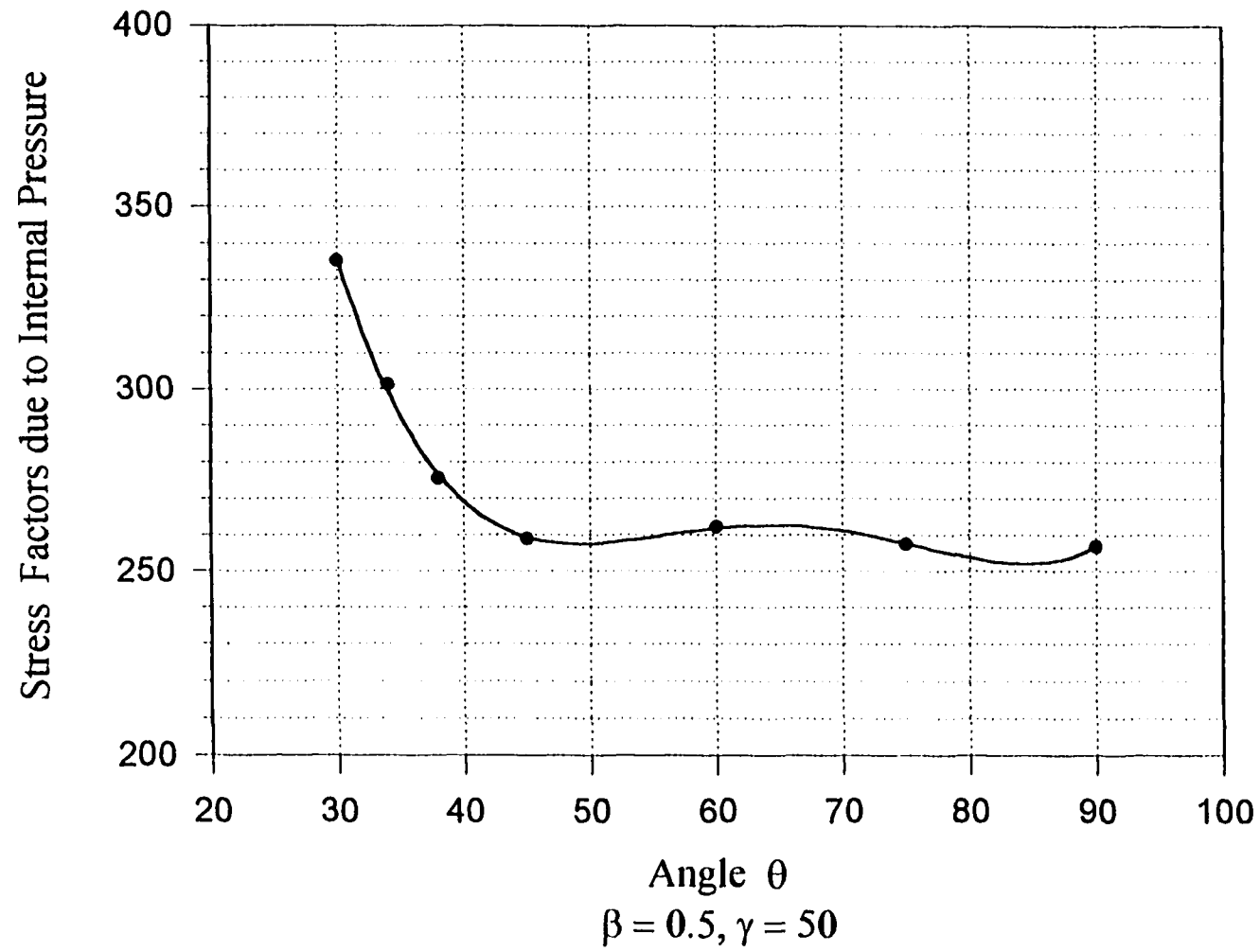in circumferential direction

$\alpha_n = 5$, $\beta = 05$, $\gamma = 50$, 96 nodes on juncture

APPENDIX C

FIGURES FOR THE CONVERGENCE STUDY OF α_n

73

$$\alpha_p = 10, \quad \beta = 05, \quad \gamma = 50, \quad 96 \text{ nodes on juncture}$$

Figure C1: Asymptotic study on α_n at point A_U of pipe in longitudinal direction

74

$\alpha_p = 10$, $\beta = 05$, $\gamma = 50$, 96 nodes on juncture
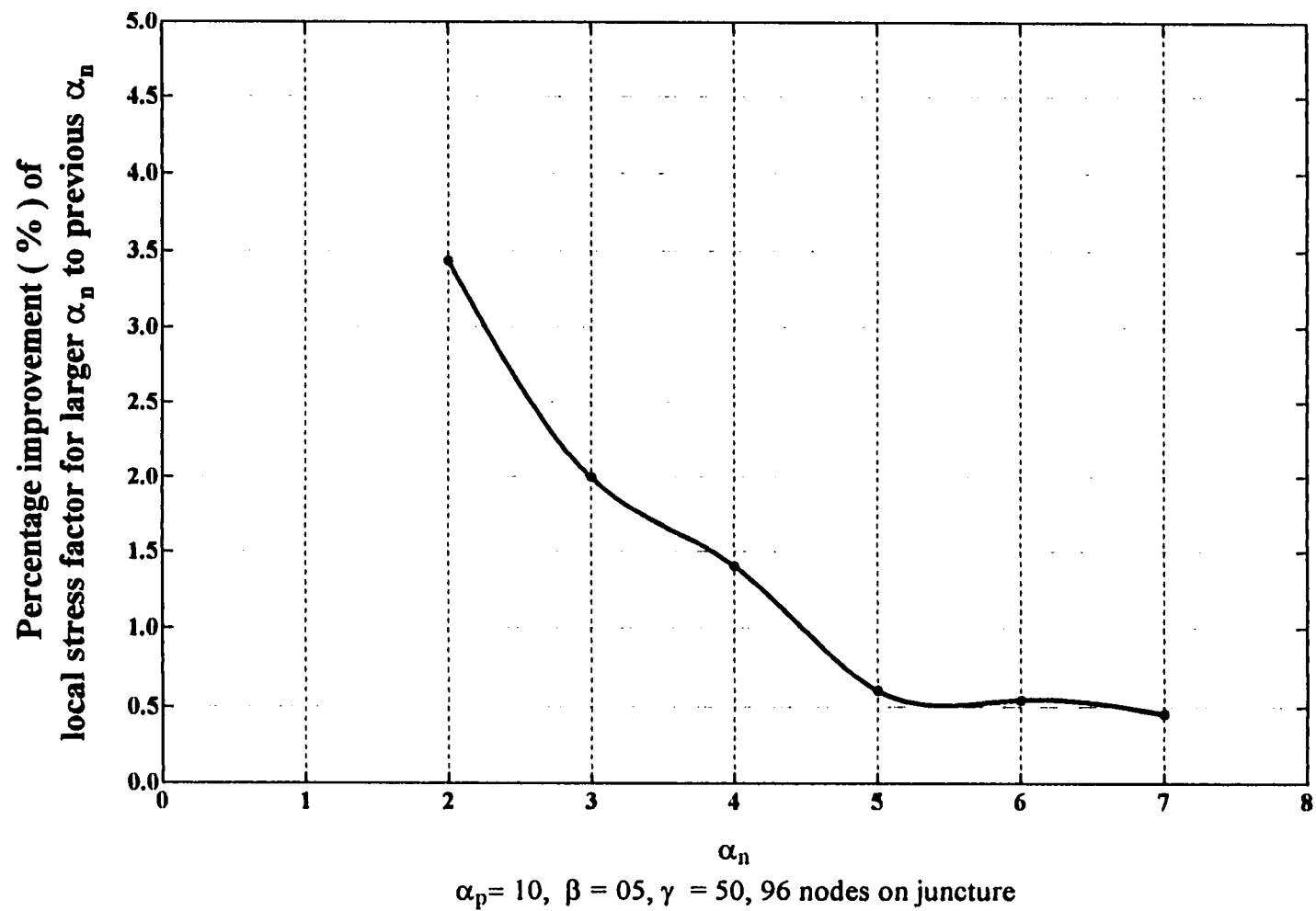
Figure C2: Asymptotic study on α_n at point A_L of pipe
in longitudinal direction

$\alpha_p = 10, \quad \beta = 05, \gamma = 50, \quad 96 \text{ nodes on juncture}$
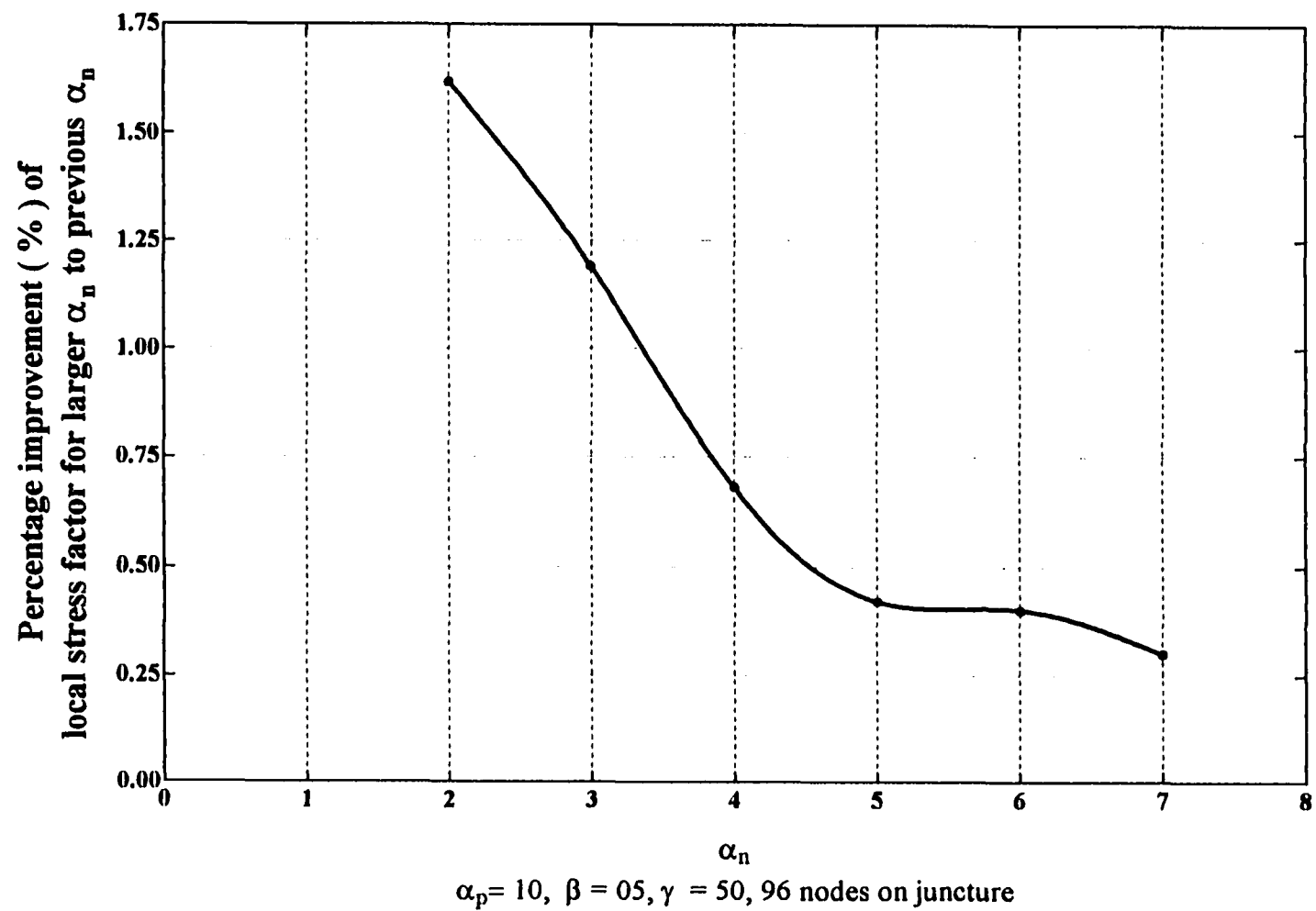
Figure C3: Asymptotic study on α_n at point A_U of pipe
in circumferential direction

$\alpha_p = 10$, $\beta = 05$, $\gamma = 50$, 96 nodes on juncture
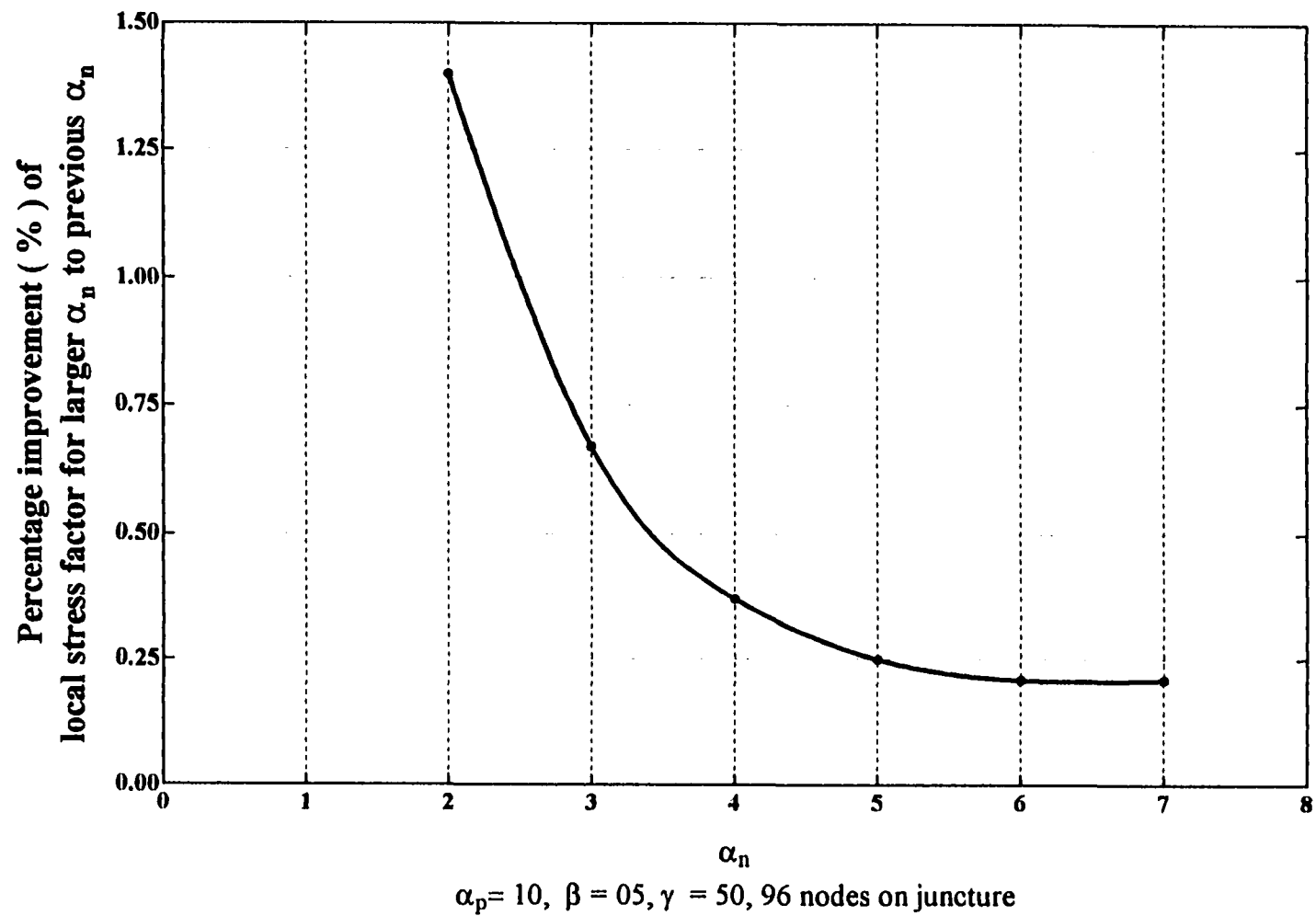
Figure C4: Asymptotic study on α_n at point A_L of pipe in circumferential direction

$\alpha_p = 10, \quad \beta = 05, \gamma = 50, 96$ nodes on juncture
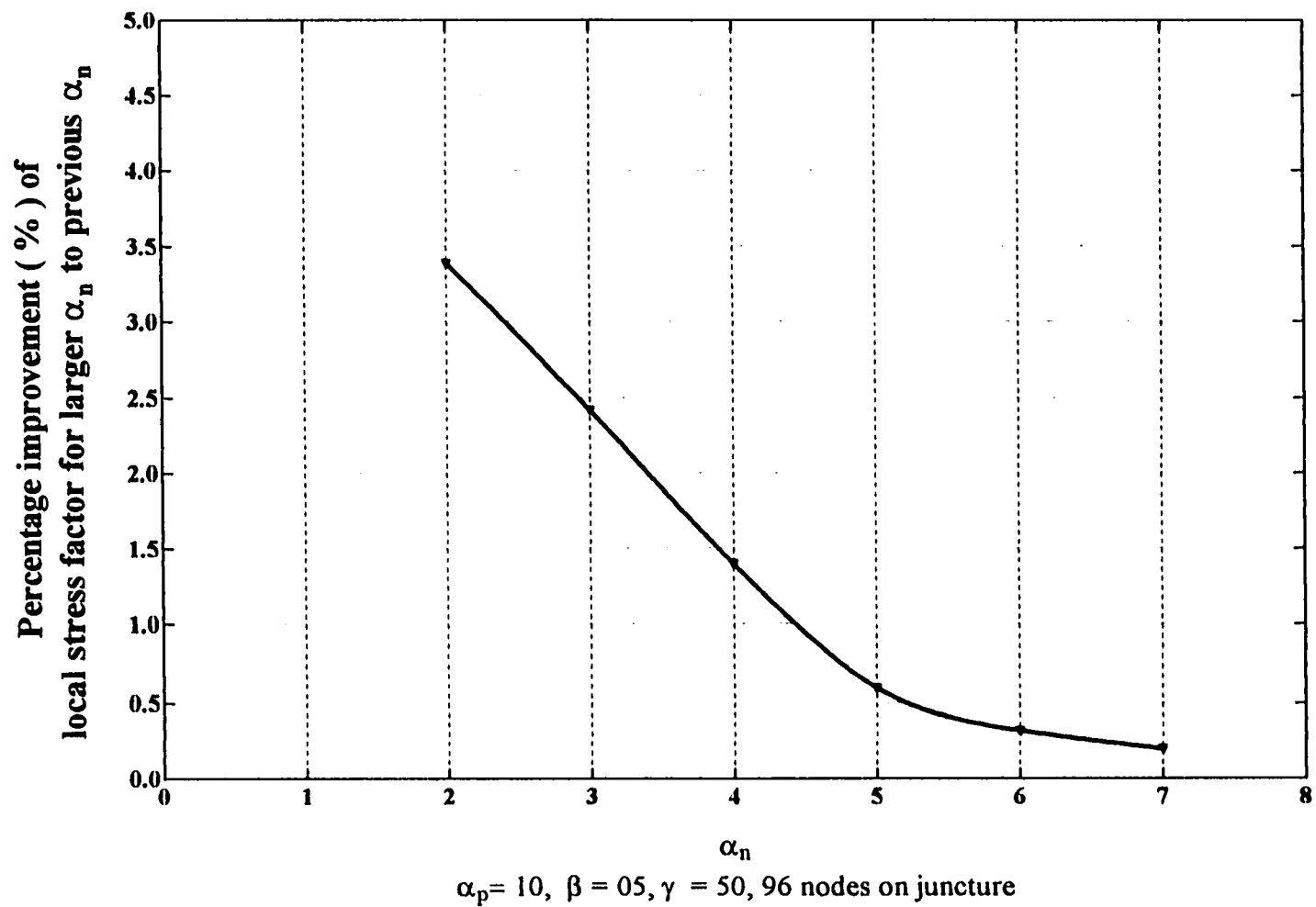
Figure C5: Asymptotic study on α_n at point B_U of pipe
in longitudinal direction

$\alpha_p = 10, \quad \beta = 05, \gamma = 50, 96$ nodes on juncture

Figure C6: Asymptotic study on α_n at point B_L of pipe in longitudinal direction

$$\alpha_p = 10, \quad \beta = 05, \gamma = 50, 96 \text{ nodes on juncture}$$

Figure C7: Asymptotic study on α_n at point B_U of pipe
in circumferential direction

$\alpha_p = 10, \quad \beta = 05, \gamma = 50,$ 96 nodes on juncture

Figure C8: Asymptotic study on α_n at point B_L of pipe
in circumferential direction

$\alpha_p = 10, \quad \beta = 05, \gamma = 50, 96$ nodes on juncture

Figure C9: Asymptotic study on α_n at point C_U of pipe in longitudinal direction

$\alpha_p = 10, \quad \beta = 05, \gamma = 50, 96$ nodes on juncture

Figure C10: Asymptotic study on α_n at point C_L of pipe
in longitudinal direction

$\alpha_p = 10, \quad \beta = 05, \gamma = 50, 96 \text{ nodes on juncture}$

Figure C11: Asymptotic study on α_n at point C_U of pipe
in circumferential direction

$\alpha_p = 10, \quad \beta = 05, \gamma = 50, 96$ nodes on juncture

Figure C12: Asymptotic study on α_n at point C_L of pipe
in circumferential direction

APPENDIX D

FIGURES FOR THE STUDY OF ANGLE EFFECT

86

Figure D1: Study on intersecting angle at point $A_{()}$ of pipe
in longitudinal direction

Angle θ

$\beta = 0.5, \gamma = 50$

Figure D2: Study on intersecting angle at point A_L of pipe

in longitudinal direction
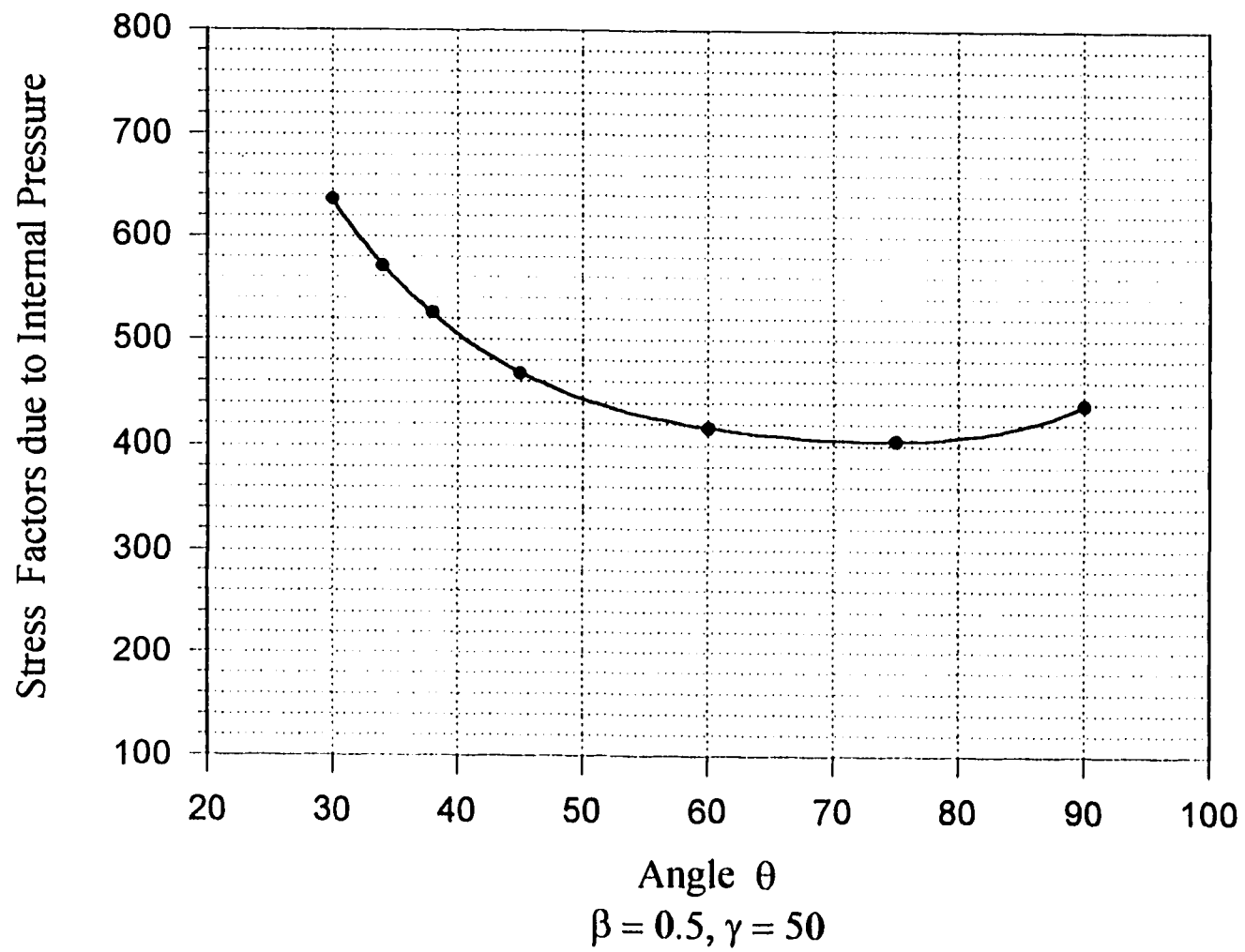
Figure D3: Study on intersecting angle at point A_{ij} of pipe
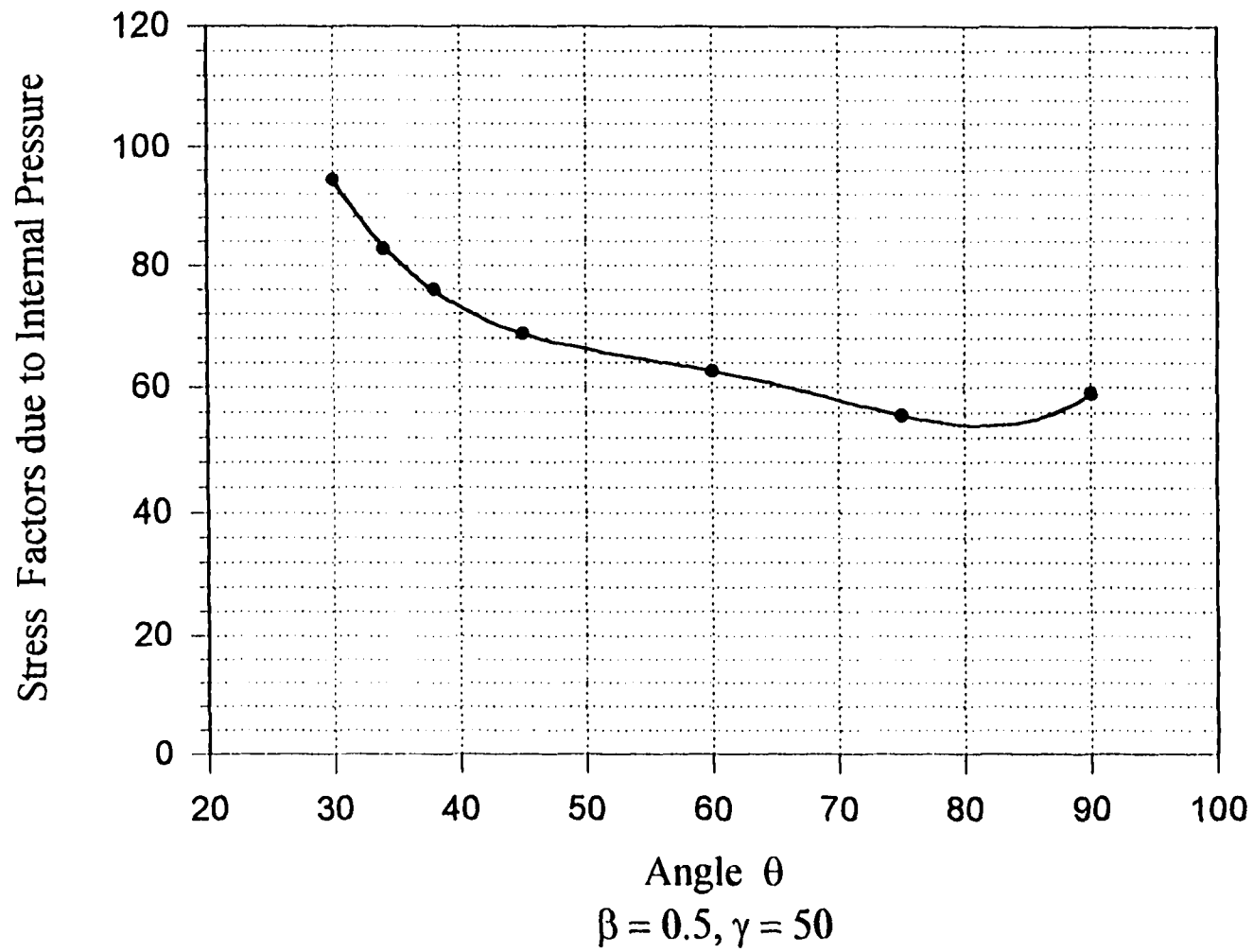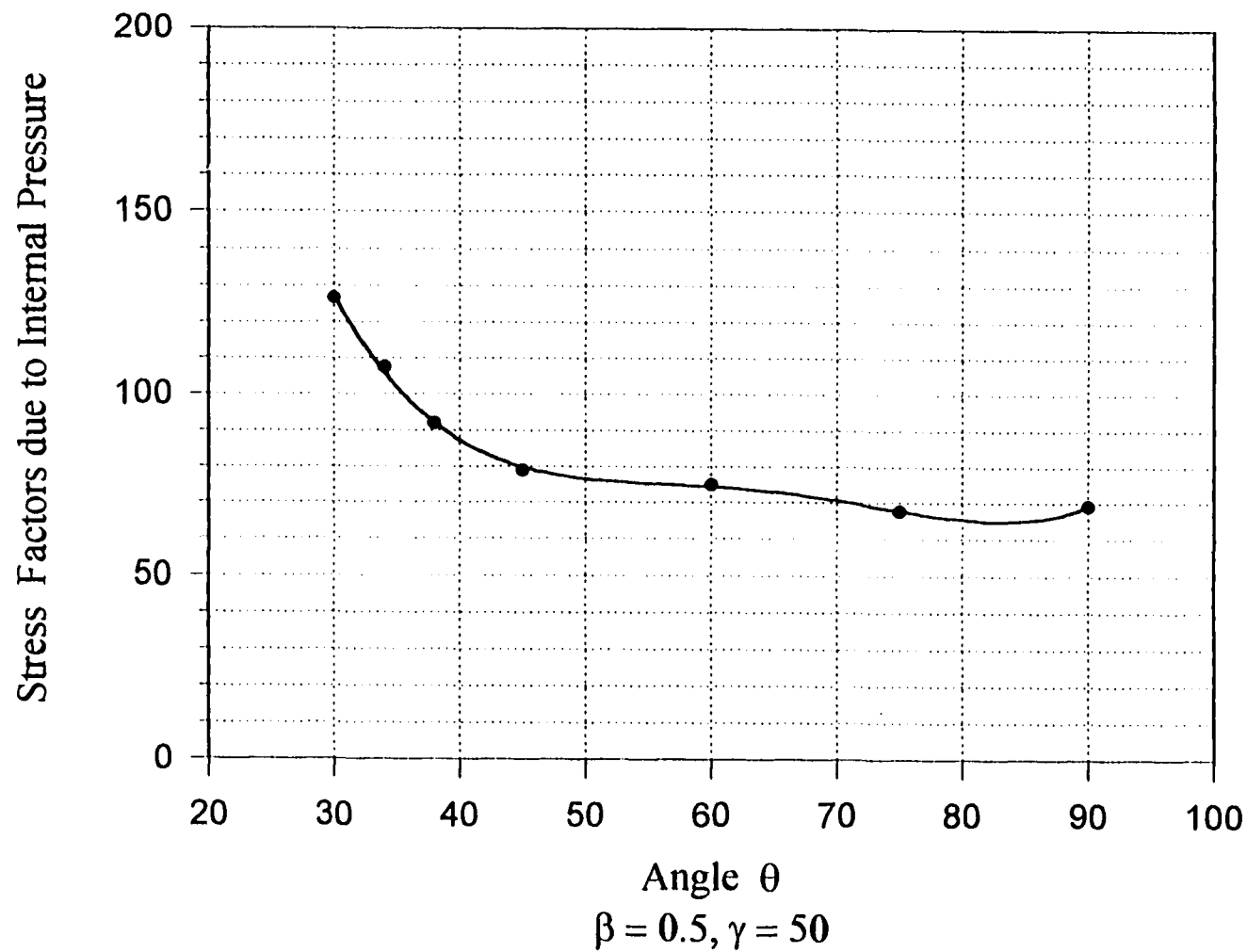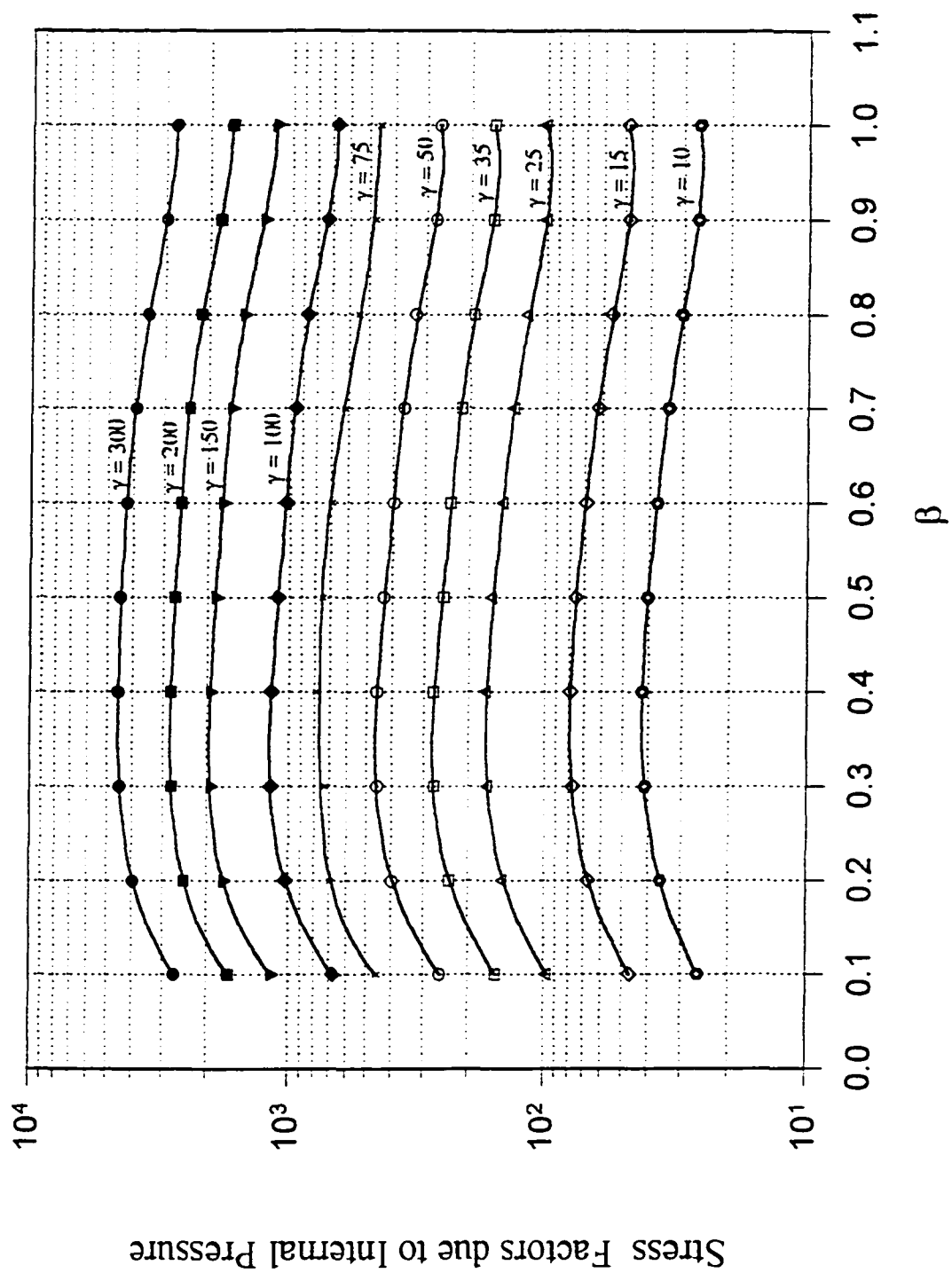in circumferential direction

$$\beta = 0.5, \gamma = 50$$
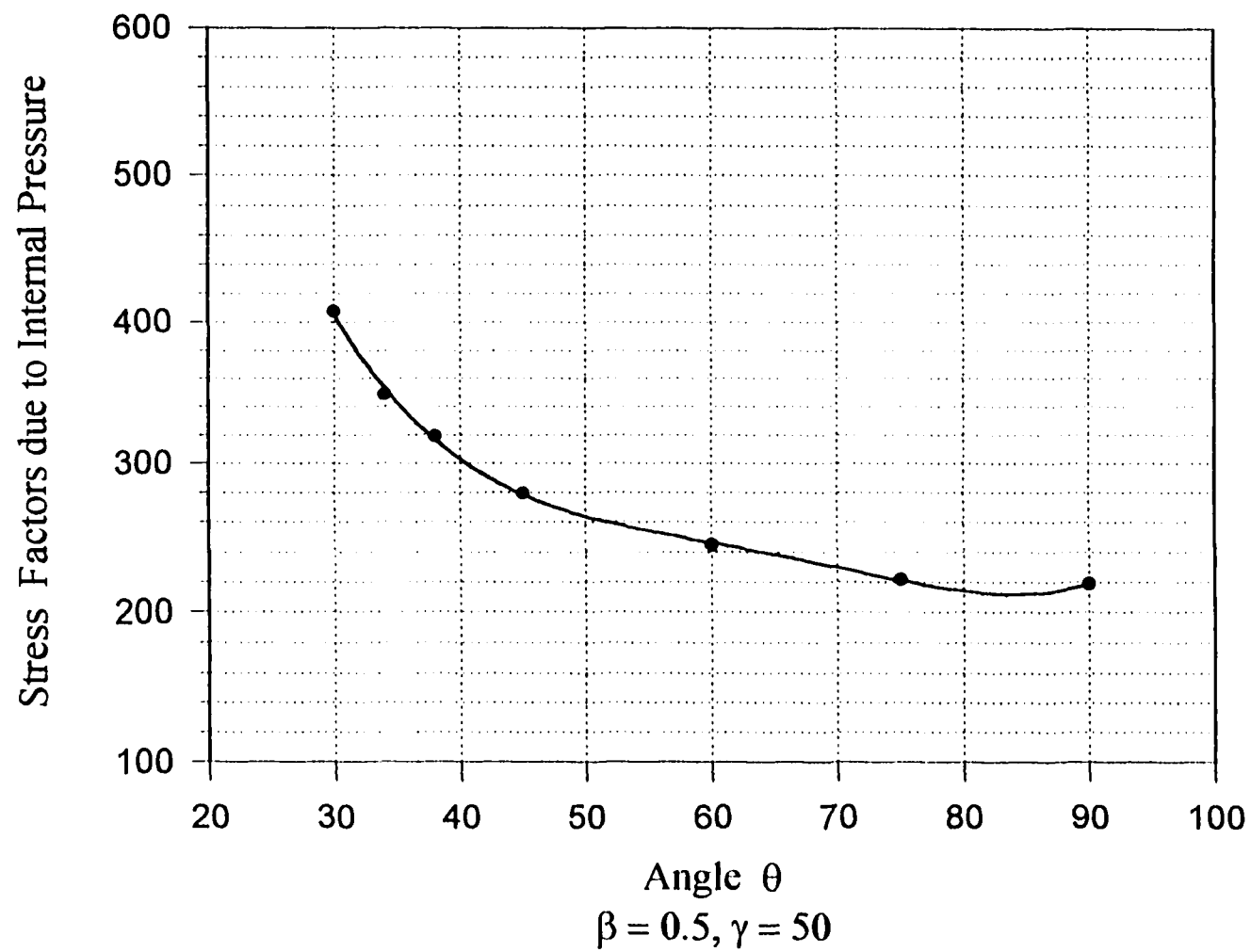
Figure D4: Study on intersecting angle at point A_1 of pipe in circumferential direction
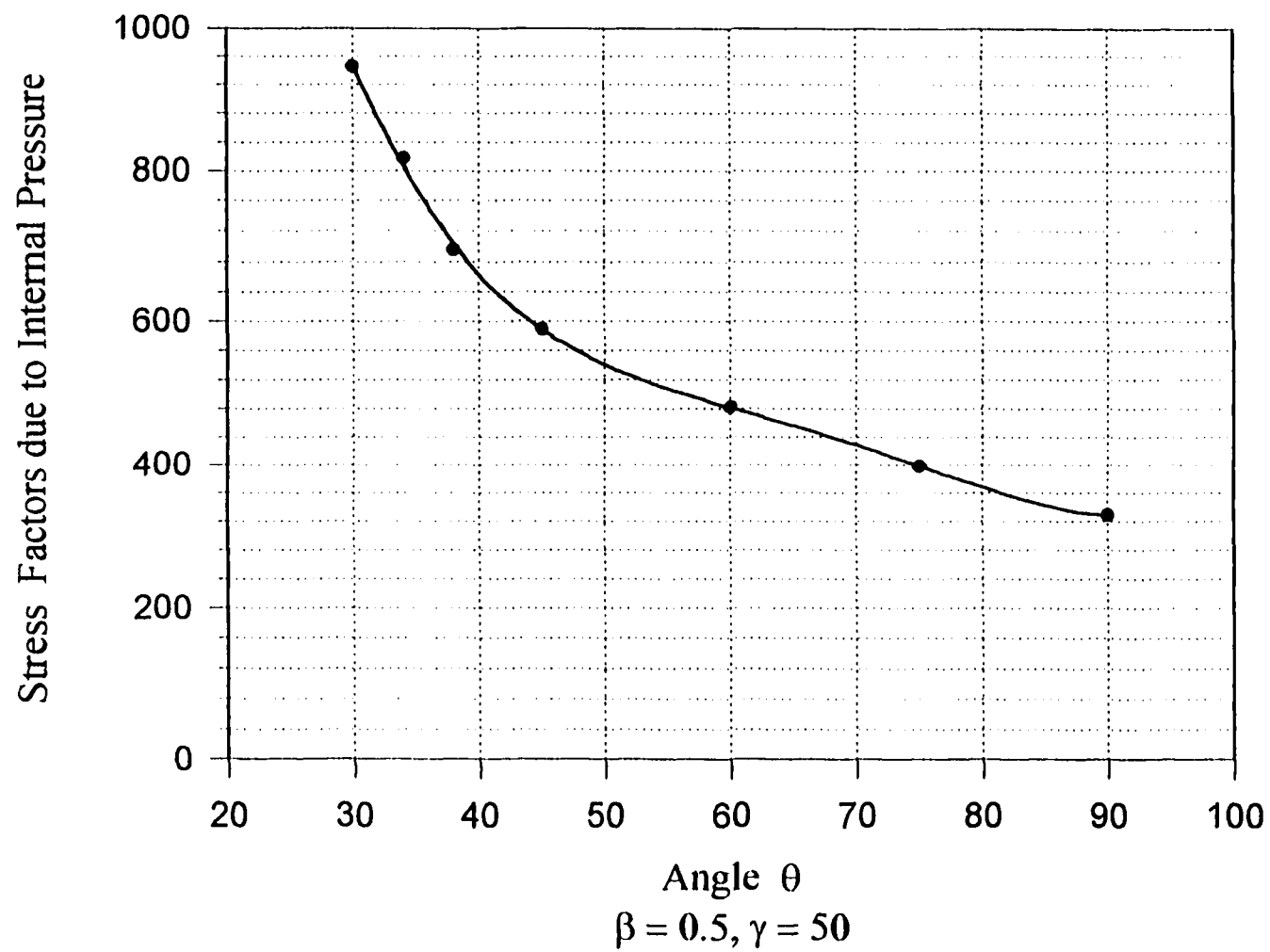
Figure D5: Study on intersecting angle at point B_{IJ} of pipe
in longitudinal direction

$\beta = 0.5, \gamma = 50$

Figure D6: Study on intersecting angle at point B_1 of pipe
in longitudinal direction
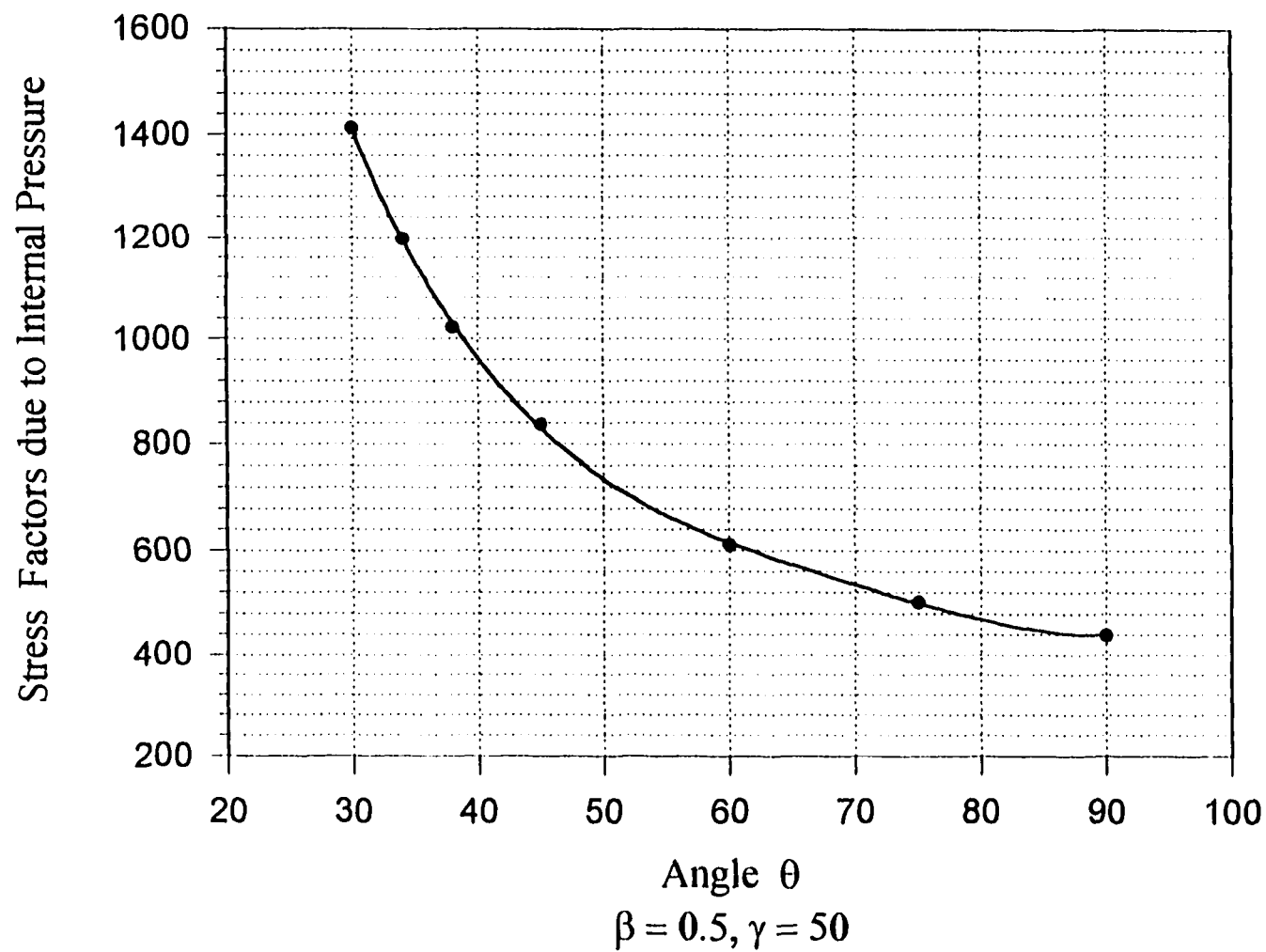
Figure D7: Study on intersecting angle at point B_U of pipe
in circumferential direction

$\beta = 0.5, \gamma = 50$
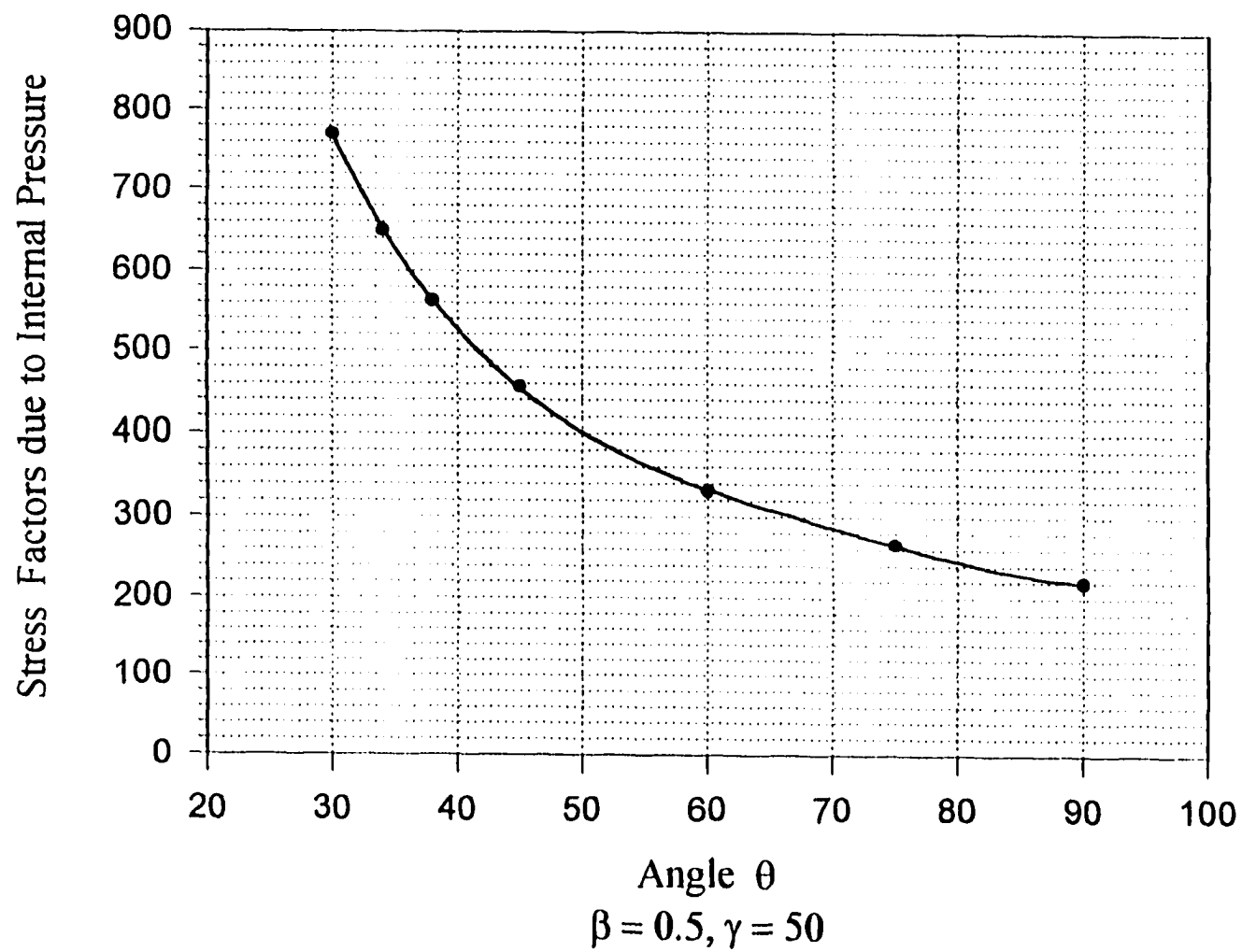
Figure D8: Study on intersecting angle at point B_1 of pipe
in circumferential direction

94
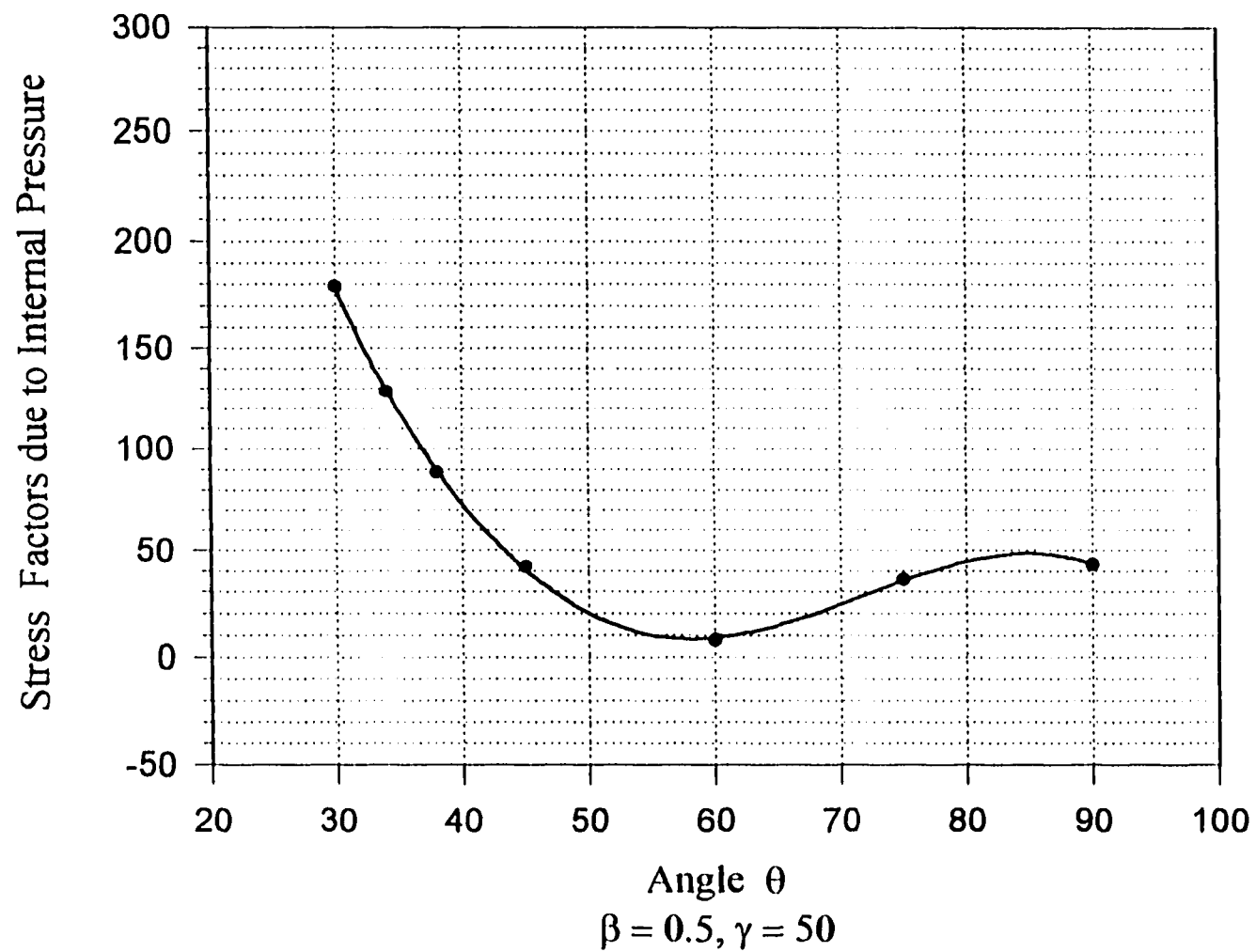
Figure D9: Study on intersecting angle at point C_{IJ} of pipe in longitudinal direction
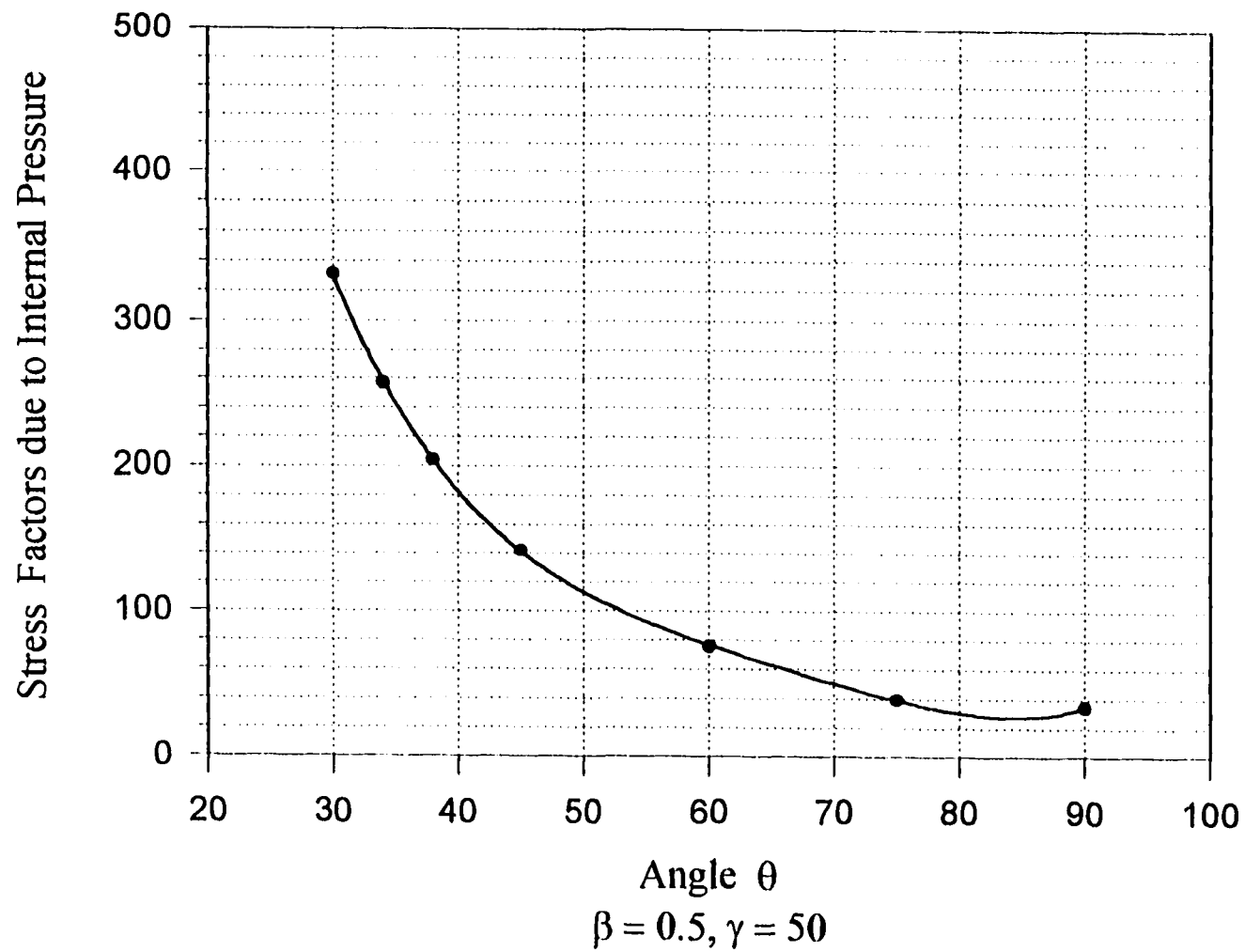
Figure D10: Study on intersecting angle at point C_L of pipe
in longitudinal direction

$$\beta = 0.5, \gamma = 50$$

Figure D11: Study on intersecting angle at point $C_{l)}$ of pipe in circumferential direction

Figure D12: Study on intersecting angle at point C_1 of pipe in circumferential direction

$\beta = 0.5, \gamma = 50$

APPENDIX E

PLOTS OF LOCAL PRESSURE STRESS FACTORS

99

Figure E1: Longitudinal pressure stress factors on the pipe at point A_{lj}

γ = 300

γ = 200

γ = 150

γ = 100

γ = 75

γ = 50

γ = 35

γ = 25

γ = 15

γ = 10

β

Stress Factors due to Internal Pressure

10^4 10^3 10^2 10^1

0.0 0.1 0.2 0.3 0.4 0.5 0.6 0.7 0.8 0.9 1.0 1.1
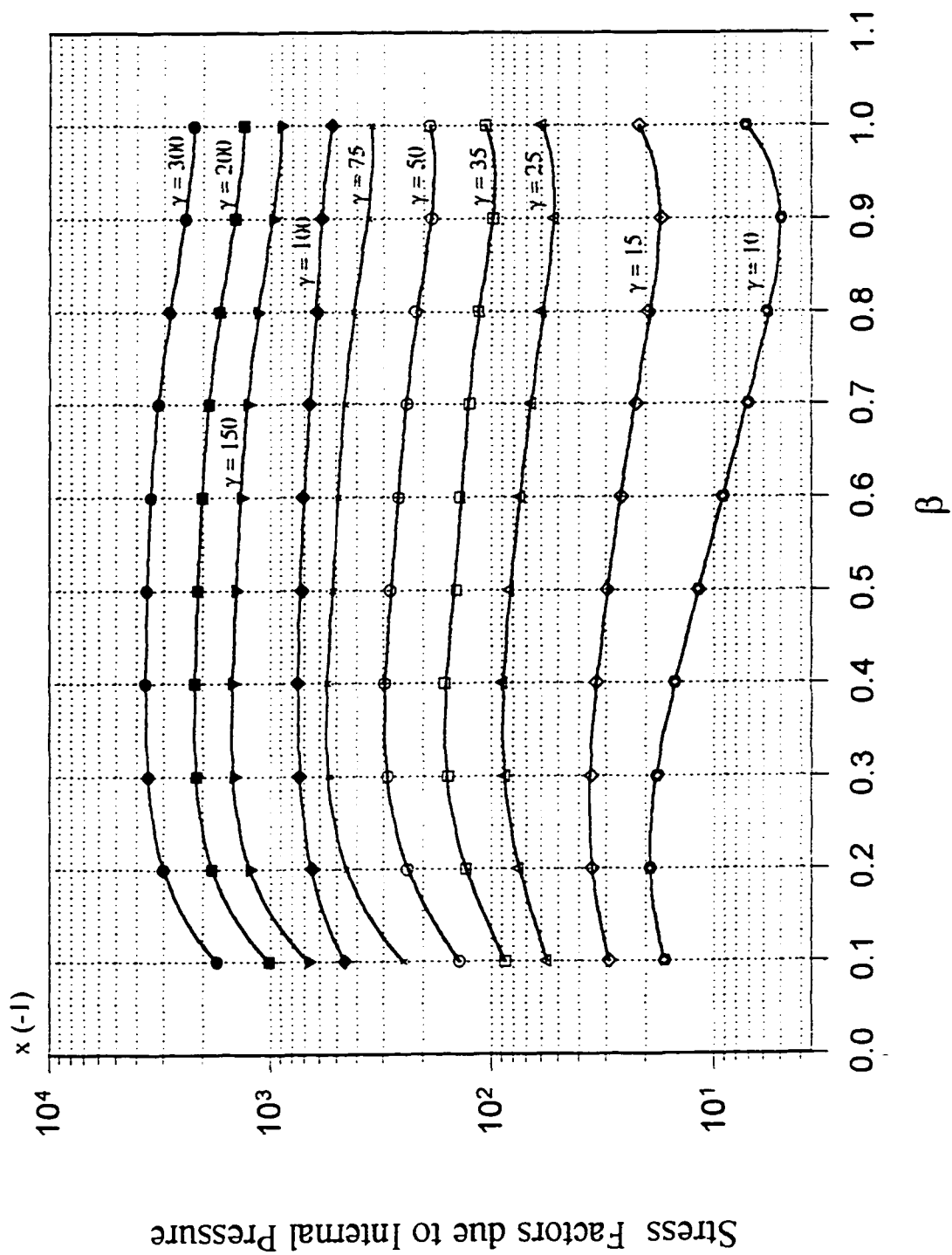
Figure E2: Longitudinal pressure stress factors on the pipe at point A_1.
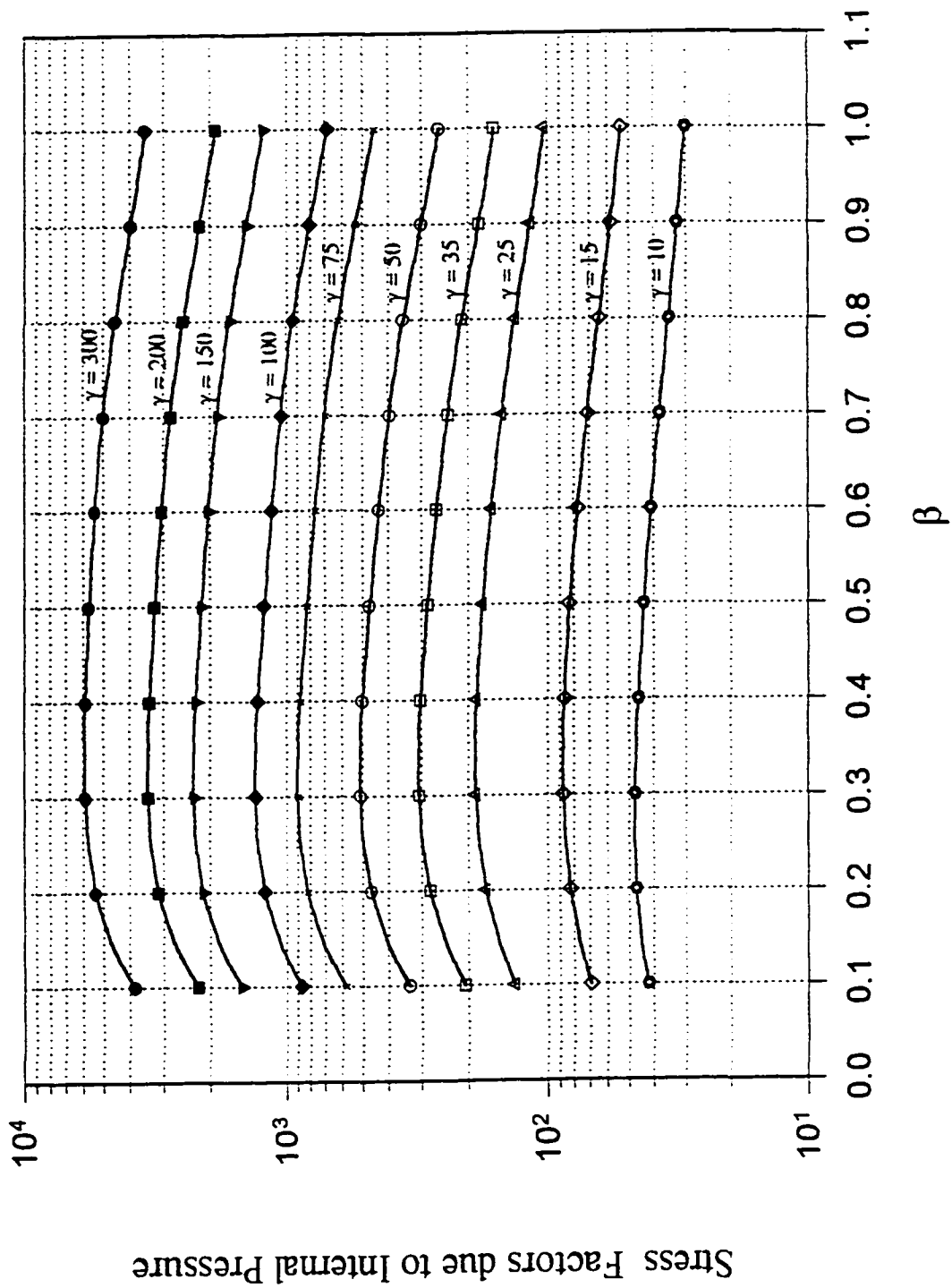
Figure E3: Circumferential pressure stress factors on the pipe at point A_U
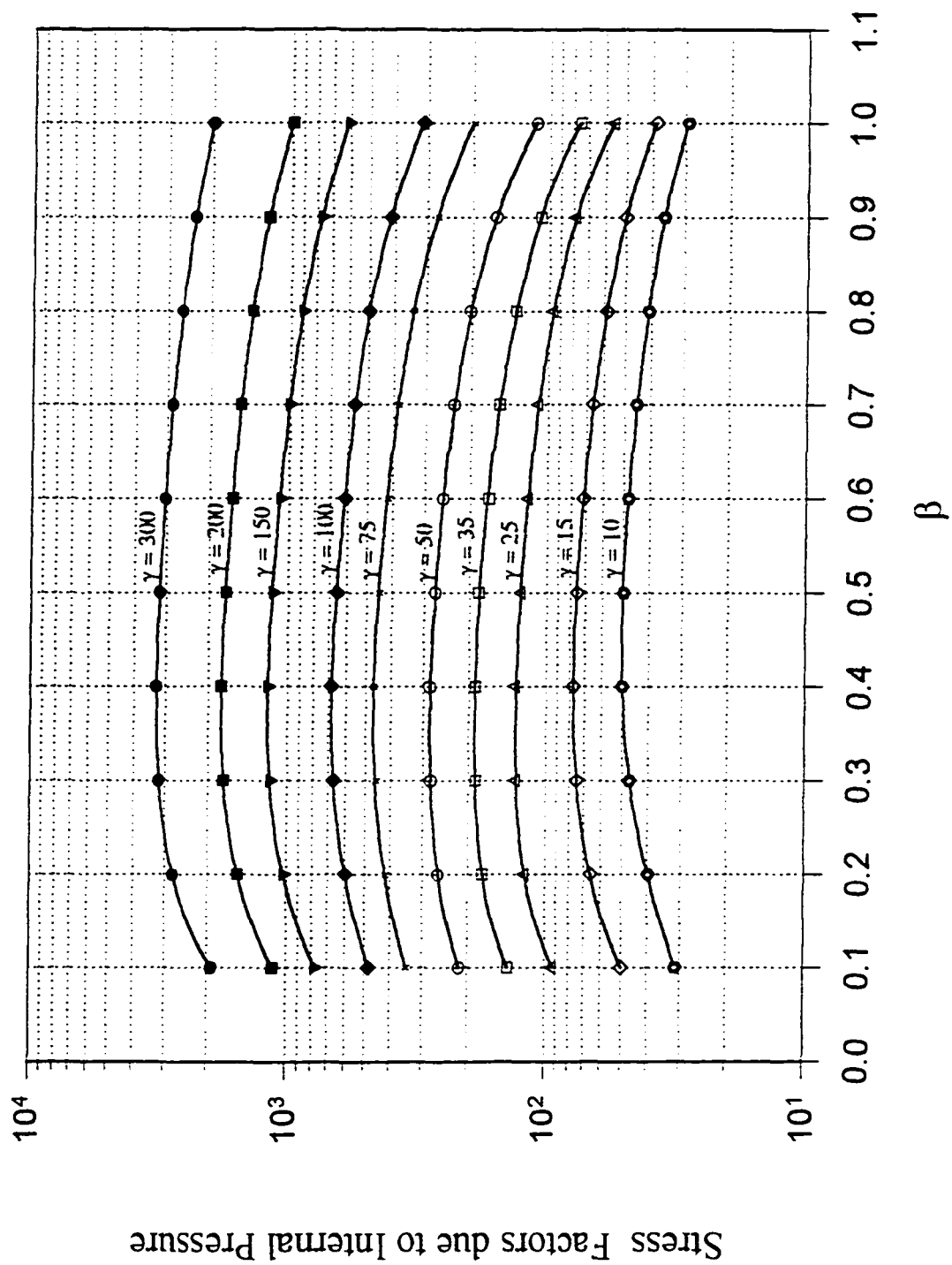
Figure E4: Circumferential pressure stress factors on the pipe at point A_1.
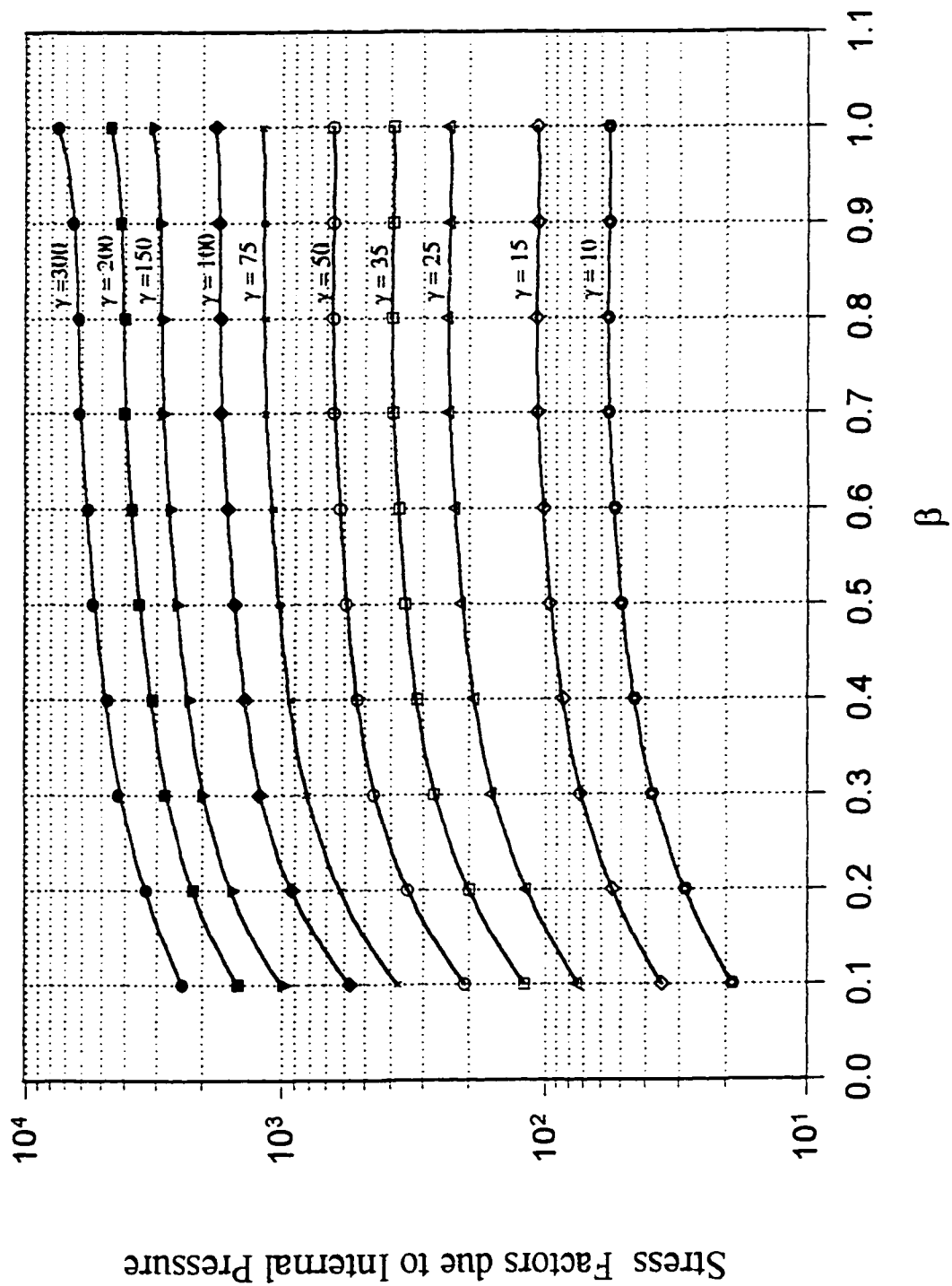
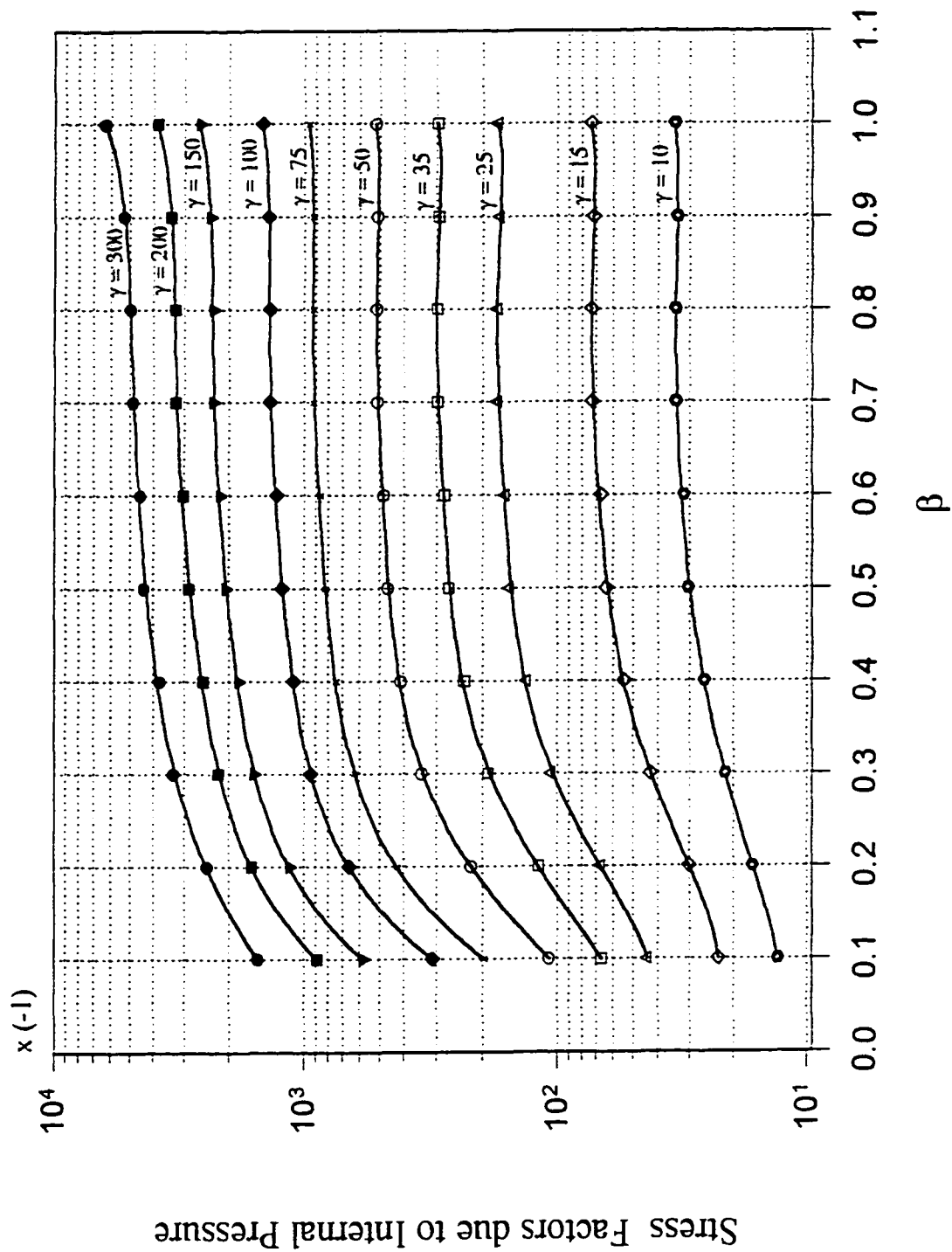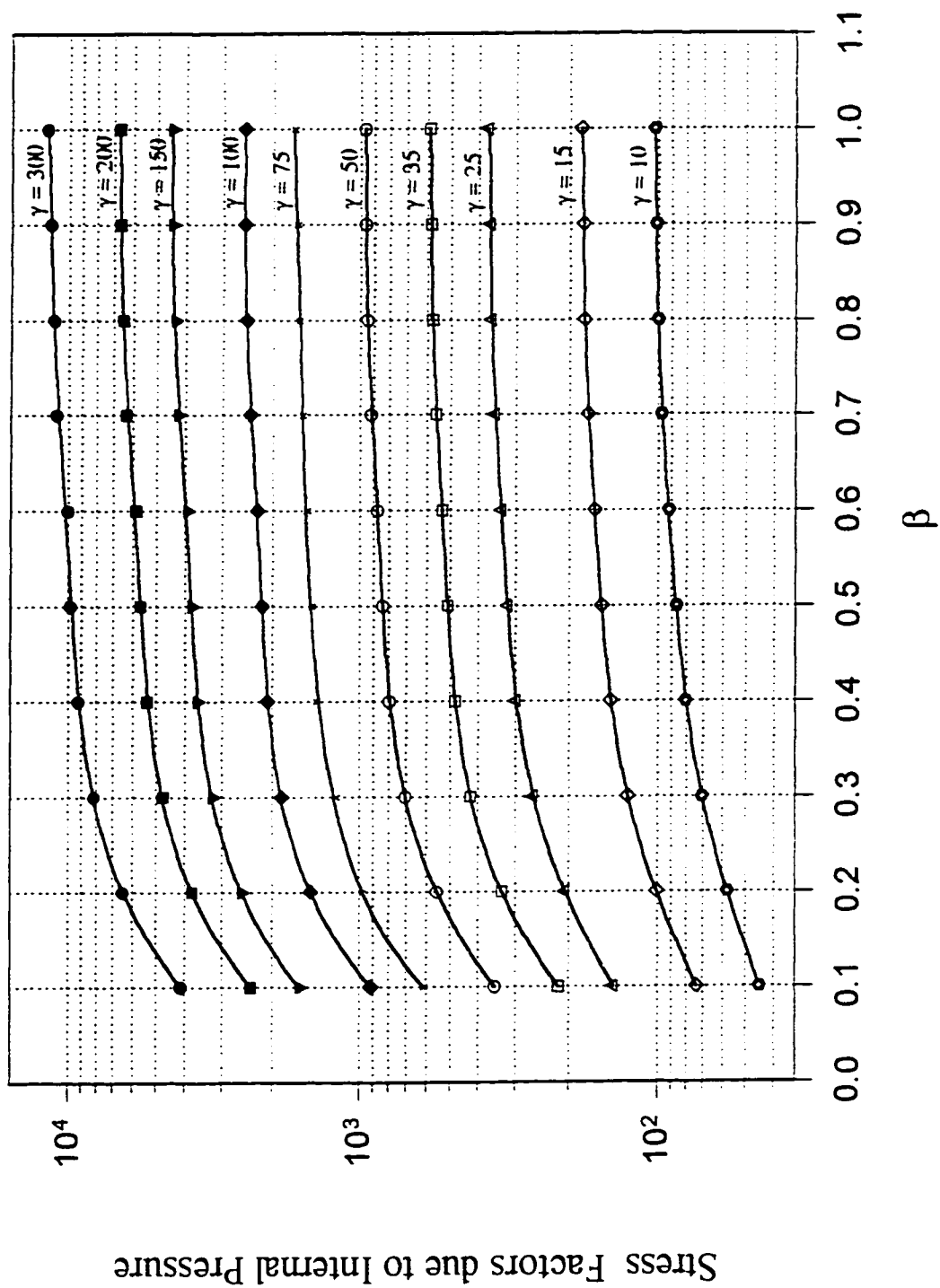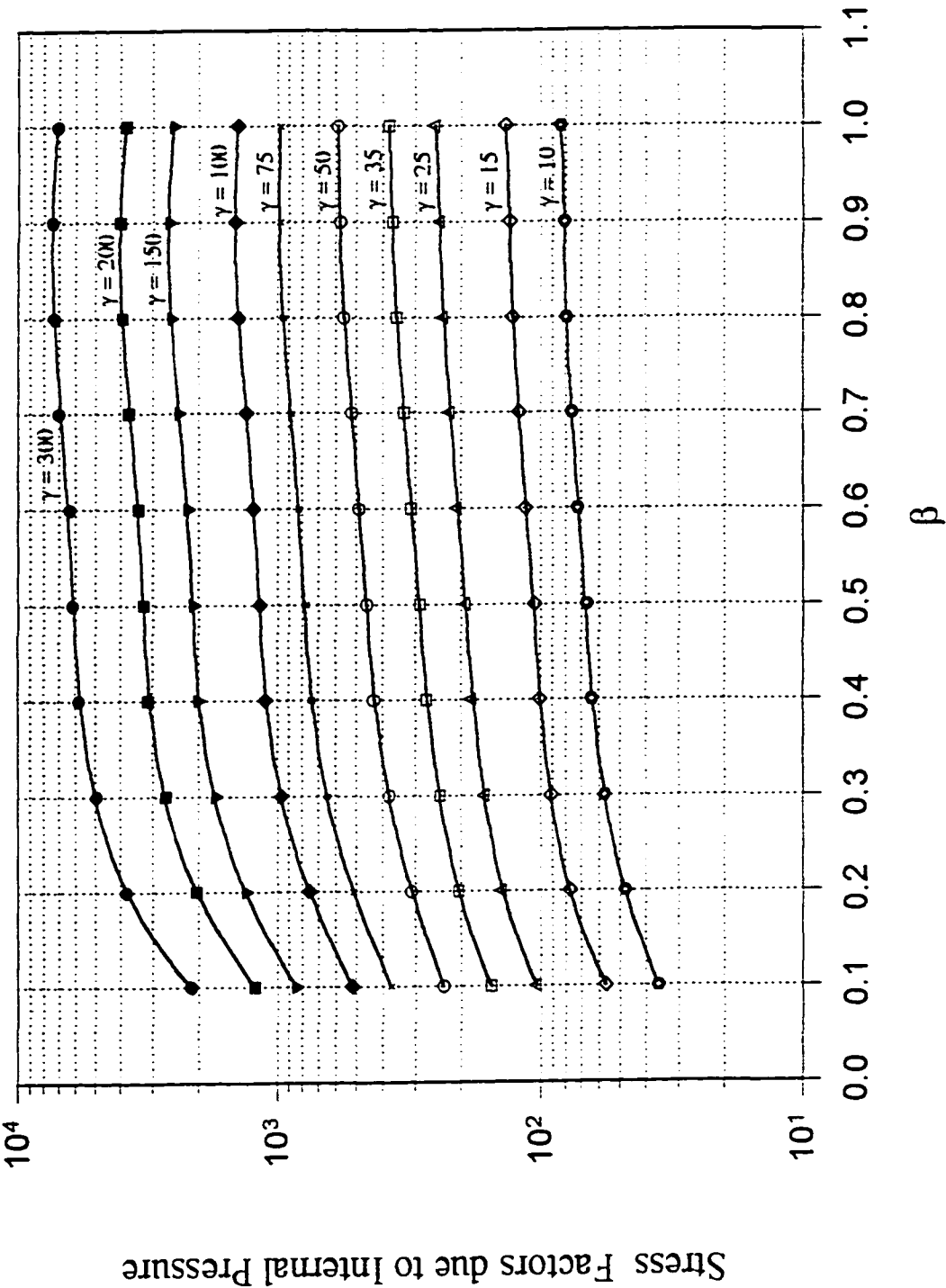**Figure E5:** Longitudinal pressure stress factors on the pipe at point B_{IJ}

Figure E6: Longitudinal pressure stress factors on the pipe at point B_1.

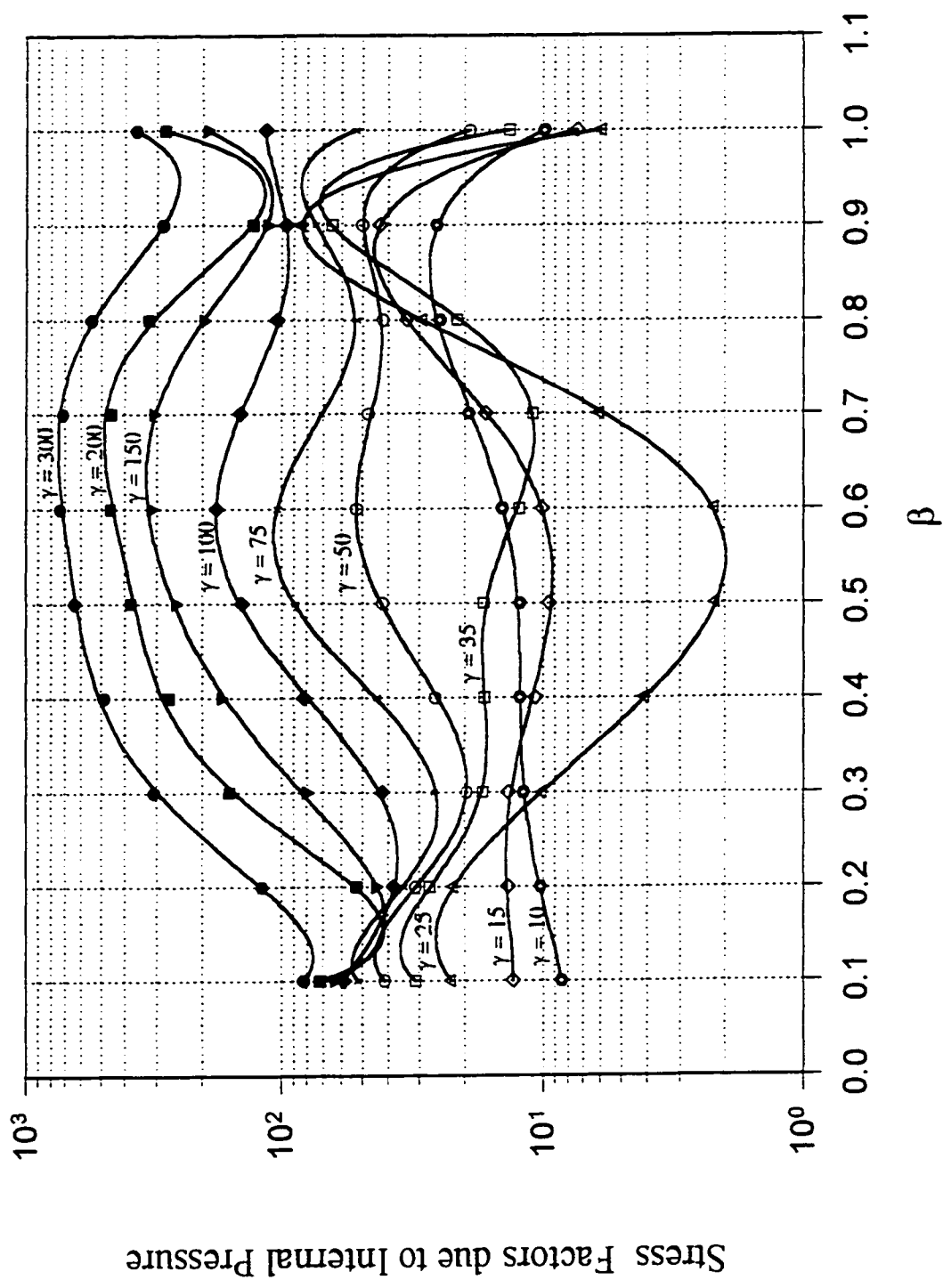**Figure E7:** Circumferential pressure stress factors on the pipe at point B_U

Figure E8: Circumferential pressure stress factors on the pipe at point B_l.

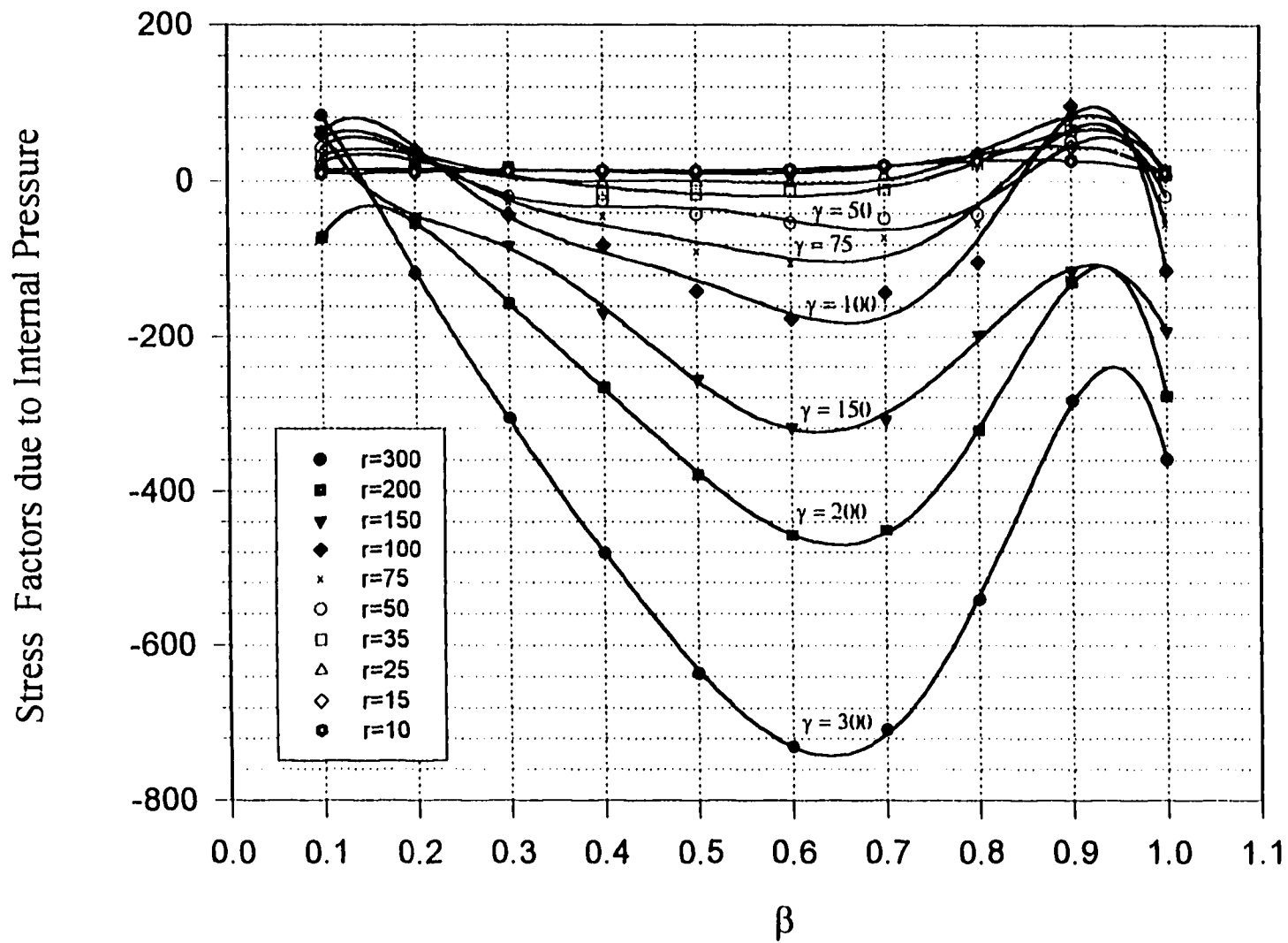**Figure E9a:** Longitudinal pressure stress factors on the pipe at point C_U

Figure E9b: Longitudinal pressure stress factors on the pipe at point C_U
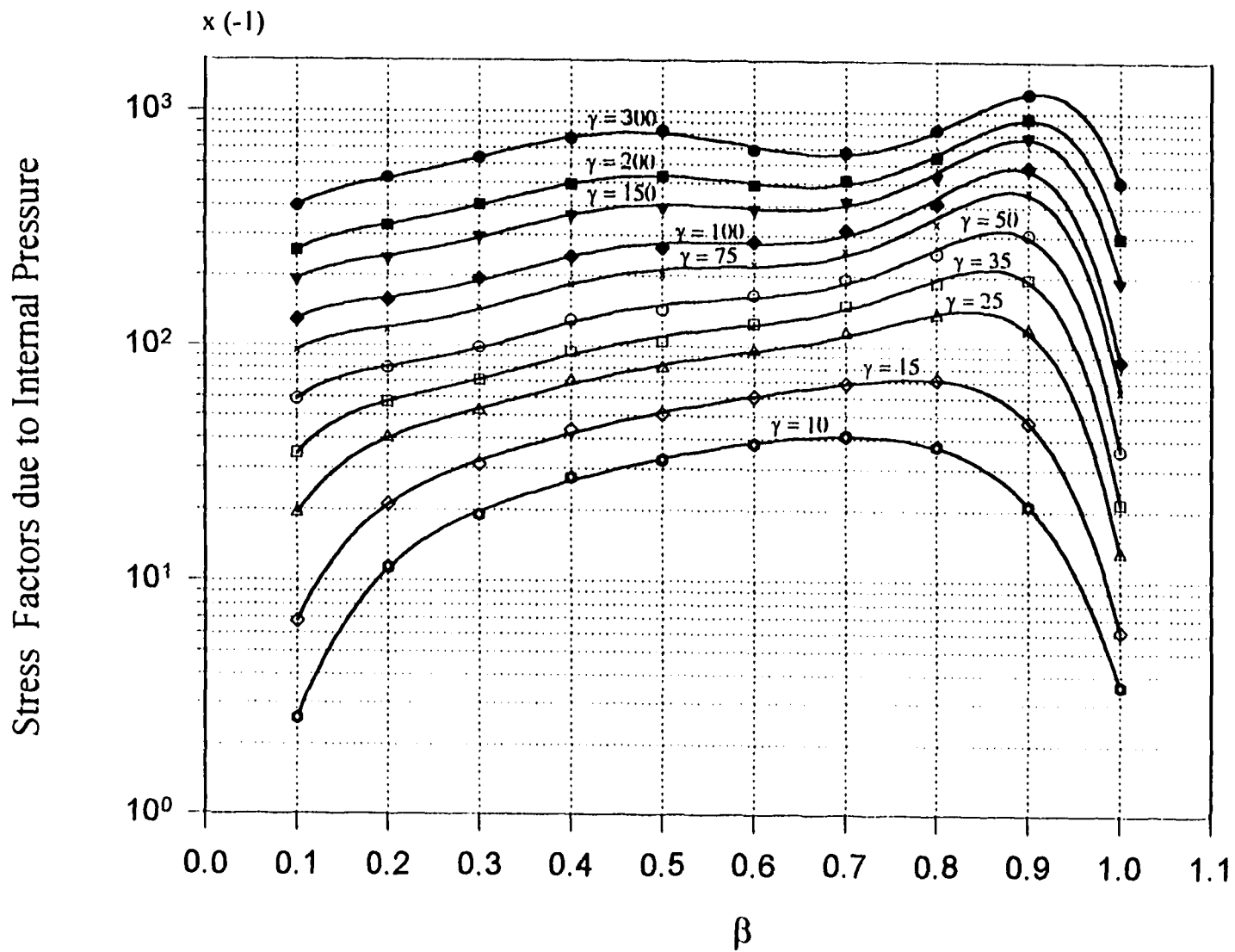
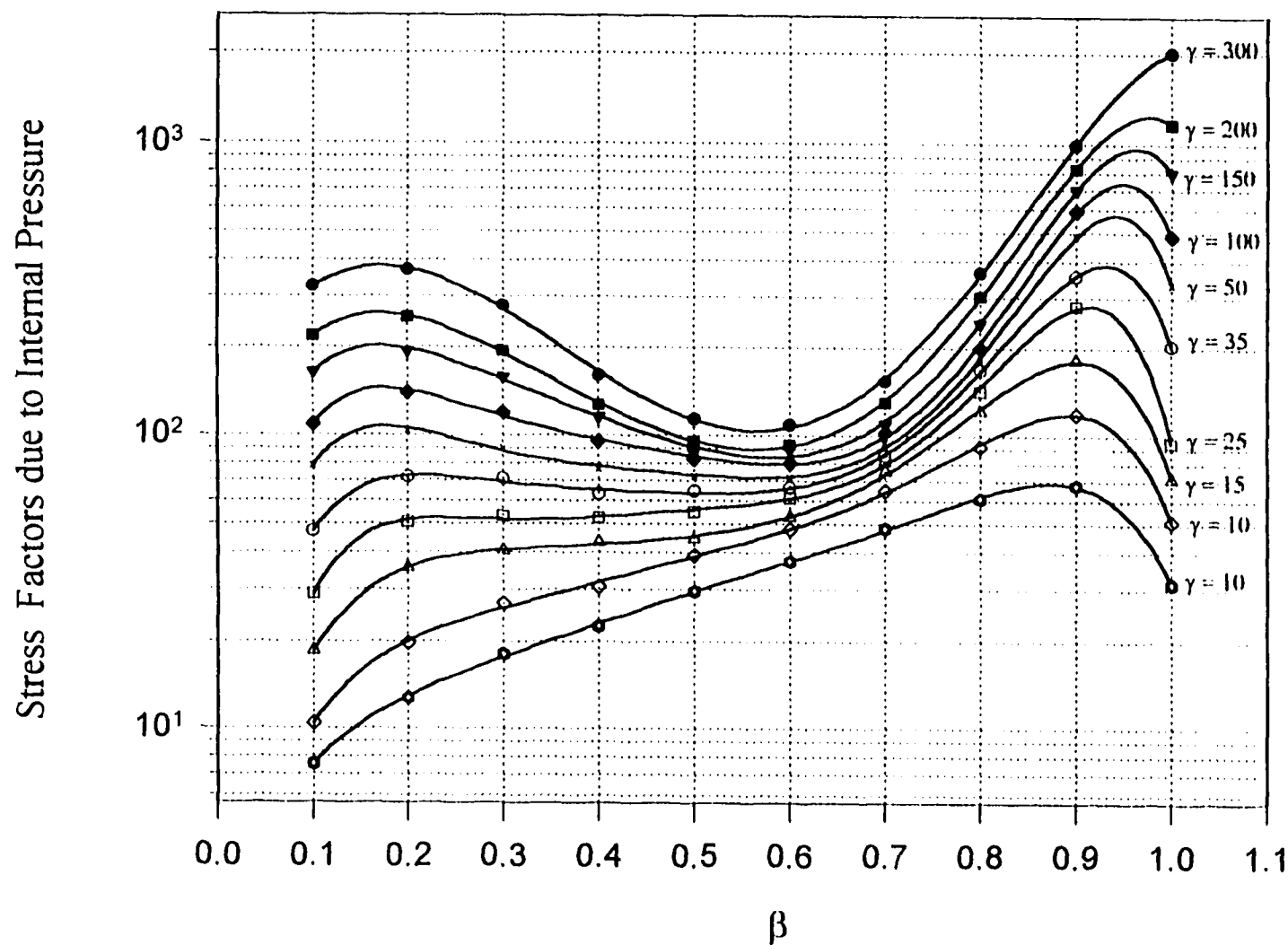**Figure E10:** Longitudinal pressure stress factors on the pipe at point C_I.

Figure E11: Circumferential pressure stress factors on the pipe at point C_u
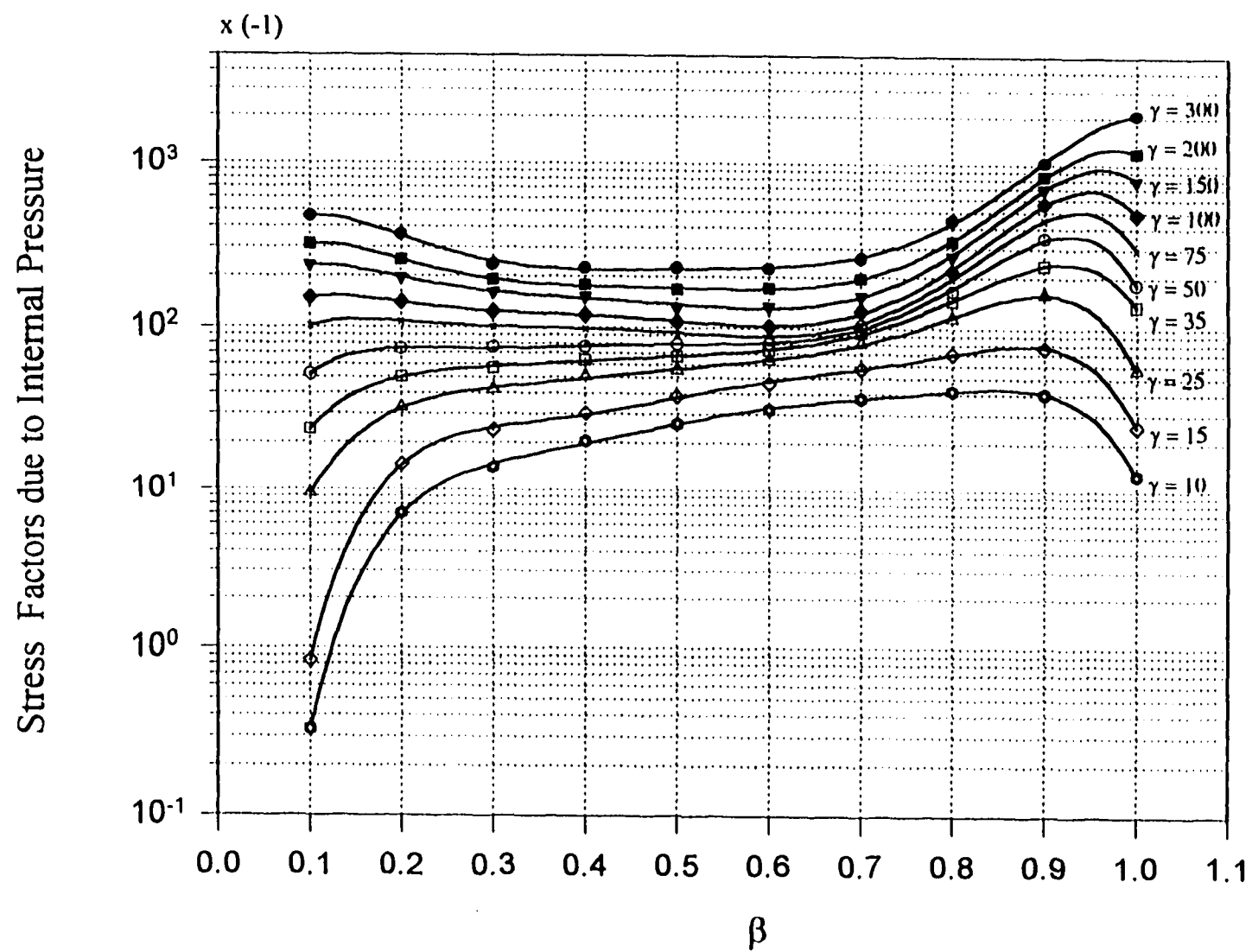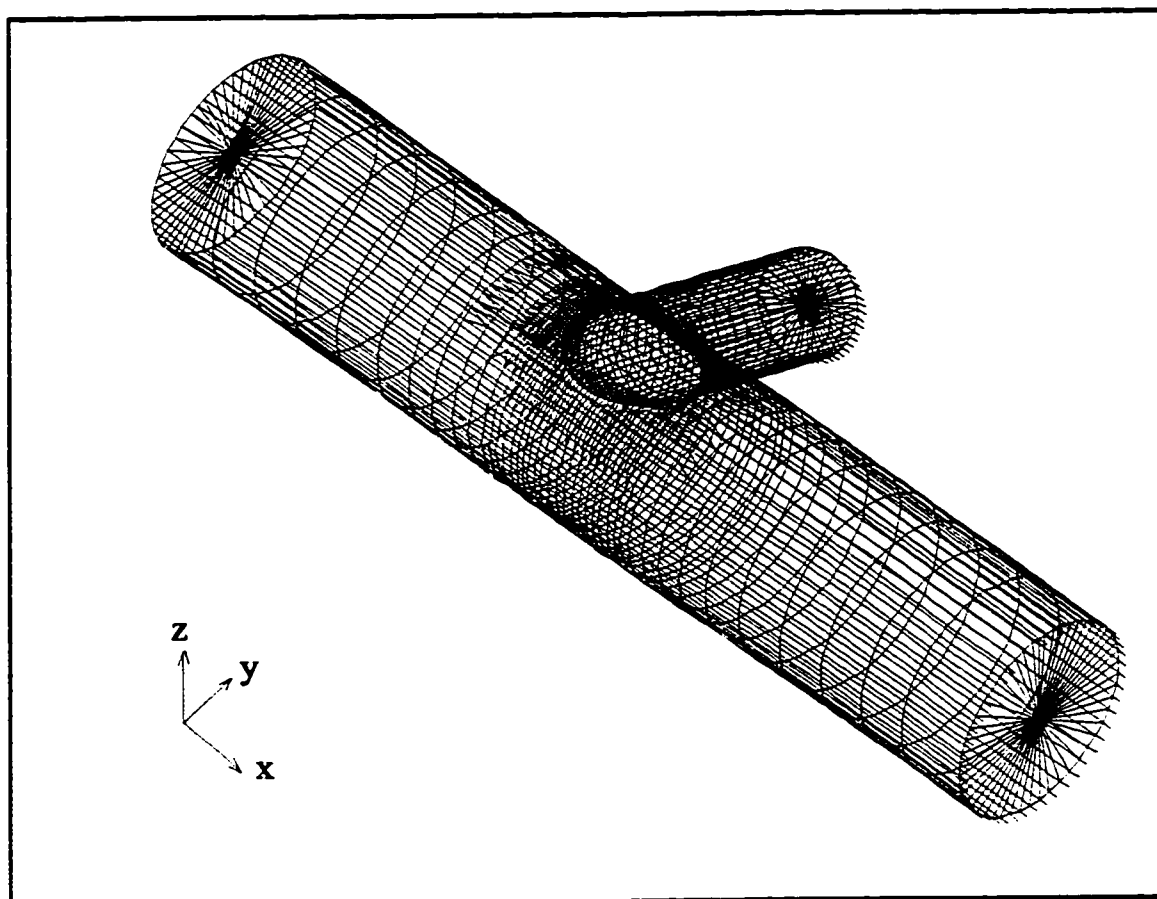
x (-1)

Stress Factors due to Internal Pressure

$\gamma = 300$
$\gamma = 200$
$\gamma = 150$
$\gamma = 100$
$\gamma = 75$
$\gamma = 50$
$\gamma = 35$
$\gamma = 25$
$\gamma = 15$
$\gamma = 10$

10^3

10^2

10^1

10^0

10^{-1}

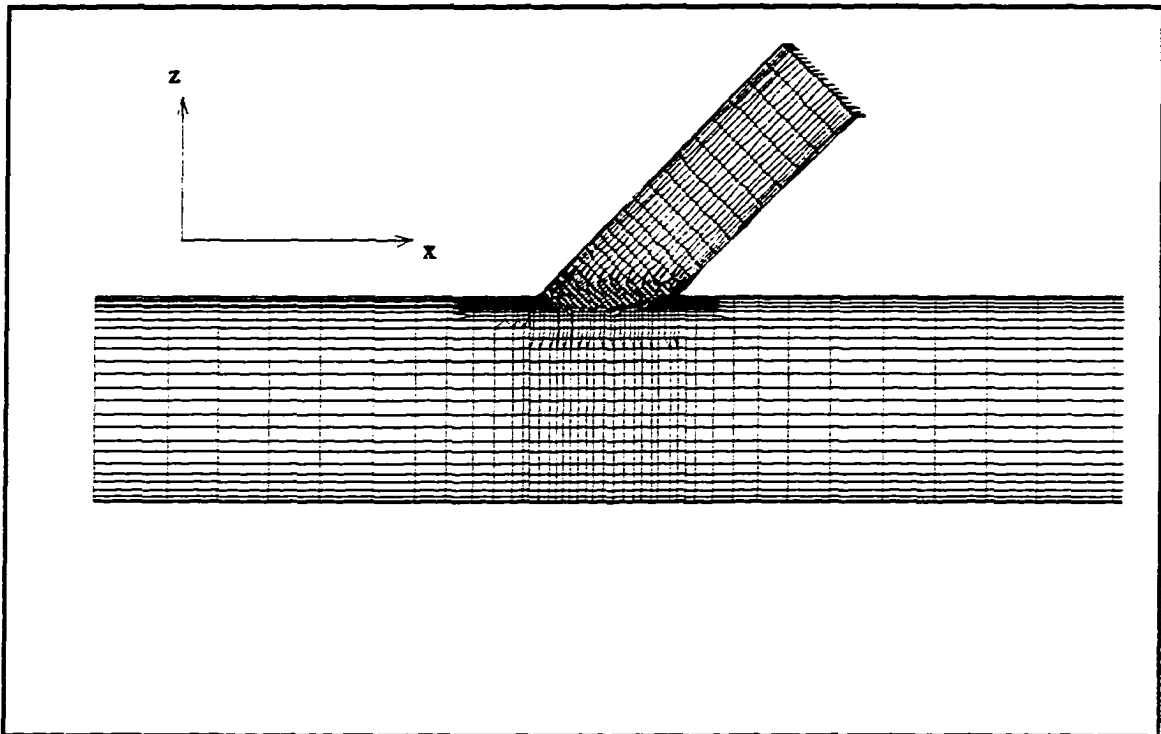0.0   0.1   0.2   0.3   0.4   0.5   0.6   0.7   0.8   0.9   1.0   1.1

β

Figure E12: Circumferential pressure stress factors on the pipe at point C_1.

APPENDIX F

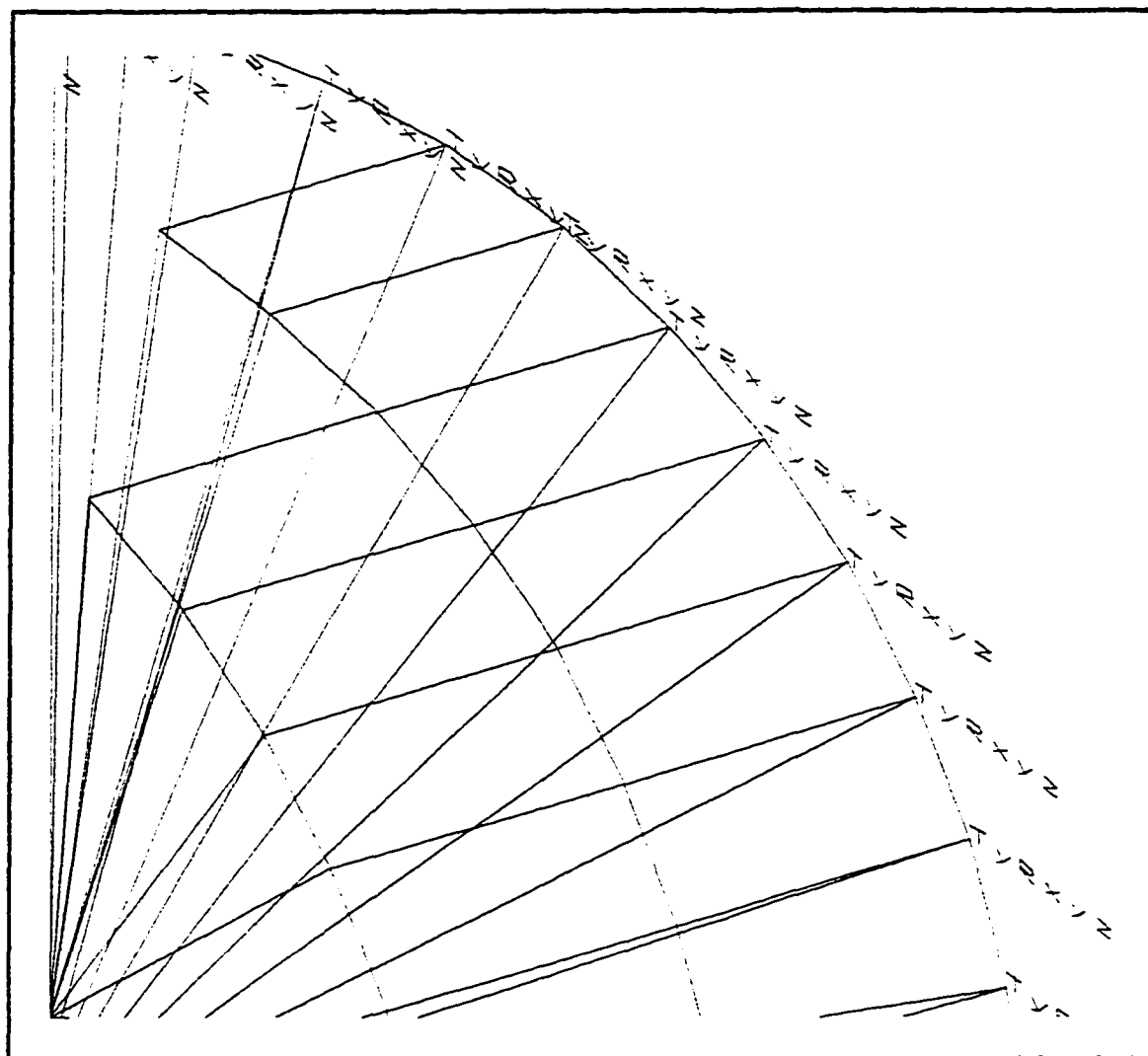# FIGURES OF 3D FINITE ELEMENT MODELS

113

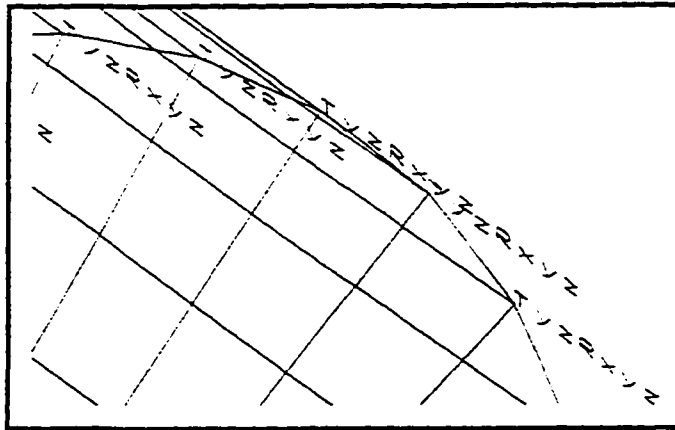**Figure F1:** A full 3D finite element model

Figure F2: A full 3D pipe-nozzle model with 45 degree angle
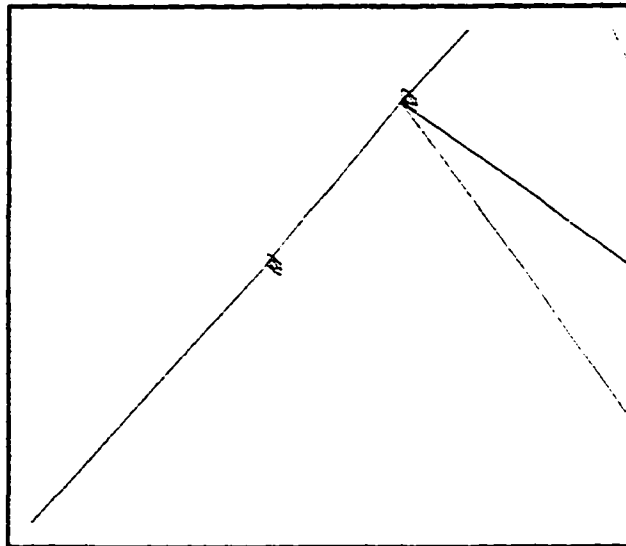
nozzle free in X and Z directions

Figure F3: The boundary conditions on the nozzle end

a. At the simple supported end
(free in X direction)

b. At the clamped end

Figure F4: The boundary conditions on the pipe end
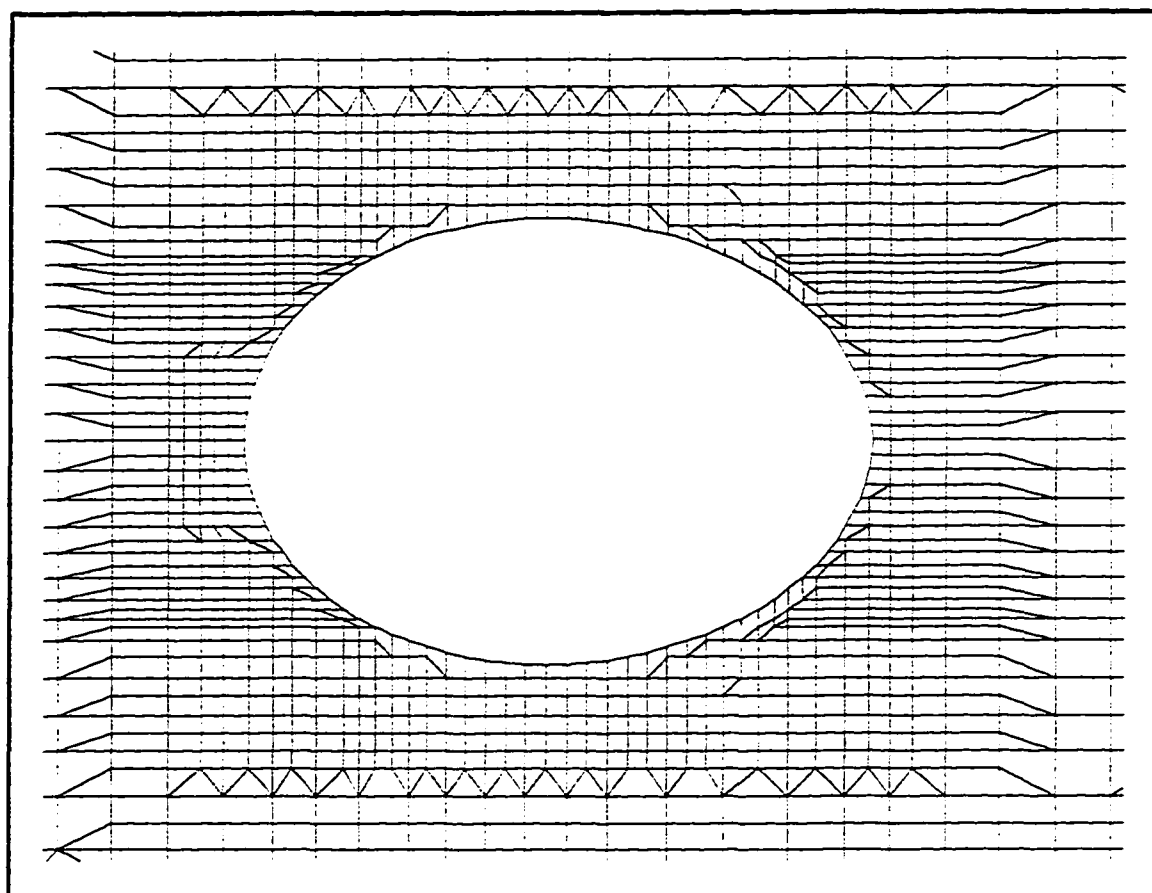
number of nodes = 10796
number of elements = 5520
96 node point on the pipe-nozzle juncture

Figure F5: Pipe-nozzle juncture with $\beta = 0.1$
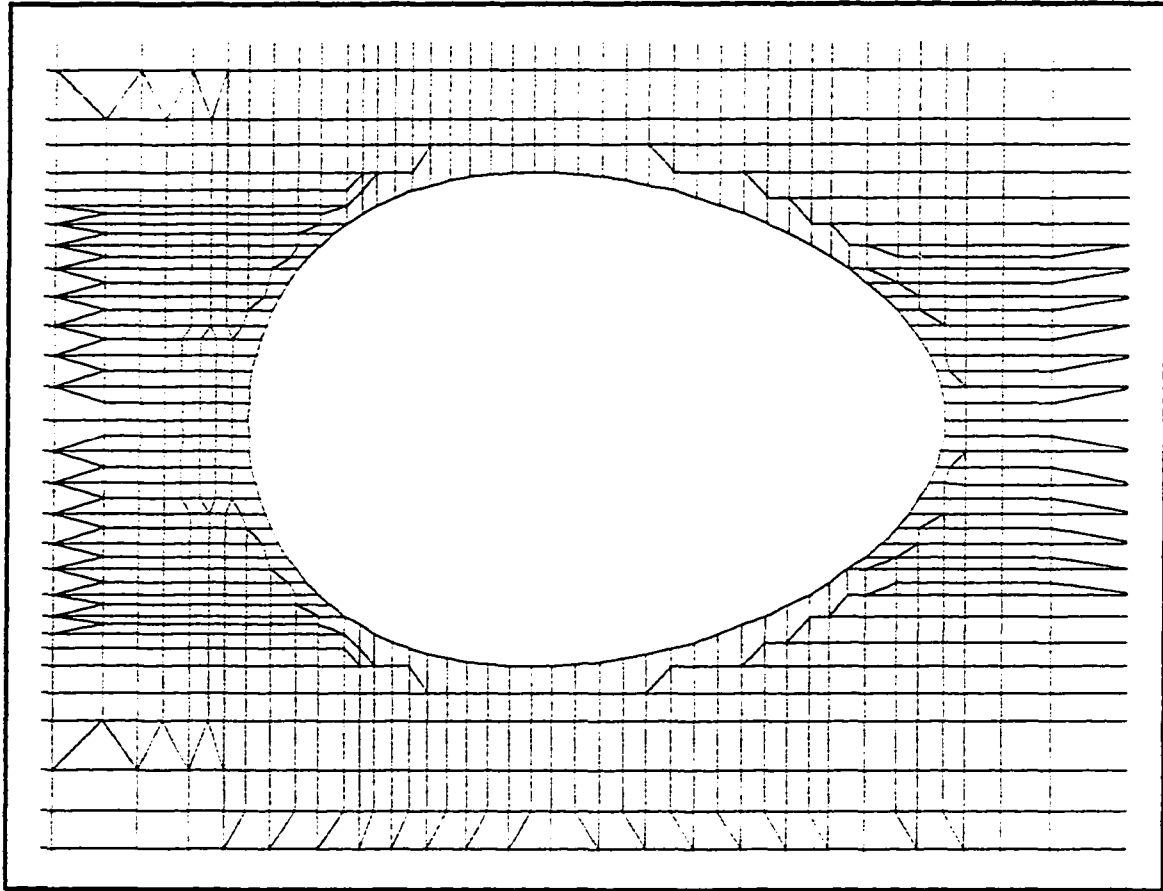
number of nodes = 8472
number of elements = 4286
96 node point on the pipe-nozzle juncture

Figure F6: Pipe-nozzle juncture with β = 0.5
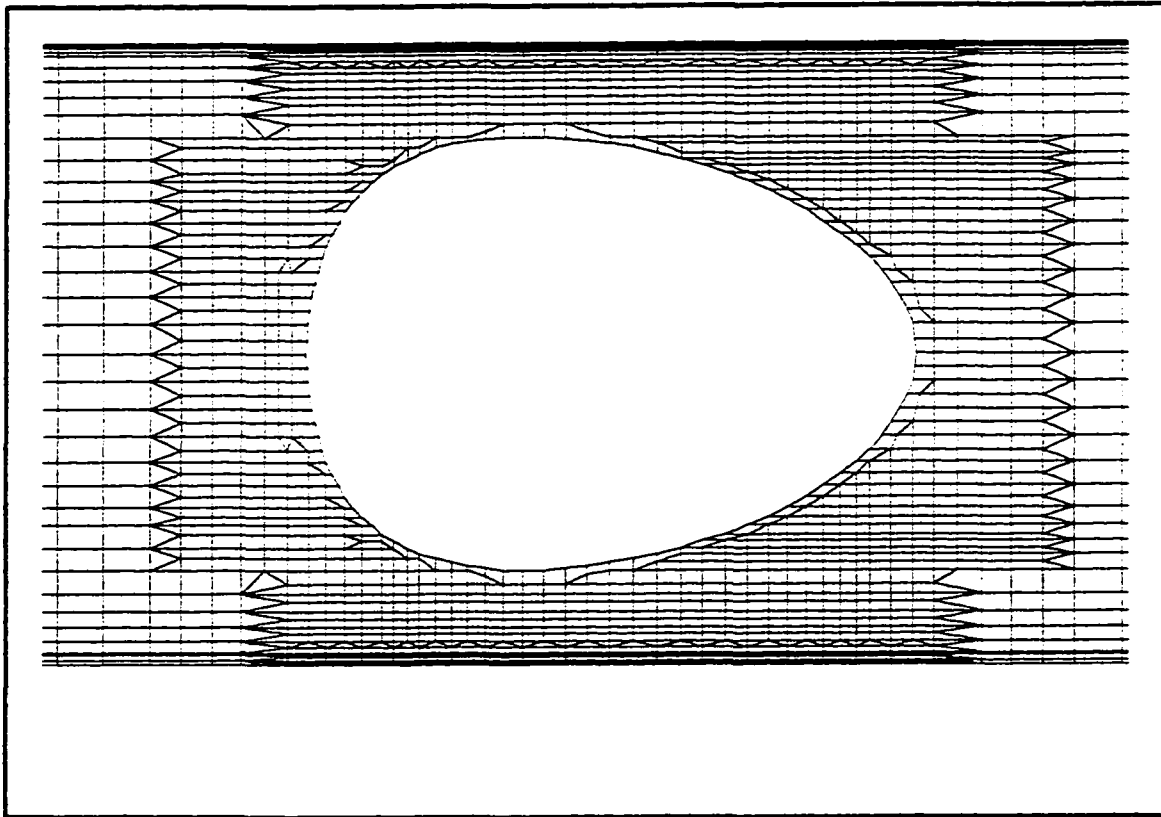
number of nodes = 8784
number of elements = 4484
96 node point on the pipe-nozzle juncture

Figure F7: Pipe-nozzle juncture with β = 0.9
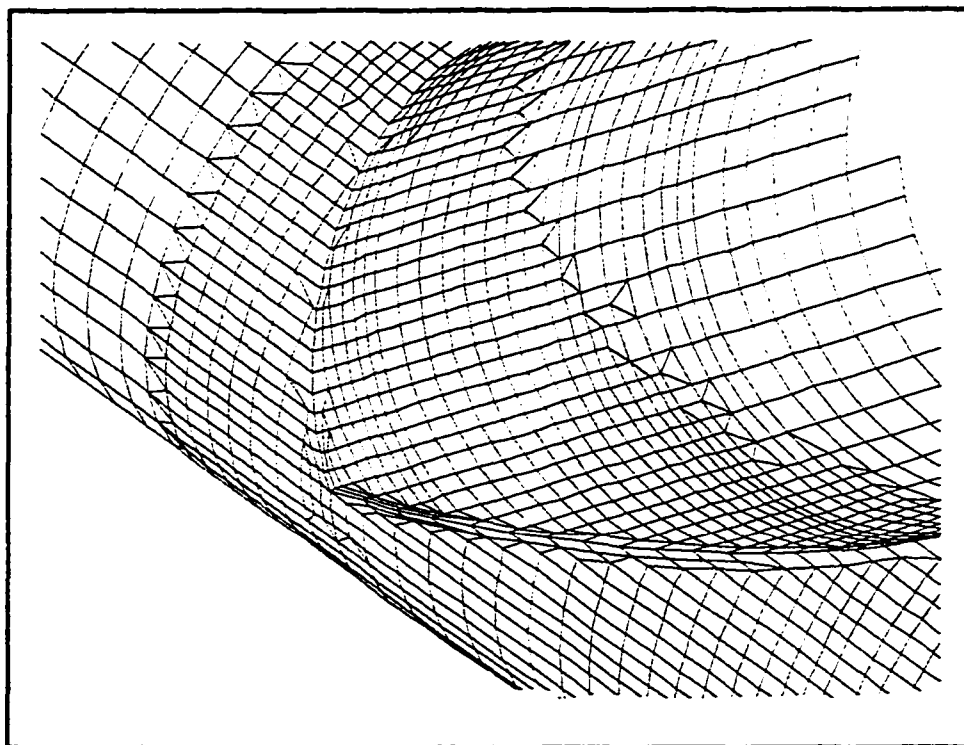
(isometric view)
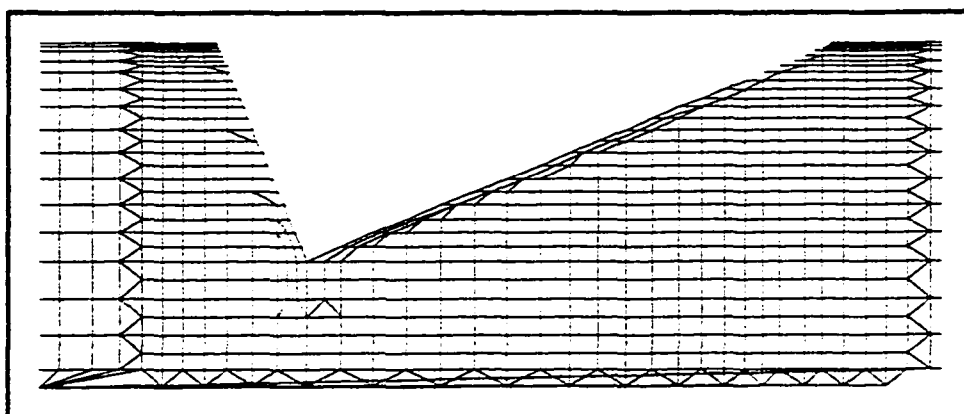
(side view)
96 node point at the pipe-nozzle juncture

Figure F8: Pipe-nozzle juncture with $\beta = 1.0$
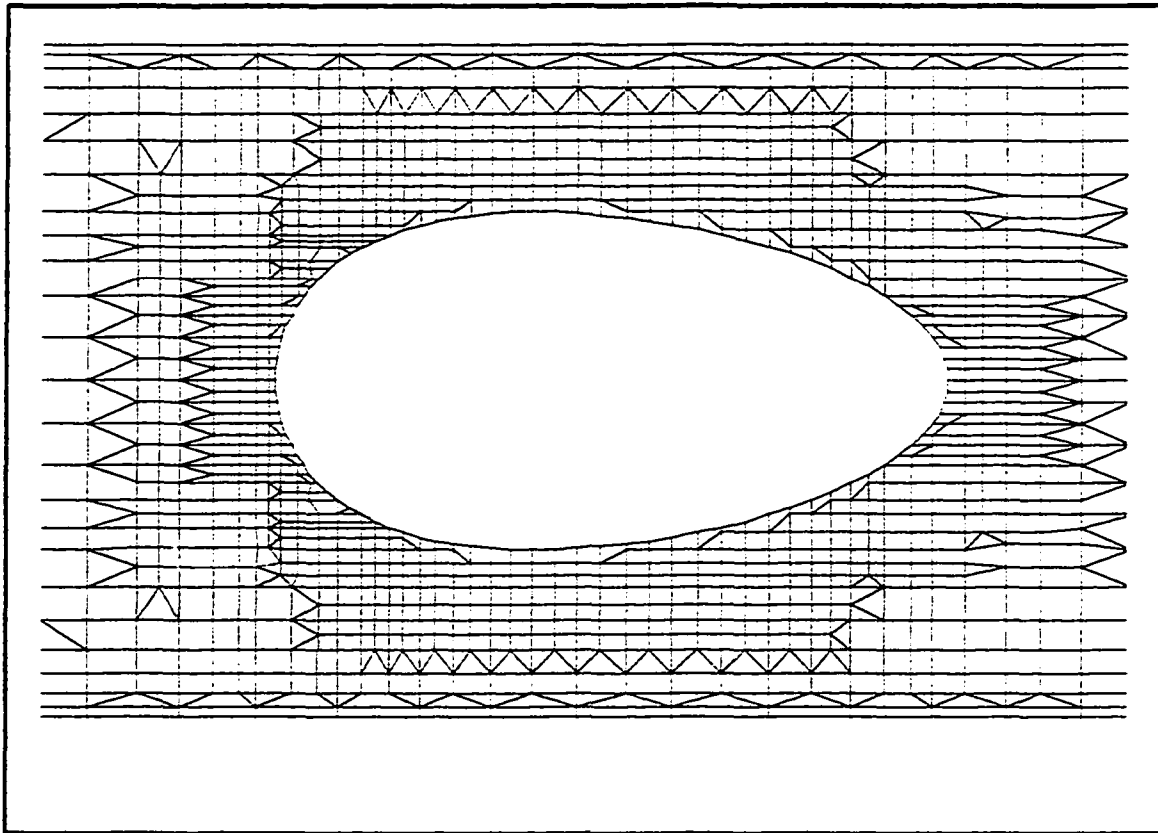
96 node point on the pipe-nozzle juncture (top view)

Figure F9: Pipe-nozzle juncture with 30° degree intersection

APPENDIX G

FIGURES FOR STRESSES NEAR THE NOZZLE JUNCTURE

123
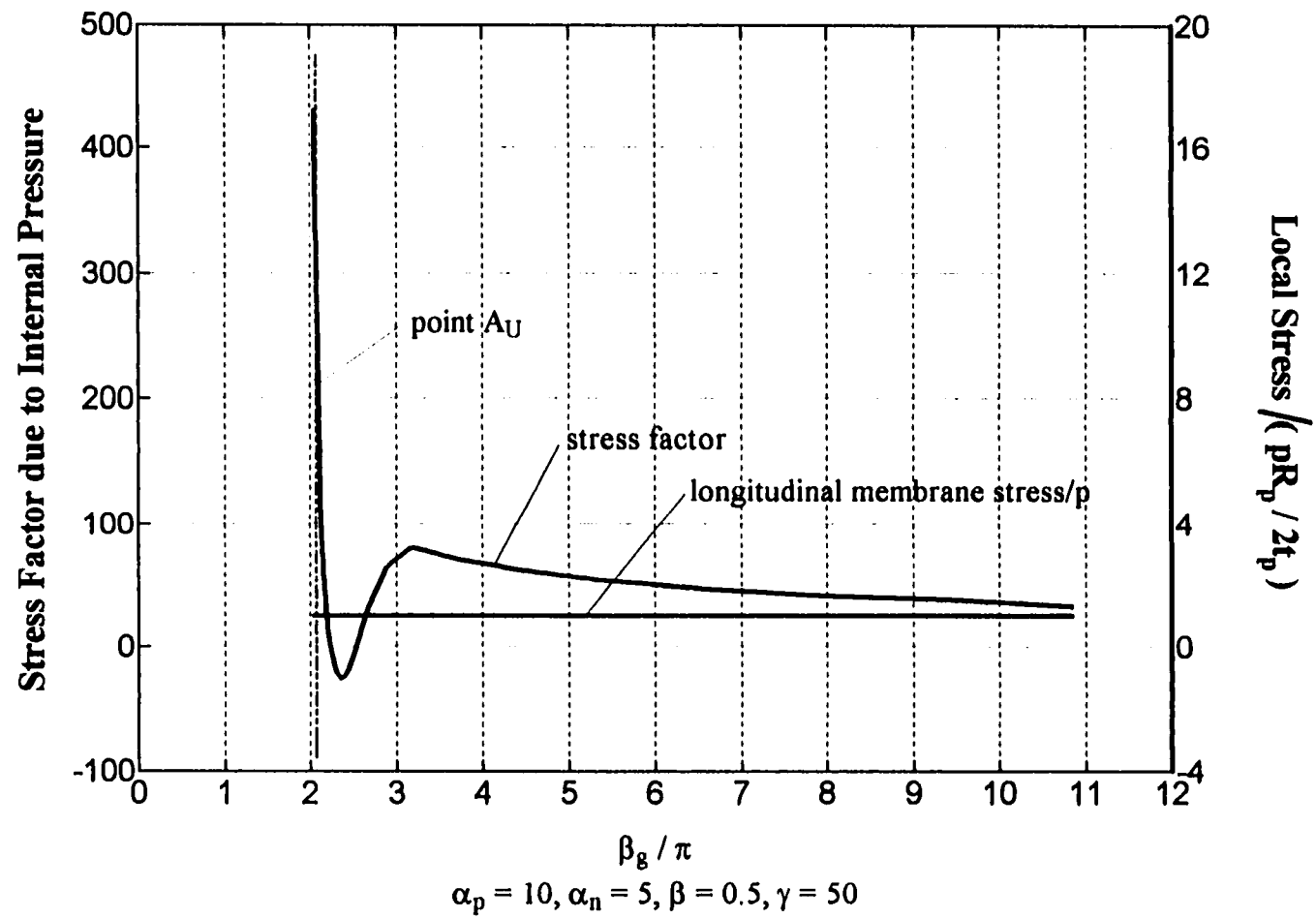
Figure G1: The variation of stress factor away from point A_U of pipe in longitudinal direction

$\alpha_p = 10$, $\alpha_n = 5$, $\beta = 0.5$, $\gamma = 50$

$\alpha_p = 10, \alpha_n = 5, \beta = 0.5, \gamma = 50$
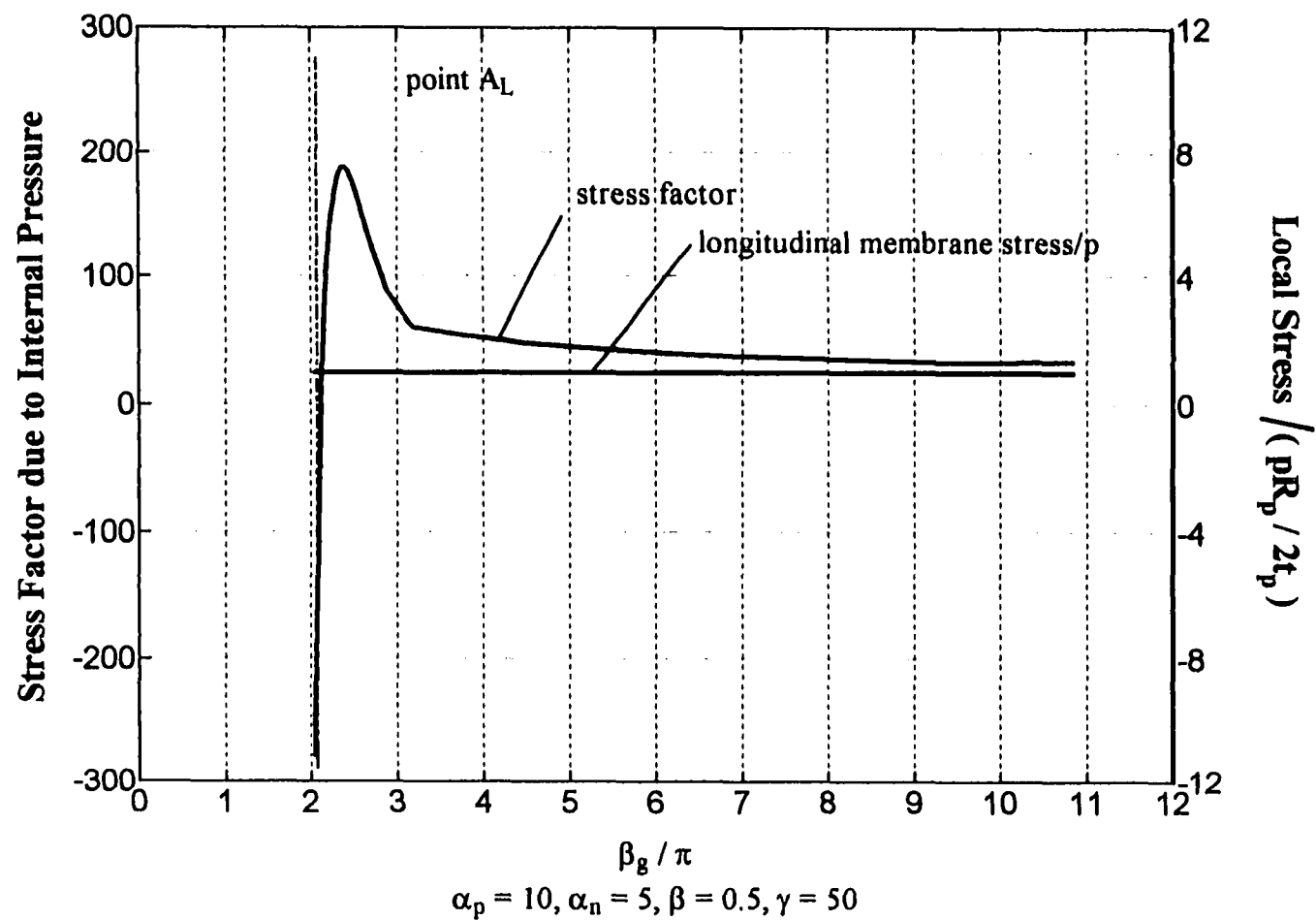
Figure G2: The variation of stress factor away from point A_L
of pipe in longitudinal direction
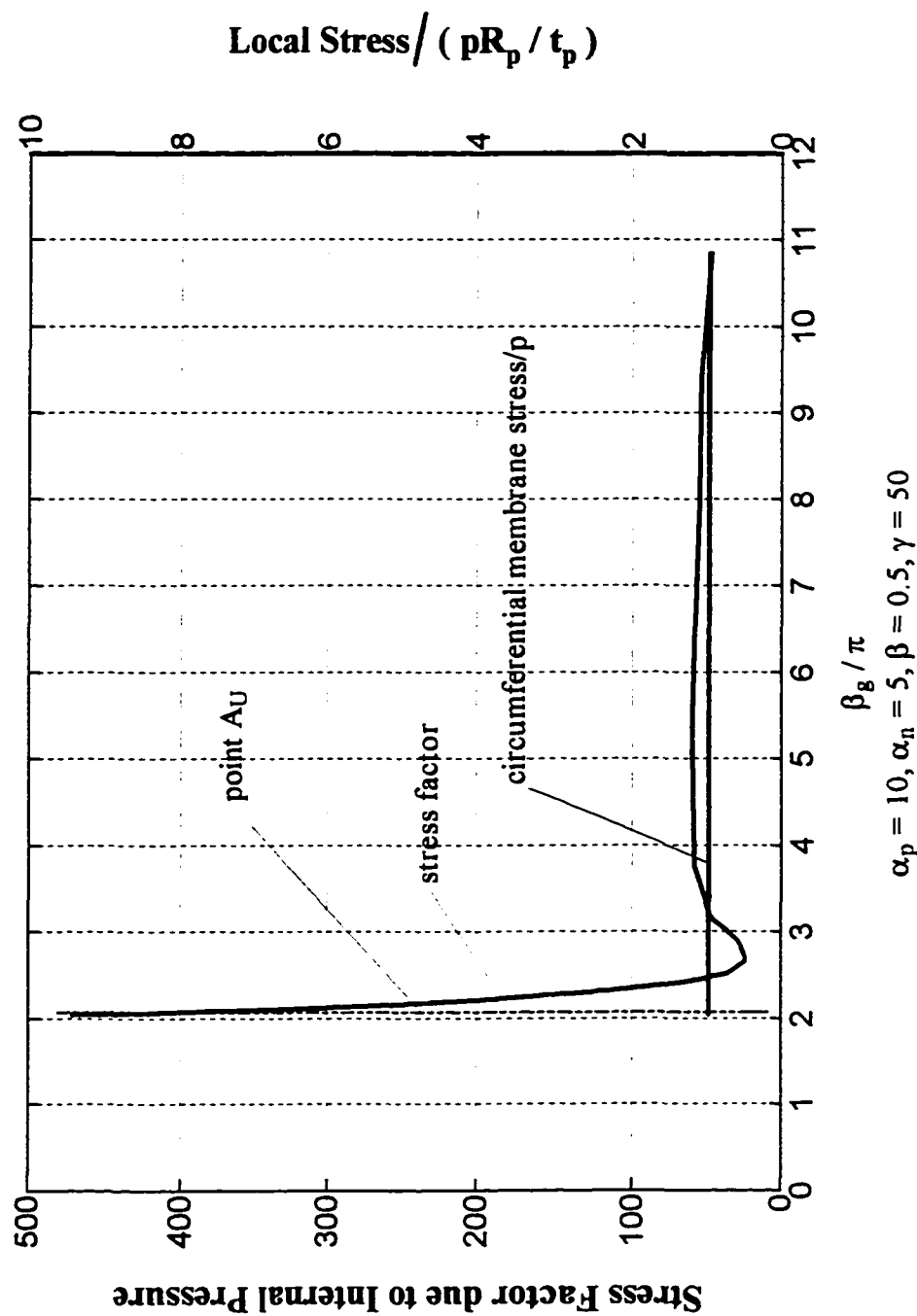
Figure G3: The variation of stress factor away from point A_U of pipe in circumferential direction

$\alpha_p = 10, \alpha_n = 5, \beta = 0.5, \gamma = 50$

$$\alpha_p = 10, \alpha_n = 5, \beta = 0.5, \gamma = 50$$
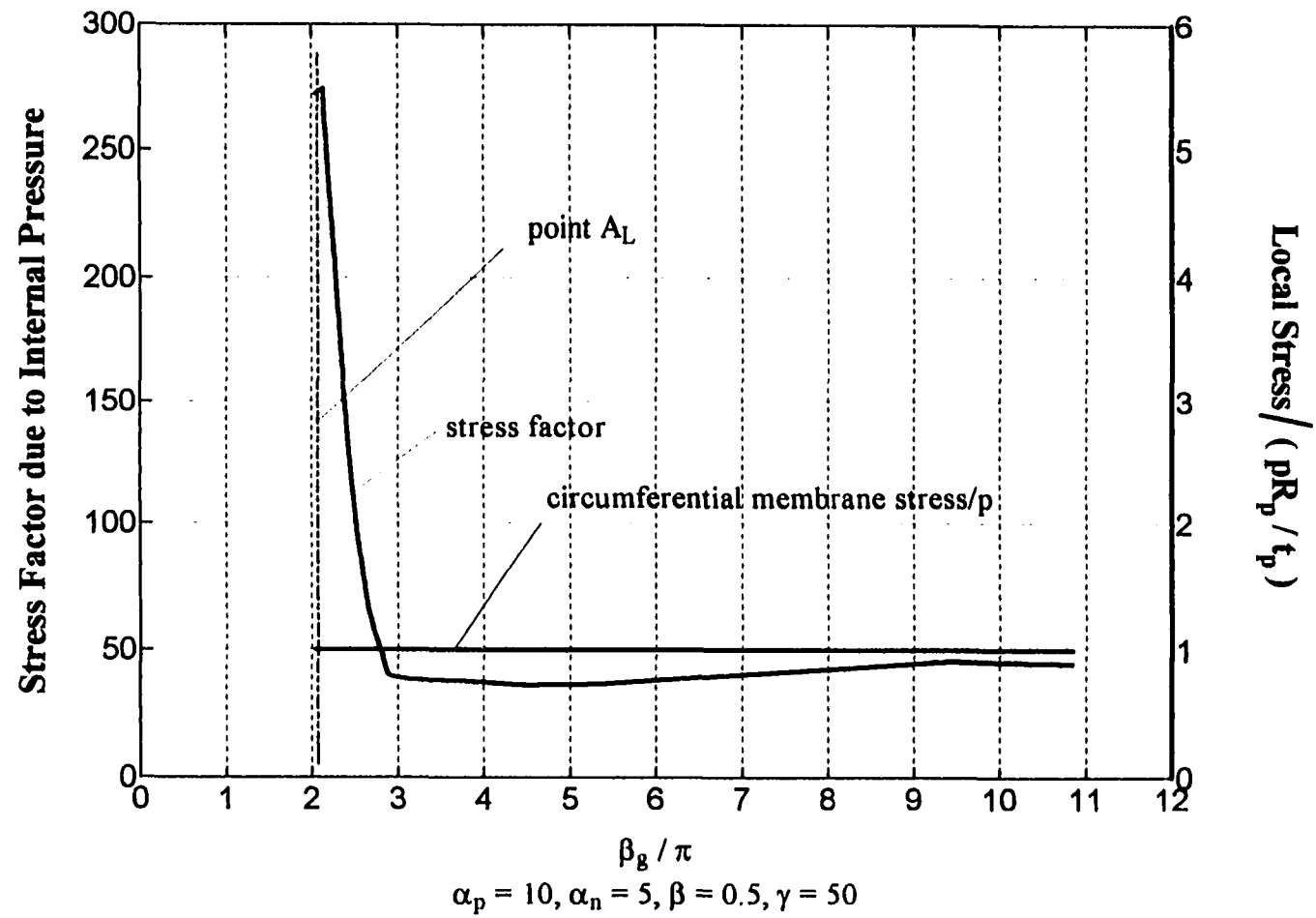
Figure G4: The variation of stress factor away from point A_L of pipe in circumferential direction

$$\alpha_p = 10, \alpha_n = 5, \beta = 0.5, \gamma = 50$$
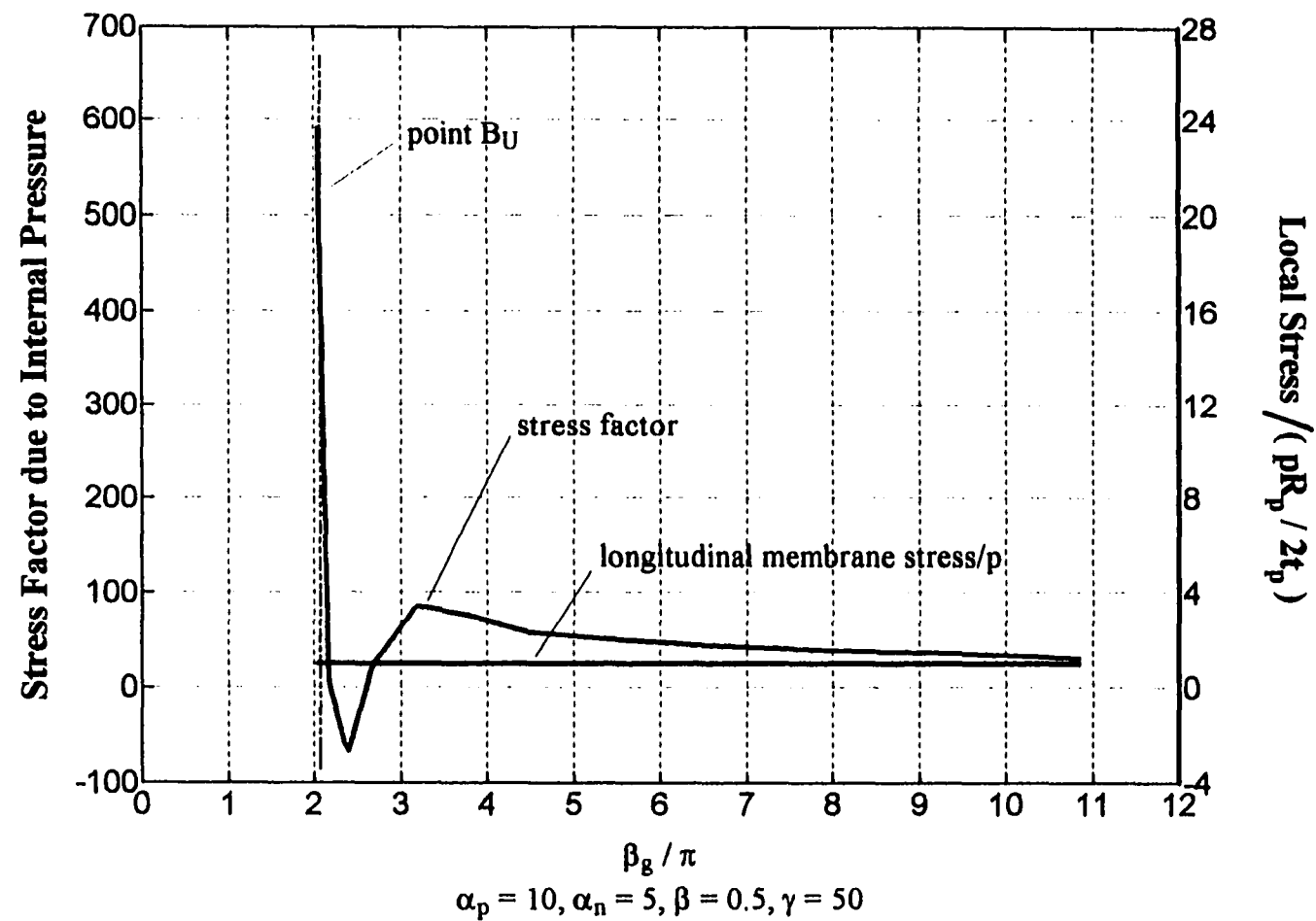
Figure G5: The variation of stress factor away from point B_U of pipe in longitudinal direction
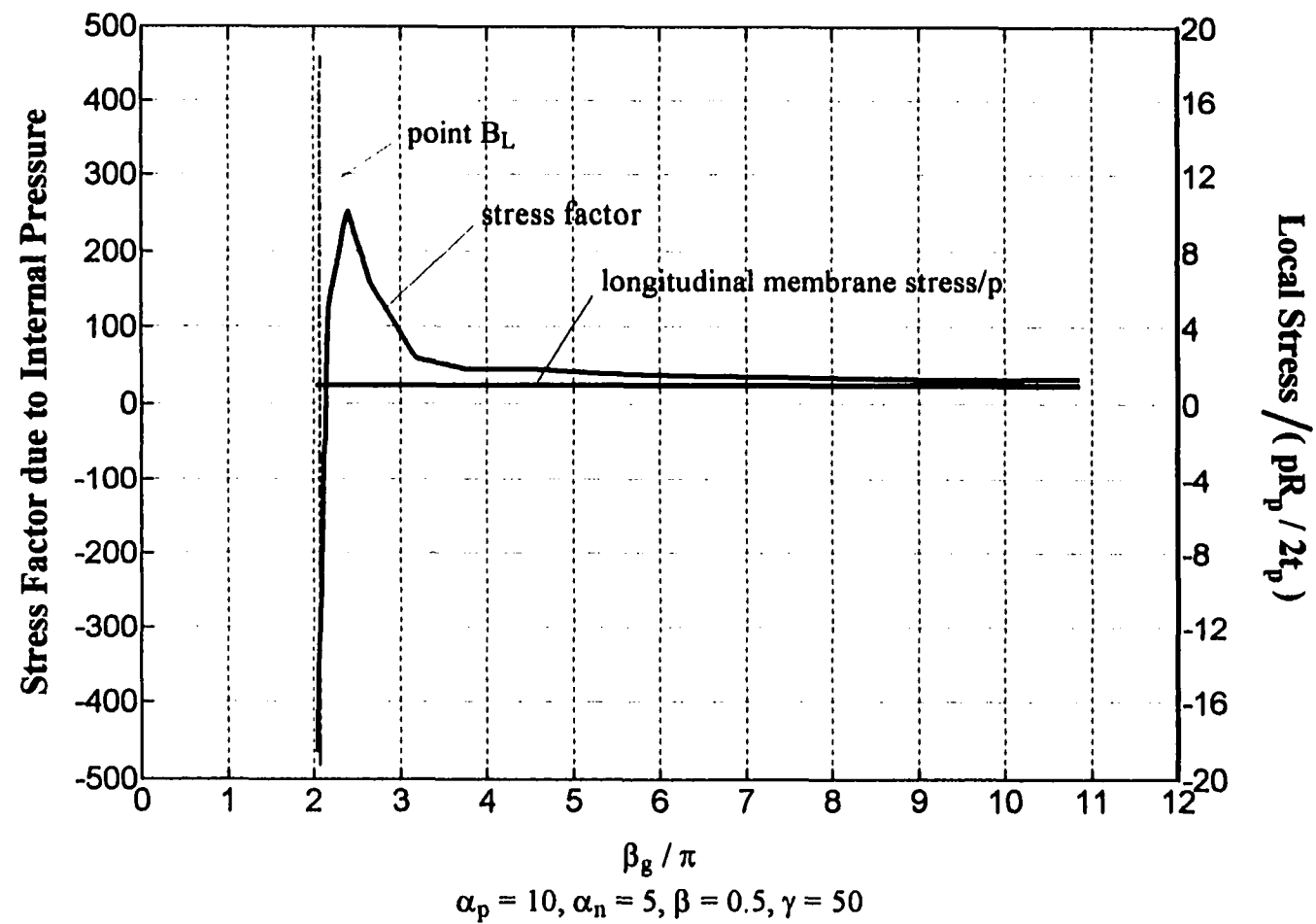
Figure G6: The variation of stress factor away from point B_L of pipe in longitudinal direction

In the figure the curves are labelled "point B_L", "stress factor", and "longitudinal membrane stress/p". The horizontal axis is β_g / π and the vertical axes are "Stress Factor due to Internal Pressure" (left) and "Local Stress /($pR_p / 2t_p$)" (right).

$$\alpha_p = 10, \ \alpha_n = 5, \ \beta = 0.5, \ \gamma = 50$$
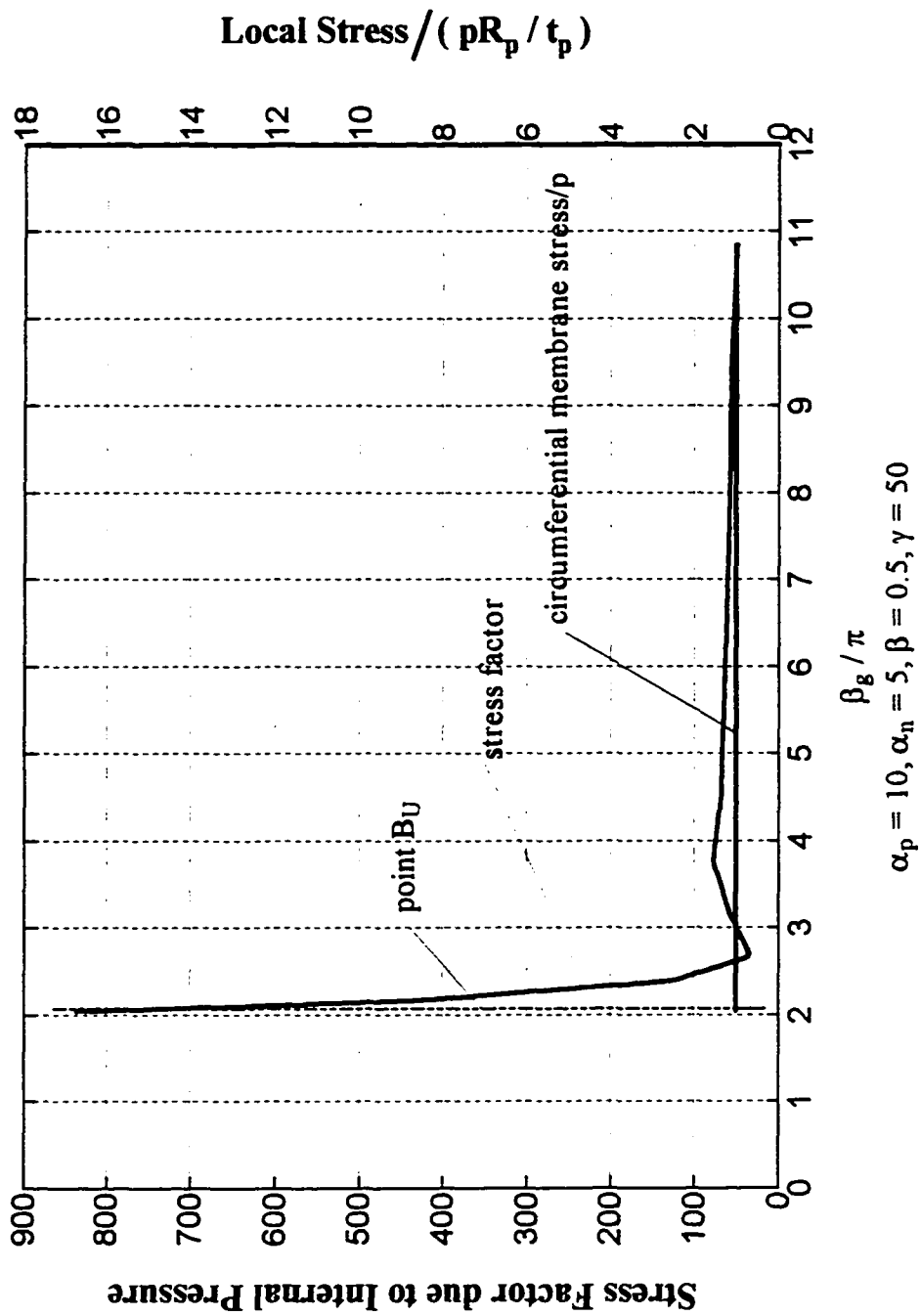
Figure G7: The variation of stress factor away from point B_U of pipe in circumferetial direction

$\alpha_p = 10, \alpha_n = 5, \beta = 0.5, \gamma = 50$

$\alpha_p = 10, \alpha_n = 5, \beta = 0.5, \gamma = 50$
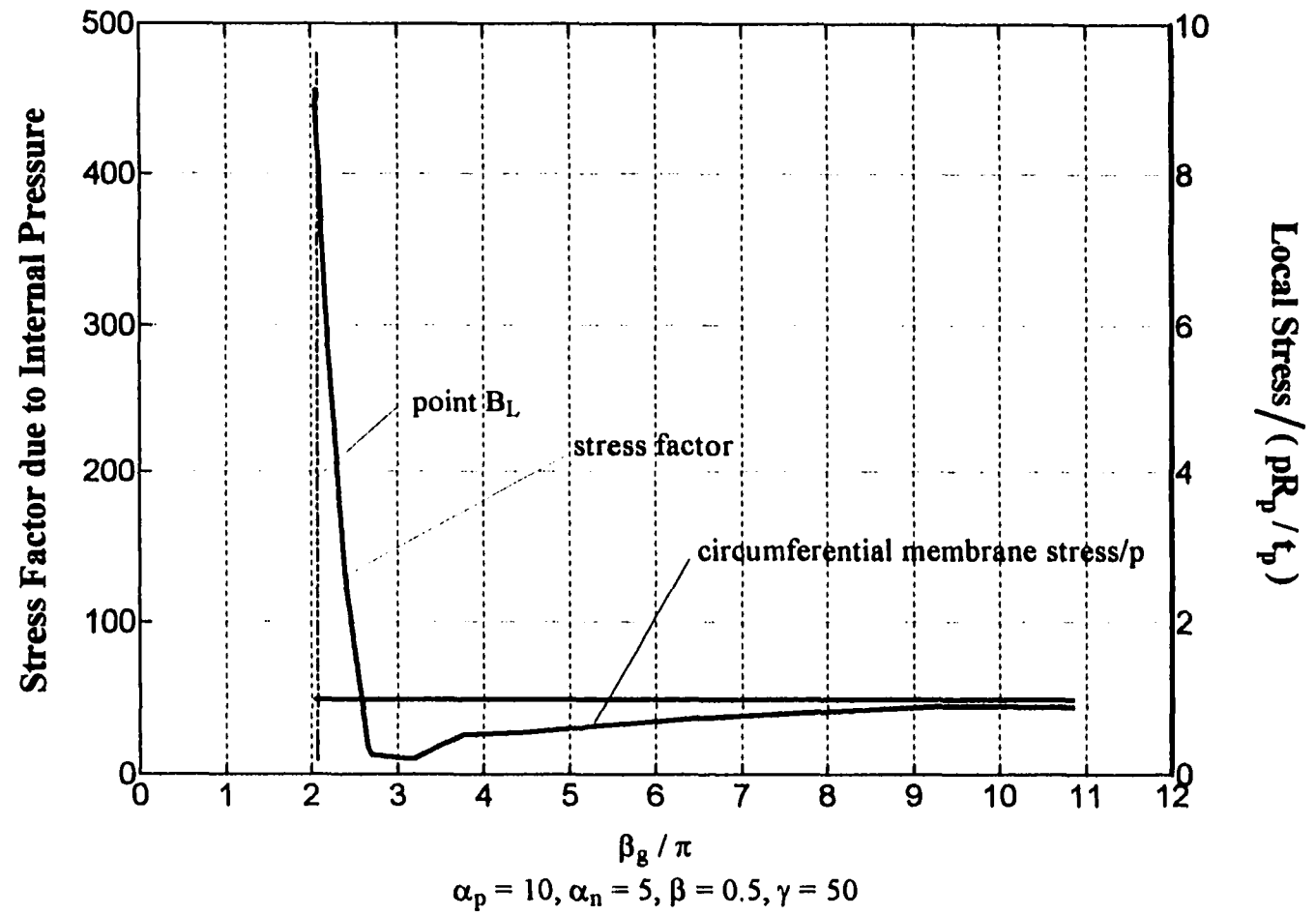
Figure G8: The variation of stress factor away from point B_L of pipe in circumferetial direction

131

REFERENCES

1. K. R. Wichman, A. G. Hopper and J. L. Mershon, "Local Stresses in Spherical and Cylindrical Shells Due to External Loading," Welding Research Council Bulletin No. 107, 1965

2. P. P. Bijlaard, " Stresses from Local Loading in Cylindrical Pressure Vessel," *Trans ASME* 77 pp. 805 - 816, 1955

3. S. Mirza, K. Gupgupoglu, " Stress Analysis of Cylindrical Pressure Vessel Subject to Bending Loading," Proceedings of the PEDAC Conference, Egypt, pp. 701 - 713, 1983

4. S. Mirza, K. Gupgupoglu, " Stress Analysis of Pressure Vessels With Uniformly Spaced Lugs." *Trans. of ASME* Vol. 110, pp. 70 - 75, 1988

5. J. L. Mershon, K. Mokhtarian, G. V. Ranjan, E. C Rodabaugh, " Local Stresses in Cylindrical Shells Due to External Loadings on Nozzle-Supplement to WRC No. 107," Welding Research Council Bulletin No. 297, 1984

6. C. R. Steele, M. L. Steele, " Stress Analysis of Nozzles in Cylindrical Vessels with External Load." *ASME, Journal of Pressure Vessel Technology*, Vol. 105, pp. 191 - 199, 1983

7. M. H. Sadd, R. R. Avent, " Stress Analysis and Stress Index Development for a Trunnion Pipe Support." *ASME, Journal of Pressure Vessel Technology*, Vol. 104, pp. 73 - 78, 1982

8. C. J. Tabone, R. H. Mallett " Pressure-Plus-Moment Limit-Load Analysis for a Cylindrical Shell Nozzle." *ASME, Journal of Pressure Vessel Technology*, Vol. 109, pp. 297 - 301, 1987

9. H. C. Sun, B. C. Sun and H. Herman, " Finite Element Analysis of Pipe-Nozzle Connections, Part II - Localized Stresses," *ASME, PVP* - Vol 194, " Analysis of Pressure Vessel and Heat Exchanger Components,", pp. 57 - 64, 1990.

10. H. C. Sun, B. C. Sun and H. Herman, " Local Stresses of Piping-Nozzle Due to Shear Forces and Torsional Moment by Finite Element Method." *ASME, PVP* - Vol 217, " Pressure Vessel and Components," 1991, pp. 33-40.

11. J. L. Ha, B. C. Sun, B. Koplik, " Local Stress Factors of Pipe-Nozzle Under Internal Pressure," *Nuclear Engineering and Design*, v.157, 1995 , pp. 81 - 91.

12. P. P. Bijlarrd, R. J. Dohrmann, " Stresses in Juncture of Nozzle to Cylindrical Pressure Vessel for Equal Diameter of Vessel and Nozzle." *Nuclear Engineering and Design*, V.5, 1967, pp. 349 - 365

13. D. H. Van Campen and H. A. Spaas, " On the Stresses Distribution in Nozzle-to-Cylinder Connections, for Small Diameter Ratios," *Nuclear Engineering and Design*, v.21, 1972, pp. 368 - 395

14. G. V. Ranjan, G. N. Brooks, and R. Huet," An Improved Method of Stress Analysis for Cylinder-to-Cylinder Intersection," *ASME Paper* 82-PVP-41, 1982

15. R. C. Gwaltney, S. E. Bolt, and J. W. Byrson," Theoretical and Experimental Stress Analysis of ORNL Thin-Shell Cylinder to Cylinder Model 4," *ERDA Report ORNL-5019*, Oak Ridge National Laboratory, June, 1975

16. V. Kumer and A. V. Singh, " Analysis of Pad-Reinforced Nozzle in Pressure Vessel Head," *Journal of Pressure Vessel Technology*, v.111, n.3, Aug., 1988, pp. 218

17. S. Timoshenko and S. Woinowsky-Krieger, *Theory of Plates and Shell.*, second edition, pp. 466 - 532, 1959

18. A. C. Ugural, *Stresses in Plates and Shells*, McGraw-Hill Book Company, New York, 1981, pp. 102 - 104, 282 - 284.

19. N. C. Lind, " Approximate Stress-Concentration Analysis for Pressured Branch Pipe Connections," *ASME* Paper 67-WA/PVP-7, 1967 pp. 1 - 8.

20. Updike, D. P. and Kalnins, A., " Approximate Analysis of Intersecting Equal Diameter Cylindrical Shells Under Internal Pressure," *ASME Journal of Pressure Vessel Technology*, Aug. 1979, pp. 194 - 199

21. ALGOR User Manual, " Visacard Plus, Vol. 1 & Vol. 2,", ALGOR Inc., 1992

22. ALGOR User Manual, " Linear Stress and Vibration,", ALGOR Inc., 1992

23. John F. Harvey, *Theory and Design of Pressure Vessel*, Second edittion, Van Nostrand Reinhold, N. Y., 1991, pp. 409 - 412

24. D. C. Chen, B. C. Sun and R. Chen, "Local Thermal Stress Factor of Pipe-Nozzle," *ASME, PVP* - Vol 318, " Structural Integrity Pressure Vessel, Piping and Components," 1995, pp. 89-102.

25. A. N. Gantayat and G. H. Powell, " Finite Element Analysis of Thin and Thick Walled Tubular Tee Joints," *Trans., International Conference on Structural Mechanics in Reactor Technology.* Paper F1/1, Aug., 1977

26. A. Y. Kuo and T. Y. Hsu, " Stress Analysis of Reinforced Nozzle-Cylindrical Shell Intersection under Internal Pressure or Thermal Expansion," *Journal of Pressure Vessel Technology,* v.110, n.3, Nov., 1988, pp. 367 - 373

27. I. M. Daniel, " Photoelastic Analysis of Stresses Around Oblique Holes, " *Experimental Mechanics,* Vol. 10, No. 11, November, 1970.

28. C. A. Ray, Jr., " Elastic-Plastic Strain Concentrations Produced by Various Skew Holes in a Flat Plate Under Uniaxial Tension, " *Experimental Mechanics,* March, 1971.

29. J. C. M. Yu and W. A. Shaw, " Stress Distribution of a Cylindrical Shell Non-radially Penetrated into a Spherical Pressure Vessel, " *ASME Paper* No. I-9, Second International Conference on Pressure Vessel Technology, San Antonio, Texas, 1973.

30. P. Stanley and B. V. Day, " Stress Concentrations at Offset-Oblique Holes in Thick-walled Cylindrical Pressure Vessels, " *ASME Paper* No. I-12, Second International Conference on Pressure Vessel Technology, San Antonio, Texas, 1973.

31. ASME Boiler and Pressure Vessel Code, Section III, Division 1, *Nuclear Power Plant Component, Appendices,* 1989, pp. 413 ~ 416